TÉCNICO LISBOA

Minimization of Fine Particles Emission from Biomass Combustion

Liquefaction, combustion additives and cyclone separators

Sriram Hariharakrishnan

Thesis to obtain the Master of Science Degree in

Energy Engineering and Management

Supervisors: Prof. Maria Joana Castelo-Branco de Assis Teixeira Neiva Correia
Dr. José Augusto Dâmaso Condeço

Examination Committee

Chairperson: Prof. Edgar Caetano Fernandes

Supervisor: Prof. Maria Joana Castelo-Branco de Assis Teixeira Neiva Correia

Members of the Committee: Dr. Maria Margarida Pires dos Santos Mateus

Eng. Joana Miguel da Silva Leal Pereira

October 2017

Acknowledgements

I'm grateful to my thesis supervisors, Prof. Joana and Dr. José; for without their guidance and help, completing this thesis would have been a Herculean task. I'm thankful to Dr. Margarida Mateus for her valuable inputs and her help with analyses. My gratitude goes to Dr. Nuno Canha from IST Center of Sciences and Nuclear technologies for providing equipment and help for measuring PSD of emissions during combustion experiments. I would like to thank Prof. Bordado for his amazing ideas regarding additives. My thanks are due for Torbel, for providing the needed raw materials and the necessary data.

I found three new friends, David, Mário, and Mónica who made working at lab more interesting and memorable. I'm thankful to my friends Shabna, Magda, Ovi, Cagdas, Abdul, Kabir, and Niko for being supportive and for putting up with my incessant ramblings and occasional idiosyncrasies.

Finally, I should thank my dad and mom for helping me become the man I am today. Thank you dad for always believing in me more than I believe in myself!

We may drift apart with time, but the memories will stay with us for eternity, to cherish!

Abstract

The global energy demand is ever-increasing due to factors such as population increase, and fossil fuels have played a major role in meeting these needs. However, the adverse environmental effects of fossil fuels call for increased use of renewable energy sources such as biomass. Biomass combustion is a common alternative of producing energy but the high concentration of fine particles in the flue gas can be a problem. Acid-catalysed liquefaction of lignocellulosic biomasses such as pinewood, olive stone/pits, olive bagasse, grape seeds, and rice husk was studied as a pre-treatment to combustion to remove the inorganic ash-forming species, while producing a liquid biofuel more easily burned. Liquefaction at 160ºC using 2-Ethyl Hexanol as solvent was optimised to have a high biomass/solvent ratio (1:1). The highest conversion achieved using this ratio under optimised conditions was ≈55% while 60 to 70% of the initial inorganic content of the biomass was removed in the liquefaction, thus proving its potential as a pre-treatment to decrease particles emissions.

Alternatively, to decrease the fine particles emitted as fly ash during combustion, some additives were selected and tested for their ability to capture fine particles and to increase the particle size of the ash particles. From the preliminary tests, TiO_2 showed promise in decreasing particulate emissions, especially, PM_1.

Aspen Plus was used to simulate a company's (Torbel) multicyclones, helical and spiral cyclones. These cyclones design were evaluated and further optimised for better performance. It was possible to obtain 16% efficiency increase.

Keywords: Biomass liquefaction; particulate emissions; combustion; additives; cyclones.

Resumo

A necessidade global de energia é crescente devido a fatores como o aumento da população e os combustíveis fósseis têm desempenhado um papel importante na satisfação destas necessidades. No entanto, os efeitos ambientais adversos dos combustíveis fósseis exigem um uso crescente de fontes de energia renováveis como a biomassa. A combustão de biomassa é muito utilizada para produção de energia mas a concentração elevada de partículas finas nos gases de combustão pode ser um problema. Neste trabalho, estudou-se a liquefacção de biomassas lenho celulósicas como madeira de pinheiro, caroço e bagaço de azeitona, sementes de uva e casca de arroz como pré-tratamento à combustão para remover os inorgânicos constituintes das cinzas, produzindo um combustível líquido mais fácil de queimar. Assim, a liquefação a 160ºC, pressão ambiente e utilizando 2-etil-hexanol como solvente e um catalisador ácido foi otimizada para uma razão biomassa/solvente de 1:1. A conversão mais elevada conseguida foi ≈55% e 60 a 70% da matéria inorgânica inicial da biomassa foi removida na liquefacção, o que demonstra o seu potencial como pré-tratamento para diminuir a emissão de partículas.

Alternativamente, para diminuir a quantidade de partículas finas emitidas na forma de cinzas volantes, foram seleccionados e testados aditivos com vista à capacidade para capturar partículas finas e aumentar a granulometria das cinzas. Nos testes preliminares, o TiO_2 mostrou-se promissor na diminuição das emissões de partículas, especialmente PM_1.

Utilizou-se o Aspen Plus para simular os multiciclones, os ciclones helicoidal e espiral da Torbel. Os sistemas foram avaliados e posteriormente otimizados para um melhor desempenho, tendo sido alcançado um aumento de eficiência de 16%.

Palavras-chave: Liquefacção de biomassa; emissões de partículas; combustão; aditivos; Ciclones.

Index

List of Figures

List of Tables

List of Abbreviations

Mtoe – Million tons of oil equivalent

OECD – Organization for Economic Co-operation and Development

Mt – Million tons

TPES – Total Primary Energy Supply

TWh – Terawatt hour

BFB – Bubbling Fluidized Bed

CFB – Circulating Fluidized Bed

PFC – Pulverized Fuel Combustion

CLC – Chemical Looping Combustion

Vol. % – Volume percentage

w. – by weight

w./w. – ratio in terms of weight

ESP – Electrostatic Precipitator

PEG – Poly Ethylene Glycol

DEG – Diethylene Glycol

MW – Molecular Weight

pTSA – para Toluene Sulfonic Acid

SMD – Sauter Mean Diameter

PM – Particulate Matter

HE – High Efficiency

2EH – 2-Ethyl Hexanol

DEEH – Mixture of 2-Ethyl Hexanol and Diethylene Glycol in the ratio 1:1 by weight

TORR – Penta Erythritol Tetra Ester

SEM – Scanning Electron Microscopy

EDS – Energy Dispersive Spectroscopy

TGA – Thermogravimetric Analysis

DTG – Differential Thermogravimetric Analysis

FTIR – Fourier Transform Infrared Spectroscopy

GCV – Gross Calorific Value

HQ – Hydroquinone

PW – Pinewood

OS – Olive stone

GS – Grape seeds

OB – Olive bagasse

RH – Rice husk

B/S – Biomass to Solvent ratio by weight

Vs. – Versus

PSD – Particle Size Distribution

CFD – Computational Fluid Dynamics

1. Introduction

1.1. Importance of bioenergy and its relevance to Portugal:

The population of the world as of now is humongous and it is still ever-increasing. The increasing population and advancements in technology has set the world on a path of seeking more sources of energy. Though, presently, fossil fuels contribute the major chunk in the energy scenario and they will continue to do so in the foreseeable future, there's a common consensus among majority of scholars that there's a pressing need for alternative energy sources owing to the drastic climate change caused by anthropogenic factors. Global warming is the most adverse effect influenced by the use of fossil fuels. Paris Agreement 2015 signed by 195 countries dictates that the governments pursue the long term goal of keeping the increase in global average temperature below 2 °C above the pre-industrial levels and to aim to limit this increase to 1.5 °C [UNCCC, 2015]. To achieve these goals, it's of paramount importance to transcend our dependence on fossil fuels by accelerating the transition from fossil fuels to renewable energy sources. Figure 1 shows the world total primary energy supply from 1971 to 2014 by fuel and by region [IEA, 2016].

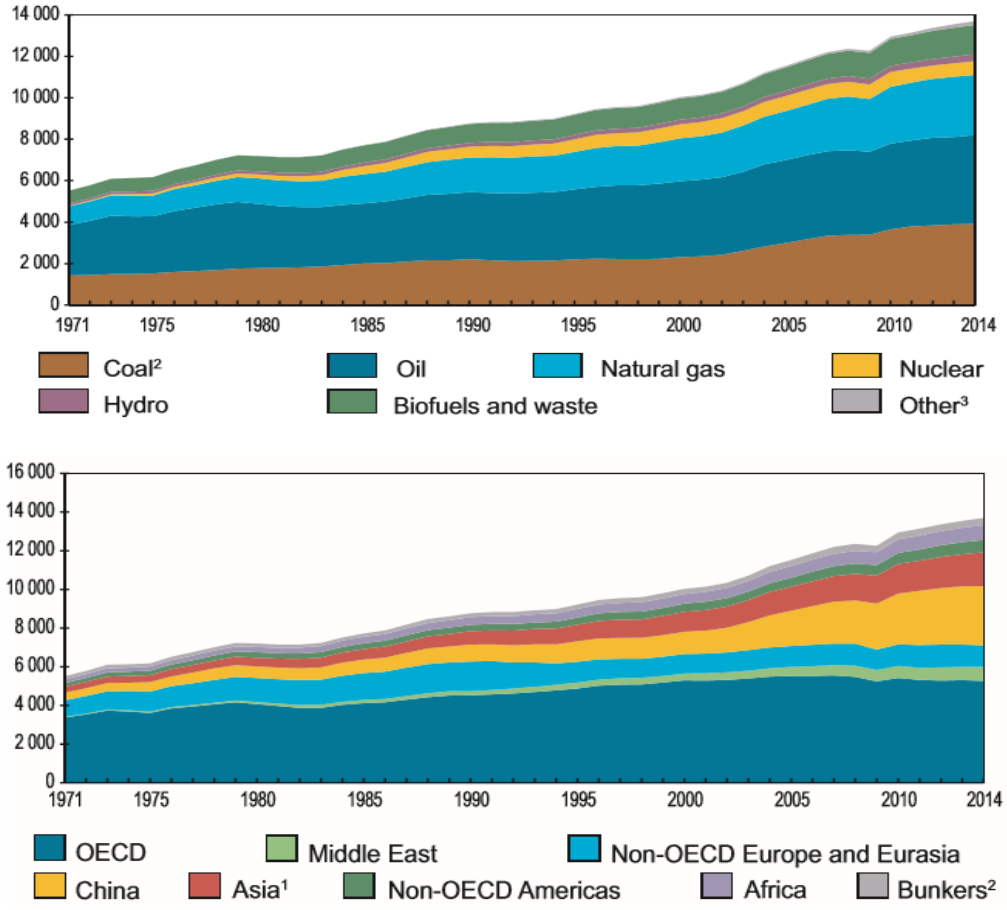

Figure 1: World total primary energy supply in Mtoe by fuel (above) and by region (below) [IEA, 2016]

Coal, natural gas and oil have been the predominant energy sources and will continue to dominate the energy sector for the foreseeable future as shown in Figure 2 [IEA, 2016]. Though, the contribution of biomass to energy supply has grown significantly, it is still a minor portion of the world energy supply; and without sufficient initiatives, it is hard to offset the production of energy from fossil fuels using biomass. It can be inferred, from Figure 3, the huge scale of CO_2 emissions by fossil fuels compared to that of other energy sources and by OECD countries & China compared to other countries. Despite the grim situation regarding greenhouse emissions, IEA stipulates a plausible optimistic scenario where, in 2040, global CO_2 emissions can be cut down by 42% by adhering to the 2015 climate policy framework of maintaining the global greenhouse emissions below 450 ppm equivalent of CO_2 [IEA, 2016].

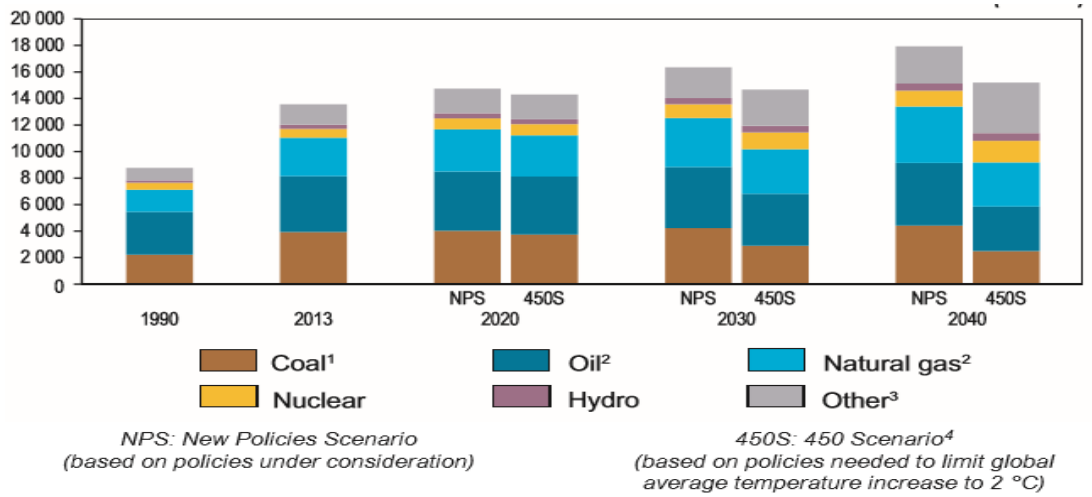

Figure 2: Total primary energy consumption of world by fuel (Mtoe) [IEA, 2016]

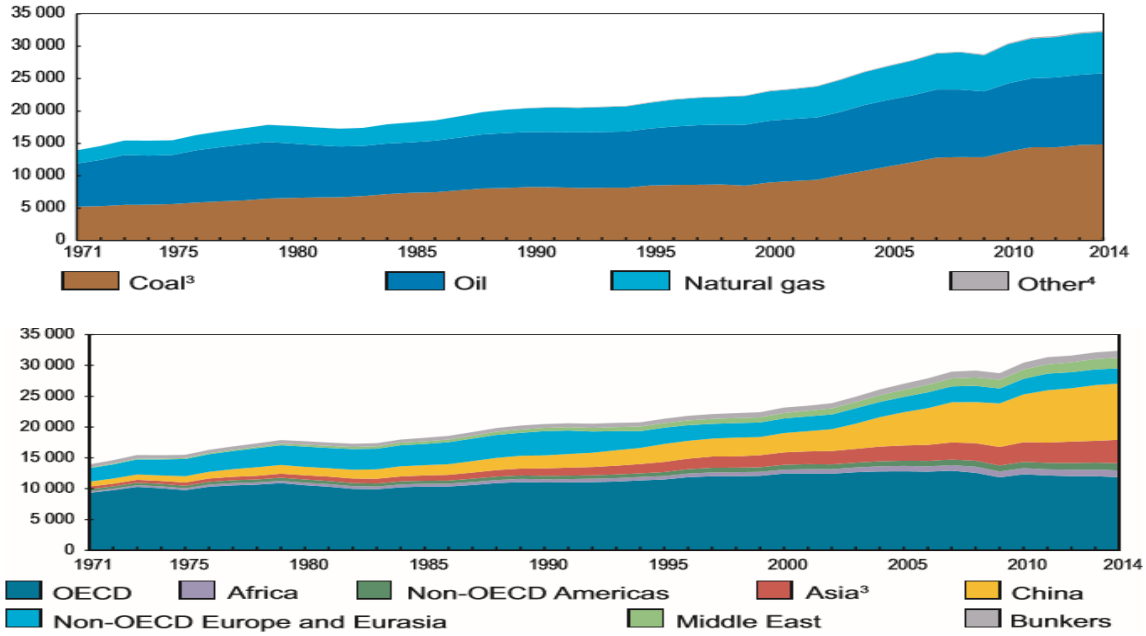

Figure 3: Global CO_2 emissions (Mt of CO_2) by fuel (above) and by region (below) [IEA, 2016]

All the data available so far indicate the need to adapt technologies and fuel sources in order to achieve negative CO_2 emissions in the long-term. Though the cost of carbon-free renewable energy sources such as solar and wind have considerably decreased in the past decade, their intermittent nature mandates the exploration of biomass sources. Moreover, the possibility to cut down the opportunity cost by utilising the locally available biomass and other wastes to produce energy is a motivating factor to further explore biomass energy. Table 1 shows the energy statistics of Portugal for 2014.

Table 1: Energy scenario of Portugal [IEA, 2016]

Energy production (Mtoe)	Net imports (Mtoe)	TPES (Mtoe)	Electricity consumption (Twh)	CO_2 emissions (Mt of CO_2)
6.00	16.38	21.16	48.50	42.81

From Figure 4 and Figure 5, it can be seen that the contribution of biomass to total energy consumption in Portugal is quite small though the contribution of biofuels has grown. Also, the use of wood and vegetal wastes for energy consumption hasn't changed much in the past two decades.

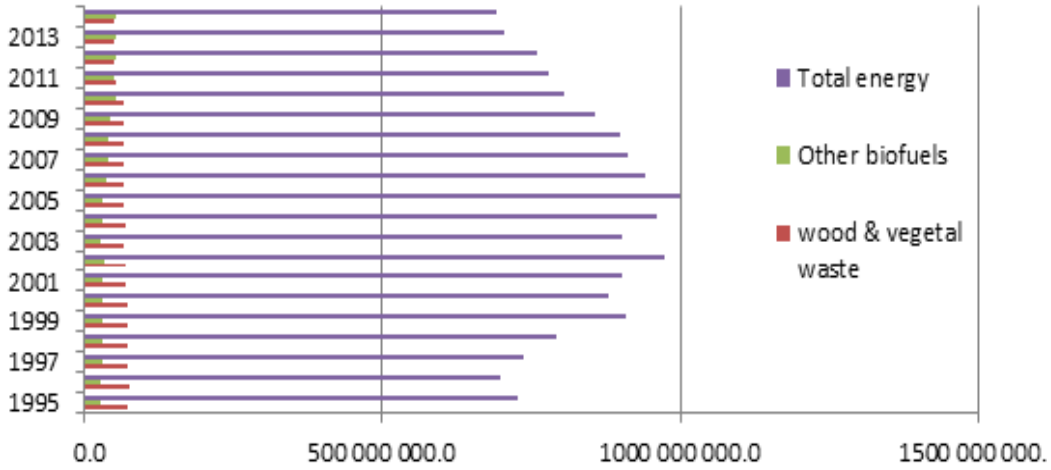

Figure 4: Energetic consumption of Portugal from biomass from 1995 to 2014 [INE]

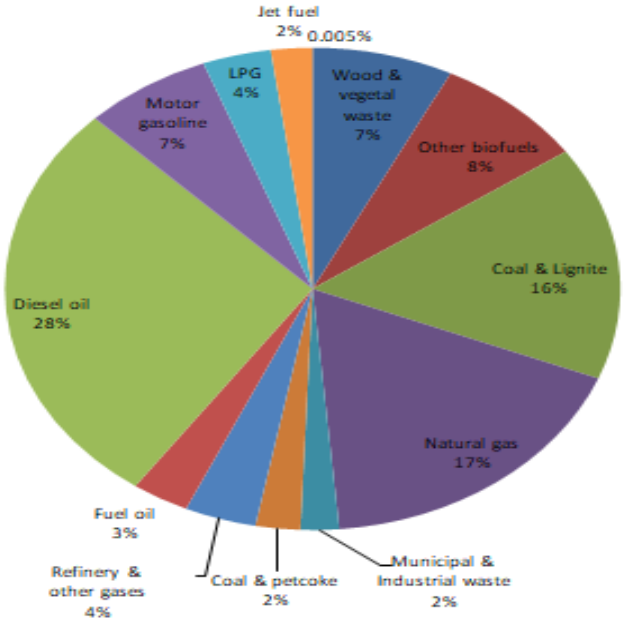

Figure 5: Energetic consumption of Portugal from different fuels in 2014 [INE]

Portugal has a huge forest cover of 35.4% including wooded areas and temporarily deforested areas. Portugal has a wide variety of forest flora as depicted in Figure 6, providing it a potential upper hand in developing bioenergy from forestry residues.

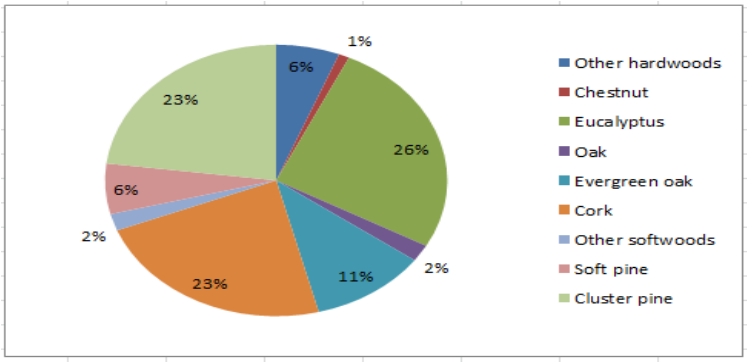

Figure 6: Composition of forest cover in Portugal [ICNF]

Though this forest cover has been more or less consistent through many years, there's a significant decrease in forest cover and also life losses every year due to forest fires. More than 2.5 million hectares of forest cover has burned due to wild forest fires between 1990 and 2012 [ICNF]. In June 2017, wildfire near Pedrógão Grande in Central Portugal killed 64 people in one of the biggest national tragedies of the decade. In July 2017, a large fire destroyed 80 to 90% of the Mação municipality. The year 2017 has seen 10000 separate forest fires in Portugal destroying 141000 hectares of forest cover [Guardian]. This necessitates implementation of good forest clearing and management plans. Establishing a biomass based circular energy economy in addition to the existing infrastructure could help mitigate this problem and to supplement the energy needs of the country.

1.2. Classification of biofuels

Biofuels are subjected to several classification methods. The most common method is to categorise them into different generations based on their source and production technology. First generation biofuels are those produced from food crops [Aro, 2016]. Corn, sugarcane, soybeans, and vegetable oils from several plants are amongst the sources of first generation biofuels. The major technologies to produce first generation biofuels are fermentation for bioethanol from sugar or starchy raw materials, and trans-esterification to produce biodiesel from plant oils. The technologies to produce and to process first generation biofuels are well-established but these fuels are controversial since these are produced from food sources.

Second generation biofuels are those produced from sources which are not food crops or from the parts/waste products from food crops which are inedible [Aro, 2016]. The main idea behind second generation biofuels was to cultivate them on non-arable lands where it is difficult, if not impossible, to cultivate food crops using lesser fertilizers and water. However, second generation biofuels fail terribly when it comes to the expected consumption of water and fertilizers [Aro, 2016]. Examples of second generation biofuels are grasses such as switch grass and elephant grass, seed crops such as jatropha and rapeseed, and waste vegetable oils. A huge bottleneck in the second generation biofuels is the inability to achieve expected high yields using only non-arable lands for their cultivation and hence they often compete with food crops for land. Unlike first generation biofuels, second generation sources need a lot of processing to produce the fuels from them. Gasification, pyrolysis, torrefaction, Fischer-Tropsch process, hydro-treatment and direct liquefaction are the main technologies used in the production of second generation biofuels.

Third generation biofuels are the fuels derived from algae and these eliminate the demerit of huge land use by second generation biofuels. Algae are versatile sources from which numerous biofuels can be produced – ethanol, biodiesel, butanol, methane, and jet fuel, to name a few. Butanol is an interesting fuel amongst these, as a fuel blend, due to its significant fuel-worthy calorific value. Besides the versatile products from algae, they can also be cultivated in multiple ways such as open ponds, custom raceways, photo-bioreactors, and closed-looping systems. Algae dominate the other biofuel sources by their ability to be grown without competing for land. Algae can even be grown on sewage water making them more advantageous [Aro, 2016]. A big disadvantage of algal biofuels is the huge requirement of nutrients needed to grow them and the energy needed for separation of water which sometimes offset the carbon emissions cut down by the algal biofuels, and researches are carried out to find or create highly efficient algal strains.

Fourth generation biofuels are those which are conceived to be produced synthetically only using renewable sources [Aro, 2016]. Aro (2016) defines the fourth generation biofuels as photobiological solar fuels produced by designer photosynthetic microorganisms, fuels produced by combining photovoltaics and microbial fuel production, or fuels produced by synthetic cell factories or synthetic tailor-made organelles. This classification of biofuels by generation does not have a definite boundary when it is done based on technology and hence it’s wise to use biomass source as a basis for this classification.

World Energy Council simply classifies biofuels into two types - bioethanol and biodiesel, the major biofuel products, irrespective of their sources [WE]. The word 'biofuels' is often used to refer only to liquid and gaseous biofuels. IEA defines biofuels as 'liquid and gaseous fuels produced from biomass' However, it is logical to also include solid biofuels under the aegis of biofuels. Then, solid biofuels could also be classified amongst the aforementioned generations depending on their source of origin. Another concept called biorefinery is noteworthy. It is similar to a petroleum refinery, where feedstock entering the refinery is converted into a wide array of products such as transportation fuels, chemicals, plastics, energy, food, and feed in an optimised way [WE].

1.3. Types and sources of biomass:

International Energy Agency defines biomass as 'any organic, i.e. decomposable, matter derived from plants or animals available for energy conversion. Biomass includes wood and agricultural crops, herbaceous and woody energy crops, municipal organic wastes, as well as manure' [IEA]. Biomass can be categorised into several different types due to its wide meaning. Food and Agricultural Organisation (FAO) of the United Nations classifies biomass based on the source as shown in Figure 7.

		WOODFUELS	AGROFUELS		
Energy crop		- energy forest trees - energy plantation trees	- energy grass - energy whole cereal crops	- energy grain	
By-products*	direct	- thinning by-products - logging by-products	crop production by-products:		- animal by-products - horticultural by-products - landscape management by-products
			- straw	- stones, shells, husks	
	indirect	- wood processing industry by-pro-ducts - black liquor	- fibre crop processing by-products	- food processing industry by-products	- biosludge - slaughterhouse by-products
End use materials	recovered	- used wood	- used fibre products	- used products of fruits and seeds	MUNICIPAL BY-PRODUCTS - kitchen waste - sewage sludge

*The term "by-products" includes the improperly called solid, liquid and gaseous residues and wastes derived from biomass processing activities.

Figure 7: FAO's classification of biomass [FAO]

The United States Department of Energy classifies the biomass feedstocks into the following types which are explained briefly as follows [US-DE]. Dedicated energy crops are non-food crops often grown on marginal non-arable lands grown specifically to harvest biomass. These are further divided into perennial herbaceous crops such as switch grass, elephant grass, bamboo and sweet sorghum, and short-rotation woody crops such as hybrid poplar, hybrid willow, sweet gum and sycamore.

Herbaceous crops are harvested annually after an initial growth period of two to three years while short rotation woody crops are harvested within five to eight years of cultivation. Agricultural crops are crops such as corn, wheat, and soybean while agricultural crop residues are parts of crops that are not commercially used for food or food-based products with examples such as rice husk, rice straw, corn stover and wheat straw. Aquatic flora such as seaweed, water hyacinths and microalgae are also sources of biomass. Forestry residues, such as pinewood and timber wastes, are the biomass wastes resulting from forest-based industries and forest management operations. Biomass processing residues such as olive stones, grape seeds, olive bagasse, waste wood pulp, wood shavings, etc., are those which are left behind after several biomass processing operations. Municipal wastes comprising organic content, such as sewage from residential, commercial and industrial sectors can also be biomass feedstocks. Animal wastes such as poultry wastes, aquaculture wastes, and swine manure are other sources of biomass. In a nutshell, biomass feedstocks can be classified, as done by Carol L. Williams, into woody and non-woody biomass or into agricultural, forest and waste residues as shown below in Figure 8 [Jose and Bhaskar].

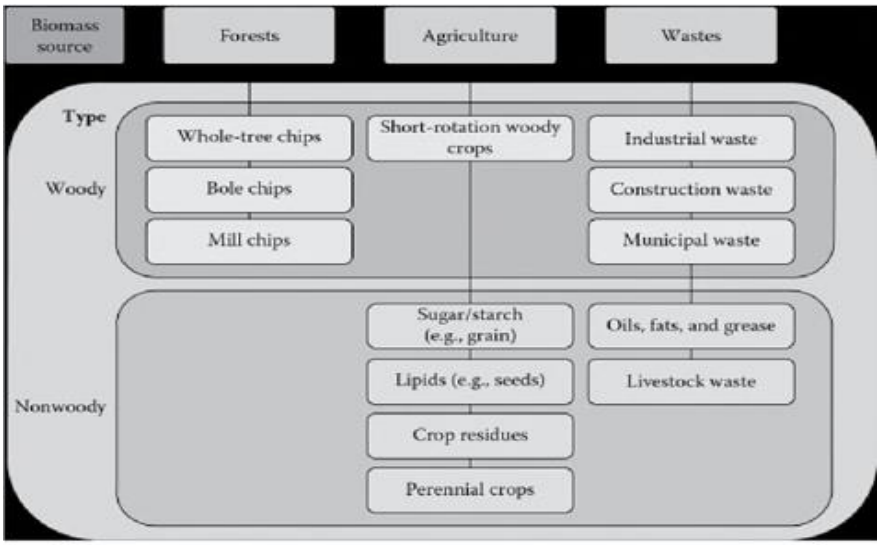

Figure 8: Classification of biomass feedstocks

1.4. Direct combustion of biomass

Although biomass is a versatile carbon-neutral source of fuels, energy and certain chemicals, direct combustion of biomass to produce energy is the most viable option in many cases as it needs less to no changes in the existing infrastructure. Biomass is already being used for co-combustion in many industries across the world and even as a sole source of energy in some industries. Monteiro, C. et al. (2011) estimated that the existing residual forest biomass is sufficient to feed the existing as well as planned thermal power plants in Portugal. Moreover, Nunes (2017) states that 82.9 MW of electricity can be produced from the existing forest waste biomass through proper forest management. Though biomass combustion has been around for many decades and well-established, there are still several hurdles to overcome.

1.4.1. Combustion technologies

Combustion technologies are developed to address the specific combustion requirements such as product needs, fuel feedstock, local regulations and utility function of the industry. Biomass combustion can be classified into combustion and co-firing. Co-firing involves combustion of biomass in addition to another fuel. Co-firing can be direct co-firing, indirect co-firing or parallel co-firing [Brem, 2005]. In direct co-firing, the biomass is subjected to mechanical pre-treatment along with other fuels to create feedstock blend which is combusted. Indirect co-firing involves gasification of biomass and to use the products obtained in combustion of another feedstock. In parallel co-firing, the biomass is combusted in separate equipment in parallel to the other feedstock in another combustion device [EUBIONET]. Combustion technologies can be broadly classified into three categories – fixed bed, fluidised bed, and pulverised fuel combustion [(Costa, 2008), (Nussbaumer, 2010)]. Examples of fixed bed combustion systems are grate furnaces and underfeed stokers, where primary air passes through a fuel bed where drying, devolatilisation, and char combustion take place whereas the volatiles combustion takes place separately in the combustion zone and not on the bed using a secondary air intake [Nussbaumer, 2010]. Underfeed stokers are suitable for low ash biomass while grate furnaces are suitable for high ash, high moisture biomass. Grate furnaces use different types of grates such as moving bed, vibrating bed, etc., depending on the fuel requirements [(Costa, 2008), (Nussbaumer, 2010)]. Fluidised bed combustion involves combustion of biomass in a suspension of biomass and an inert material such as dolomite, silica, olivine, etc., as fluidising medium. The fluidised bed provides better mixing and hence, it can be used for various blended biomass feedstock [Nussbaumer, 2010]. However, the particle size and impurity limitations imposed by the design of these combustors necessitate proper pre-treatment of the feed [Costa, 2008]. Fluidised bed combustors can be classified into bubbling fluidised bed (BFB) and circulating fluidised bed (CFB) depending on the velocity of the fluidising medium [Nussbaumer, 2010]. In pulverised fuel combustion (PFC), fine particles of biomass are injected into the combustor along with primary air to enable explosive devolatilisation of the feed particles [Nussbaumer, 2010]. In PFC, small particle size enables simultaneous devolatilisation and char combustion whereas volatiles combustion is done by secondary air intake [Nussbaumer, 2010]. Figure 9 and Figure 10 illustrate these combustion technologies. Table 2 compares some of the characteristics of these combustion technologies as given by Mário Costa (2008).

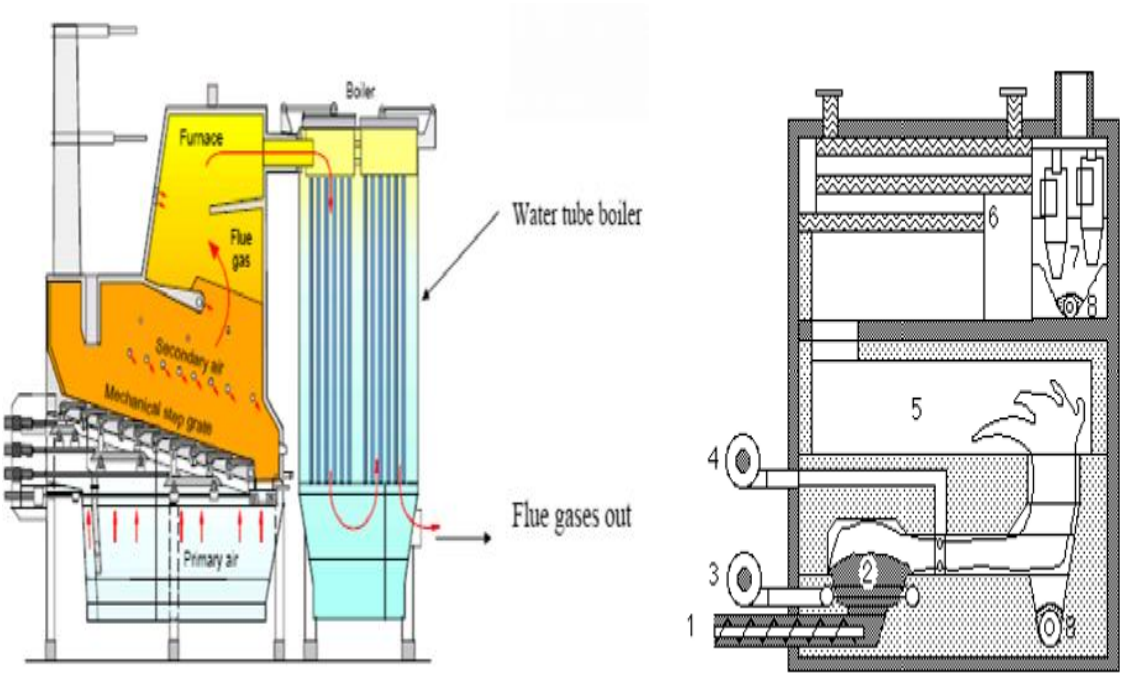

Figure 9: Left - Fixed bed grate furnace and right – Understoker boiler with primary and secondary air, mixing zone and post combustion chamber showing 1 screw feeder, 2 understoker zone with glow bed, 3 primary air, 4 secondary air, 5 post combustion chamber, 6 heat exchanger, 7 cyclone, 8 ash removal. [(Costa, 2008), (Nussbaumer, 2010)]

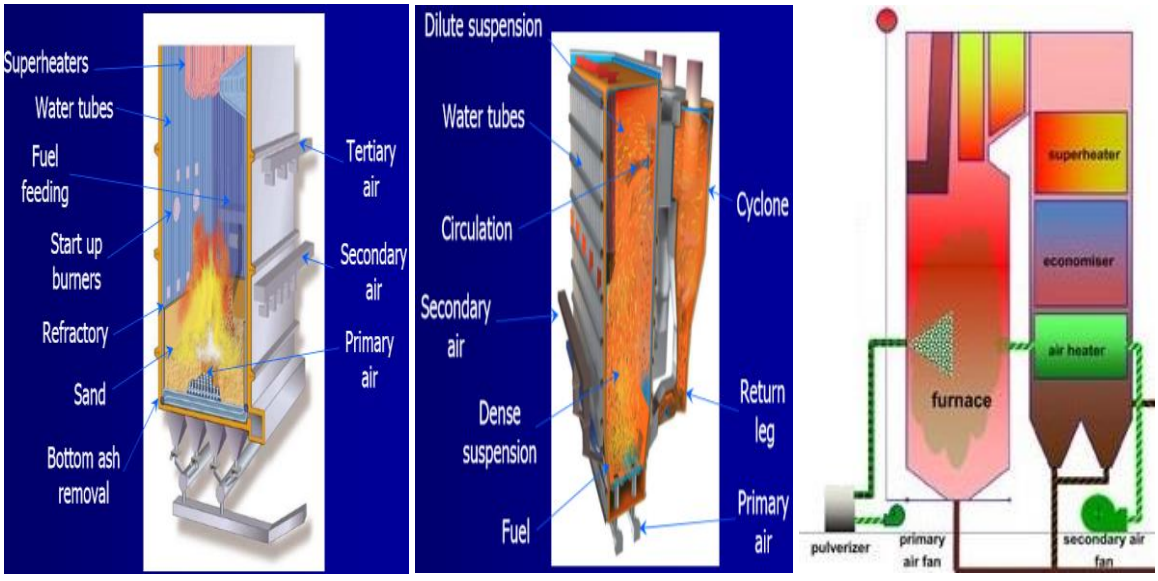

Figure 10: From left to right: Bubbling Fluidised bed furnace, Circulating fluidised bed furnace, and Pulverised combustion boiler [(Costa, 2008), (BHE)]

Table 2: Characteristics of different combustion technologies [Costa, 2008]

Characteristic	Combustion Technology		
	Pulverised	**Fixed (Grate)**	**Fluidised bed**
Combustion efficiency (%)	99	70-90	90-99
Global thermal efficiency (%)	35-45	25-35	40-55
Excess air (%)	15-50	20-40	10-25
Particle size (mm)	<0.5	12-20	8
Operating temperature (°C)	1400-1700	1400-1700	800-1000
NO_x emissions	High	High	Low
SO_x capture (%)	-	-	80-90

Apart from these technologies, new technologies such as oxy-combustion and chemical looping combustion (CLC) also exist. In oxy-combustion, pure oxygen is used instead of air to reduce NO_x emissions from air and for enhanced combustion characteristics and to derive a CO_2 concentrated stream [Riaza, 2012]. CLC uses a combination of a CFB & an air reactor, an oxygen carrier, typically metal oxide or a combination of metal oxides instead of air directly, in order to get a concentrated stream of CO_2 for carbon capture and sequestration. CLC is a novel technology that is still in the research phase in places like Chalmers University, Sweden and it has a great potential to pursue negative CO_2 emissions on overcoming the difficulties such as finding a non-toxic, low-cost, high-efficiency oxygen carrier; decreasing the char entrainment, ash agglomeration; and decreasing the carbon capture in air reactor.

To summarize, fixed bed combustion of biomass is widely used in industries and pulverised combustion of biomass in fewer places. Fluidised bed combustion is more widely used in coal power plant: a prime example is the world's largest CFB boiler in Łagisza power plant in Poland [TAURON]. However, very less information is available regarding the commercial use of fluidized bed technology for biomass combustion. For instance, according to the information available in its internet site, Torbel has the capability to manufacture fluidized bed boilers up to 15 MW for biomass combustion. However, additional information regarding these furnaces is not available.

1.4.2. Bottlenecks of biomass combustion

Biomass combustion has its own difficulties such as high moisture content, low bulk density, ash formation, etc. The high moisture content of biomass causes poor ignition and lowering of temperature during combustion. In addition to this, high moisture content also causes high transportation and storage costs. Biomass has low bulk density causing logistical problems and storage hazards such as spontaneous combustion due to high surface area and volume. Figure 11 shows the bulk density of typical agricultural residues. Biomass also has a lower energy density compared to coal.

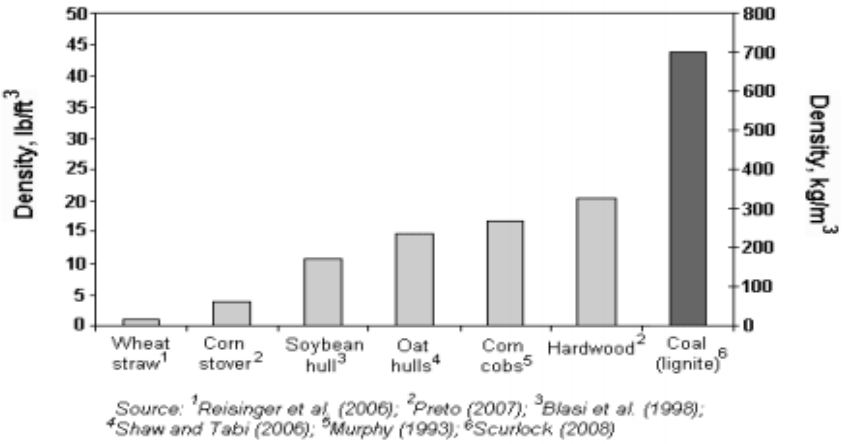

Figure 11: Bulk density of typical agricultural residues [Clarke and Preto, 2011]

These problems can be solved by pre-treatment and densification of biomass. Grinding is one of the pre-treatment techniques used to decrease the energy consumed during densification process and to give denser products as output during compaction [Clarke and Preto, 2011]. Drying of the biomass is needed to decrease the moisture content which in turn increases the density and durability of the biomass feedstock [Clarke and Preto, 2011]. The biomass needs certain moisture content for ease of compaction and above that level of moisture, the durability and density of the biomass is reduced. Also, the density and durability depends on the natural binding agents of the biomass material. Sometimes, binding agent additives such as vegetable oil, starch, clay, wax, etc. are added for effective compaction of biomass to pellets, bales, etc [Clarke and Preto, 2011]. Steaming is a method of pre-treatment where addition of steam aids in the release and activation of the natural binders in the biomass [Clarke and Preto, 2011].

Another pre-treatment process is torrefaction. Torrefaction is a form of mild pyrolysis at temperature of about 200 to 320 ˚C which is carried out under atmospheric pressure but in the absence of oxygen [Chew, 2011]. During this process, the water contained in the biomass and the superfluous volatiles are released and the polymeric part containing cellulose, hemicellulose, and lignin partly decomposes [Chew, 2011]. The final product from this process is a denser biomass commonly called bio-char in literature. This process consumes more energy which is a demerit in the overall Life cycle impact of the energy from agricultural and forest residues [Clarke and Preto, 2011]. This can however be offset by using the volatiles from this process to provide heat for torrefaction and by minimizing the loss of low value heat by optimizing the process further. The pre-treatment processes provide value addition

to the biomass by giving it higher energy density, more homogeneous composition, hydrophobic behaviour, and less biological activity thus preventing the rotting of biomass [Chew, 2011].

Pyrolysis is also used as a pre-treatment to produce bio-oil and bio-char which can further be combusted [FAO]. However, a major demerit associated with this process is the high energy consumption [FAO]. The slurry of this bio-oil and bio-char may be used as combustion feedstock. As mentioned in the next item, another major problem with biomass is the typically high inorganic content which leads to problems such as slagging, fouling and agglomeration. Some biomass such as rice husk have higher silica content causing ceramic material like deposits which are hard to clean during blow down. Most biomasses have high potassium and Chlorine content. K content leads to lower ash melting temperatures and Cl content favours the formation of fly ash which is a major environmental concern regarding biomass combustion [Obernberger].

In this perspective, liquefaction is a potential pre-treatment to decrease the problems associated with the inorganic content before combustion, high moisture content of biomasses and to facilitate easier combustion by using bio-liquids instead of direct biomass combustion. In the literature, liquefaction has been studied widely as a pathway to liquid fuels and some chemicals but not as a pre-treatment before combustion.

1.4.3. Ash characteristics of common biomass

Ash from biomass can be classified into inherent and extraneous ash fractions [Livingston, 2006]. Inherent inorganic fraction exists as a part of the molecular structure of the biomass whereas the extraneous fraction includes inorganic material added to the biomass by geological, agricultural or handling processes [Livingston B., 2006]. Extraneous inorganic fraction is mainly caused by contamination of biomass by soil during harvest, handling and storage. Biomass ashes can also be classified into three types based on their compositions and fusion temperatures - high silica/high potassium/low calcium ashes with low fusion temperatures; low silica/low potassium/high calcium ashes with high fusion temperatures; and high calcium/high phosphorus ashes with low fusion temperatures [(Livingston B., 2006), (Livingston W.R., 2007)]. The fusion temperatures influence the agglomeration and slagging of ash particles on the surface of the combustion equipment. The biomass ash can further be classified into three fractions – water-soluble components such as nitrates, chlorides, and sulphates of alkali metals; organically associated compounds such as organometallic complexes, sulpholipids, amino acids and proteins; and precipitates such as calcium oxalate and phytolite [(Livingston B., 2006), (Livingston W.R., 2007)]. The inorganic compositions of some common biomasses are tabulated in Table 3.

Table 3: Inorganic composition of common biomasses [Livingston B., 2006]

Biomass	Forest residue	Willow	Cereal straw	Oil seed rape straw	Olive residue	Palm kernel	Poultry litter
Ash (%)	2	2	5	5	7	4	13
Analysis (mg/kg)							
Al	-	-	50	50	1500	750	600
Ca	5000	5000	4000	15000	6000	3000	20000
Fe	-	100	100	100	900	2500	900
K	2000	3000	10000	10000	23000	3000	5000
Mg	800	500	700	700	2000	3000	5000
Na	200	-	500	500	100	200	3000
P	500	800	1000	1000	1500	7000	14000
Si	3000	-	10000	1000	5000	3000	9000

1.4.4. Fine particles formation mechanism

The fly ash produced from combustion comprises two fractions – coarse fly ash, and aerosols. Coarse fly ash particles are those carried away from the char combustion whereas aerosols are formed by several different gas phase reactions followed by nucleation, agglomeration and/or condensation of resultant compounds. Coarse fly ash particles can have aerodynamic diameters from 1 to 250 µm while aerosols have diameters below 1 µm [Obernberger]. Particles below 10 µm are classified as fine particle emissions in the literature. These fly ash fractions are formed from a series of different reactions following the char formation during devolatilisation of the biomass particles. These pathways are given by Obernberger as illustrated in Figure 12 [Obernberger].

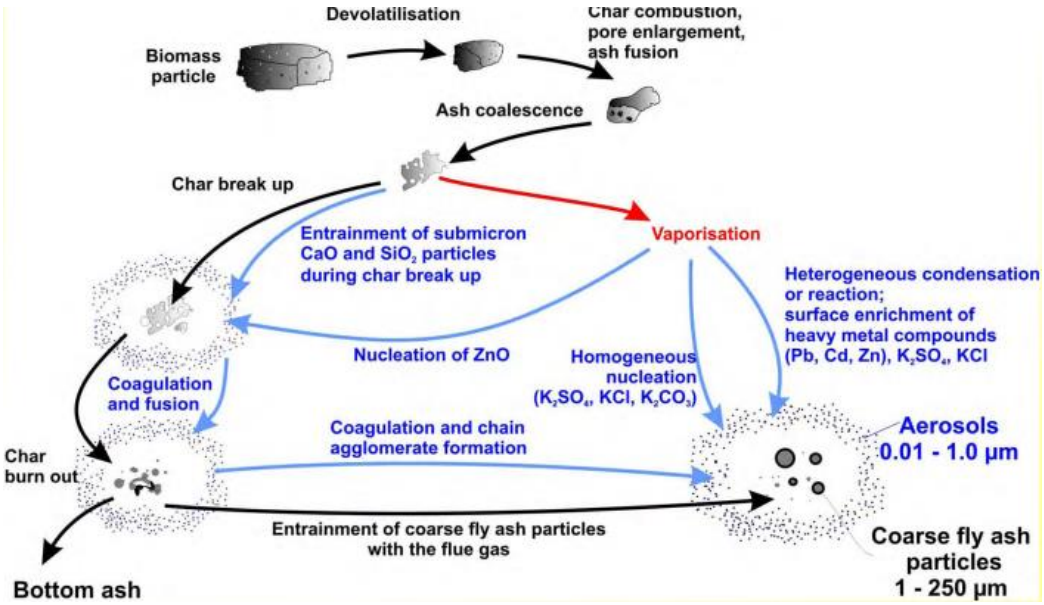

Figure 12: Aerosol and coarse fly ash formation pathways [Obernberger]

The particle size distribution (PSD) of the fly ash varies widely with the type of biomass feedstock, combustion technology used and the process parameters. T. Brunner, et al. (2002) found that the PSD of fly ash from fixed bed combustion systems follow a logarithmic normal distribution as shown in Figure 13.

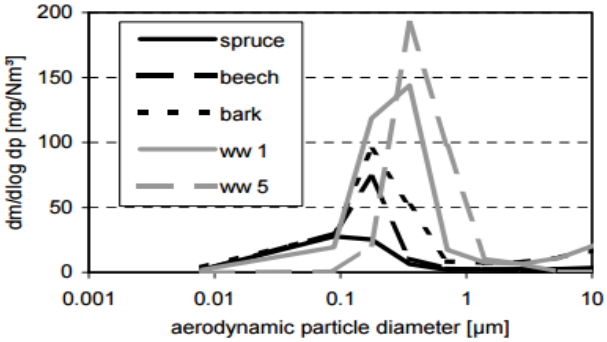

Figure 13: PSD of fly ash from different biomass in fixed bed combustion systems, ww1 - waste wood with high Si content; ww5 - waste wood with high Ca content. Data normalized to dry flue gas and 13 vol. % O_2 [Brunner, 2002]

The composition of aerosols varies with the chemical composition of the biomass feedstock. They usually contain alkali metal phosphates, sulphates, and heavy metals. Table 4 represents a sample data for aerosols composition from different biomass [Obernberger]

Table 4: Sample elemental composition of aerosols from combustion of different biomass feedstocks [Obernberger]

Element	Composition (atom %)			
	Spruce	Beech	Bark	Waste wood
K	28.5	34.6	27.3	8.7
Na	2.7	1.5	-	4.4
S	9.0	9.7	8.7	-
Cl	1.6	5.7	18.1	36.6
Zn	7.3	-	3.4	12.6
Ca	-	-	1.3	-
Pb	-	-	-	25.2
O	50.4	47.8	40.7	12.6

The aerosol compounds usually have low melting points causing deposition problems and high amounts of S and Cl in some aerosols causes downstream corrosion problems during post combustion capture [Livingston B., 2006]. Aerosols formation mechanisms available in literature do not give a uniform predictive model and more research is needed to establish a firm ground in this domain. These fine particle emissions pose severe health risks and hence necessitate post-combustion capture equipment such as high efficient cyclones, ESP and bag house filters.

1.4.5. Emission regulations

One of the major environmental and health hazard is air pollution. The air quality guidelines provided by World Health Organization (WHO) stipulates the health hazards of several air pollutants. The WHO estimated that in 2014, 92% of the world population was living in places which do not meet the WHO air quality guideline limits. It also estimated that air pollution causes 3 million premature deaths worldwide, every year, solely due to PM_{10} and particles smaller than PM_{10}. The WHO 2005 guidelines prescribe emission limits for common air pollutants as shown in Table 5.

Table 5: Atmospheric pollutant concentration limits according to WHO air quality guidelines 2005 [WHO]

Pollutant	Limit
$PM_{2.5}$	10 µg/m^3 annual mean 25 µg/m^3 24-hour mean
PM_{10}	20 µg/m^3 annual mean 50 µg/m^3 24-hour mean
SO_2	20 µg/m^3 24-hour mean 500 µg/m^3 10-minute mean
NO_2	40 µg/m^3 annual mean 200 µg/m^3 hourly mean

The directive 2008/50/EC of the European Parliament and of the council of 21 May 2008 on ambient air quality and cleaner air for Europe delineates several targets, limits and critical emission levels for common air pollutants, some of which are tabulated below in Table 6 [DIR08]. This directive gives a target limit value of 20 µg/m^3 for $PM_{2.5}$ in the atmosphere, by 1st of January 2020.

Table 6: Limit for common pollutant in ambient air according to 2008/50/EC European Parliament directive [DIR10]

Pollutant	Limit	Margin of tolerance
PM_{10}	Daily: 50 µg/m^3, not to be exceeded more than 35 times a calendar year	50%
	Yearly: 40 µg/m^3	20%
SO_2	Hourly: 350 µg/m^3, not to be exceeded more than 24 times a calendar year	43%
	Daily: 125 µg/m^3, not to be exceeded more than 3 times a calendar year	None
NO_2	Hourly: 200 µg/m^3, not to be exceeded more than 18 times a calendar year	0%
	Yearly: 40 µg/m^3	0%

Directive 2010/75/EU of the European Parliament and of the Council of 24 November 2010 on industrial emissions (integrated pollution prevention and control) gives the emission limits for large combustion plants for different solid, liquid and gaseous fuels for different plant capacities based on their construction approval dates [DIR10]. Some of these limits for solid and liquid fuels are summarised below in Table 7. These emission limits have some exceptions based on the date of permits which are described in detail in the directive.

Table 7: Emission limits according to 2010/75/EU directive [DIR10]

Pollutant	Total rated thermal input (MW)	Biomass (mg/Nm^3)	Liquid fuels (mg/Nm^3)
SO_2	50-100	200	350
	100-300	200	250
	> 300	200	200
NO_x	50-100	300	450
	100-300	250	200
	> 300	200	150
PM	50-100	30	30
	100-300	20	25
	> 300	20	20

In Portugal, the *Portaria 677-2009* imposes that for plants with less than 50 MW, the PM emission limit is 150 $mg/Nm^{3.}$ However, it is expected that in near future the limit for this type of plants can decrease to 50mg/Nm^3 as imposed by the European Directive transposed on to the Portuguese Decree DL 127/2013.

This thesis was carried out within a research project between Instituto Superior Técnico and Torbel, a Portuguese company that develops and builds systems for energy production, namely biomass furnaces and boilers, and environmental treatment systems such as cyclones and filters. The project aims to study alternatives to decrease fine particles emission in biomass combustion to comply with the PM emission limit of 50 mg/Nm^3.

1.5. Fine particles emission control

1.5.1. Liquefaction of biomass as a pre-treatment:

The main objective of liquefaction as a pre-treatment is to convert the biomass into a combustible liquid of significant calorific value and decreasing the content of undesirable components such as sulphur, nitrogen, oxygen, minerals and the fine particle emissions resulting from combustion. The liquefied product can easily be stored, transported and used directly in combustion or be processed further to produce liquid fuels and/or other chemicals. Hence, biomass liquefaction can be an alternative pathway to produce fuels and chemicals. However, biomass liquefaction has its own merits and demerits depending on the liquefaction techniques used, type of biomass and the process parameters.

1.5.1.1. Liquefaction process:

Liquefaction of biomass is a solvolytic process that is either acid-catalysed or base-catalysed, most commonly the former. During liquefaction, biomass gets degraded into smaller molecules by dissolution and reaction with a solvent, at atmospheric pressure and at temperature of 150 to 250 °C. Usually, one or more polyhydric alcohols are used as solvent [Li, 2015]. The structural and chemical composition of the biomass determines the mechanism and results of liquefaction. Any lignocellulosic biomass is composed mainly of three types of polymers- cellulose, hemicellulose and lignin and the composition of these in a lignocellulosic biomass influences the liquefaction process. Besides these polymers, comparatively small amounts of pectin, proteins, extractives and inorganic content constitute lignocellulosic biomass [Bajpai et al., 2016]. The structure and chemical composition of these components are described in brief as follows.

Cellulose is a linear polymer with repeating disaccharide units of β-glucose monomer linked by 1,4-β glycosidic bonds, as shown in Figure 14.

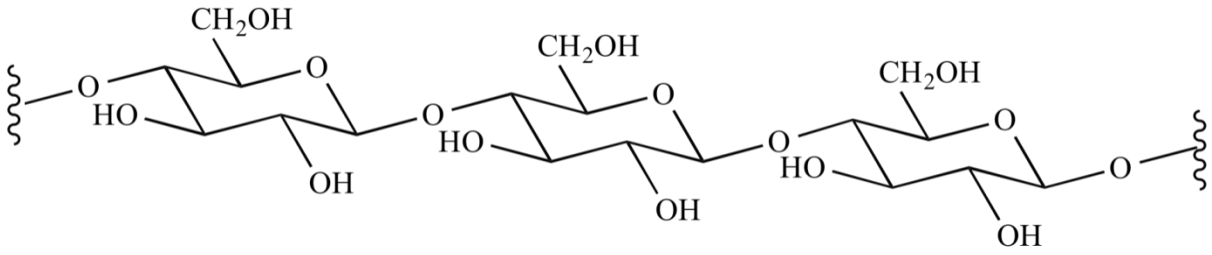

Figure 14: Chemical structure of one cellulose polymer chain [UCLA]

The branched off carbon chain on two linked monomers are on alternate sides enabling a cellulose polymer chain to occupy less space and to form a compact cellulose framework with more polymer units lying side to side. These polymer units are connected to each other by hydrogen bonds forming a compact structure, the crystalline regions of cellulose found in lignocellulosic biomass. This enables cellulose to bundle into cellulose microfibrils which give the inherent structural integrity to the cell walls of plants [Bajpai et al., 2016]. Cellulose also contains amorphous regions but much less compared to its counterpart starch.

Hemicellulose, unlike cellulose, is branched and highly heterogeneous in composition. It encompasses families of polysaccharides such as xylans, xyloglucans, mannans, glucomannans and β-glucans [Scheller and Ulvskov, 2010]. These polysaccharides are composed of different monosaccharides, majorly either xylose or mannose, and also galactose, arabinose and rhamnose. The chemical structures of these polysaccharides vary widely with plant species and even among different parts of one plant [Scheller and Ulvskov, 2010]. As an example, the structures of xylan from different biomass sources are shown below in Figure 15.

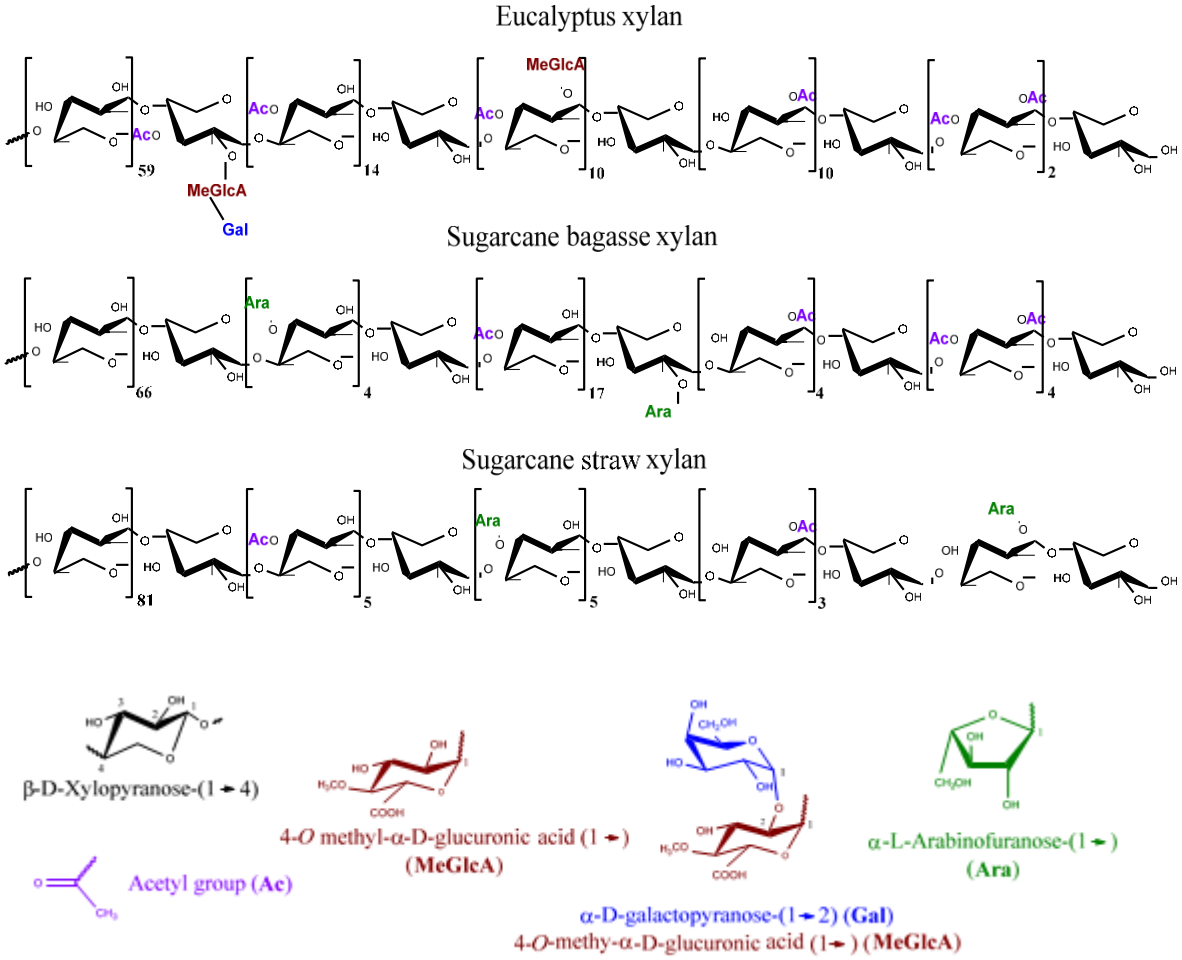

Figure 15: Structure of xylan from different biomass sources [Carvalho, 2015]

Hemicellulose aids the strengthening of cell wall by functioning as an intermediary in connecting the cellulose microfibrils to each other and sometimes to lignin and pectin.

Lignin is defined by John Ralph et al. (2004) as “complex natural polymers resulting from oxidative coupling of 4-hydroxyphenyl-propanoids”. Phenyl-propanoids are plant-based organic compounds biosynthesized from two amino acids – phenylalanine and tyrosine [Barros et al., 2016]. The chemical structure of lignin varies so widely that there are hypotheses claiming that formation of lignin results from random biosynthesis by plants. Though the combinatorial possibilities of resultant products from lignification reactions are statistically finite and limited by the inherently present precursors and conditions, the number of possible combinations is so humongous that it eliminates the likelihood of

any two lignin compounds exhibiting the same chemical structure [Ralph et al., 2004]. Though, most literatures delineate lignin as potentially three dimensional cross-polymers, Banoub and Delmas (2003) claim that this could be a result of analysing lignin from paper & pulp industries which could have recombined to form these complex polymers and might be significantly different from lignins in native form. The structures of some lignins as stated by Banoub and Delmas (2003) are as shown below in Figure 16.

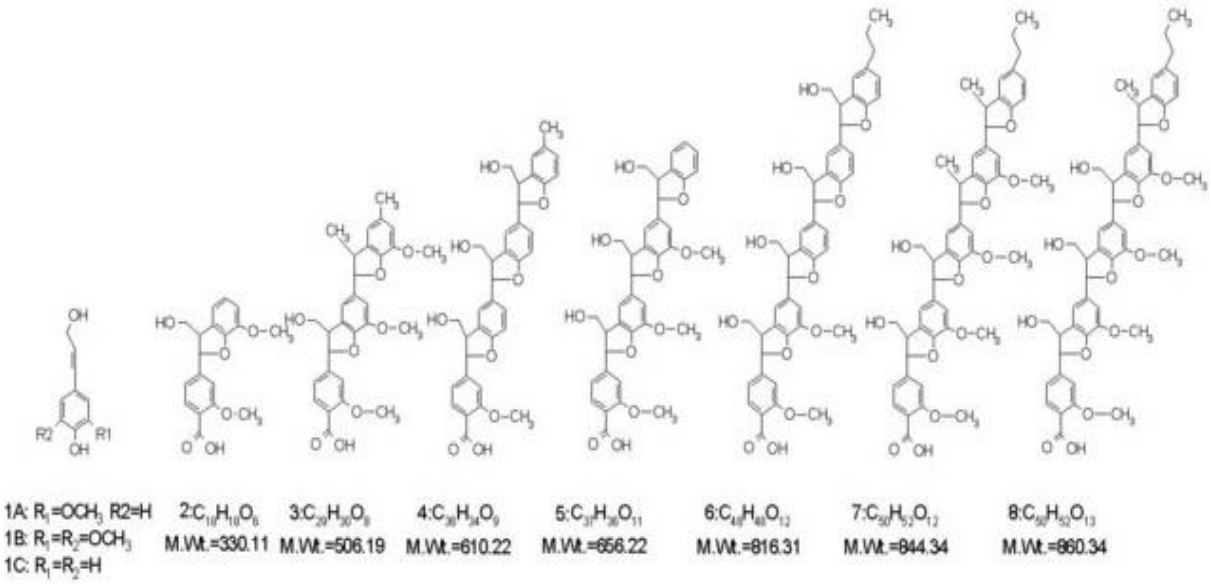

Figure 16: Structure of lignins from different sources as elicited by Banoub and Delmas (2003)

Biologically, lignin provides rigidity to cell wall with the aid of cellulose, acts as a seal against water loss and serves as an effective conduit for water and nutrient uptake by plant cells.

These three polymers – cellulose, hemicellulose and lignin bind together in a huge network to form the cell walls of lignocellulosic biomass as shown in Figure 17.

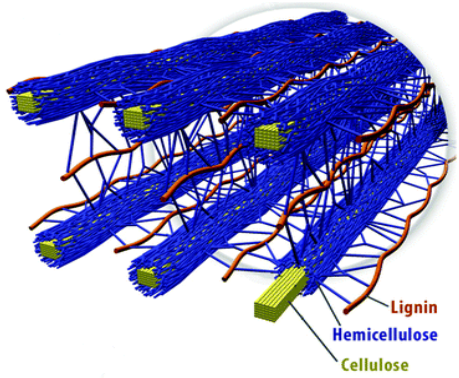

Figure 17: Structure of plant cell wall of lignocellulosic biomass showing interwoven network of cellulose, hemicellulose and lignin [Brandt et al., 2013]

The liquefaction of amorphous cellulose, lignin and hemicellulose occurs fast in the initial stages of liquefaction process due to their amorphous structure while crystalline cellulose undergoes liquefaction at a slower rate and continues till the end of the process due to its less accessibility to the solvent. As crystalline cellulose majorly constitutes the cellulose in lignocellulosic biomass, the conversion of cellulose is the limiting reaction in the liquefaction process [Li et al., 2015]. Figure 18 shows the reaction mechanism of one of the major reactions during acid-catalysed cellulose liquefaction in polyhydric alcohols as solvents [Li et al., 2015].

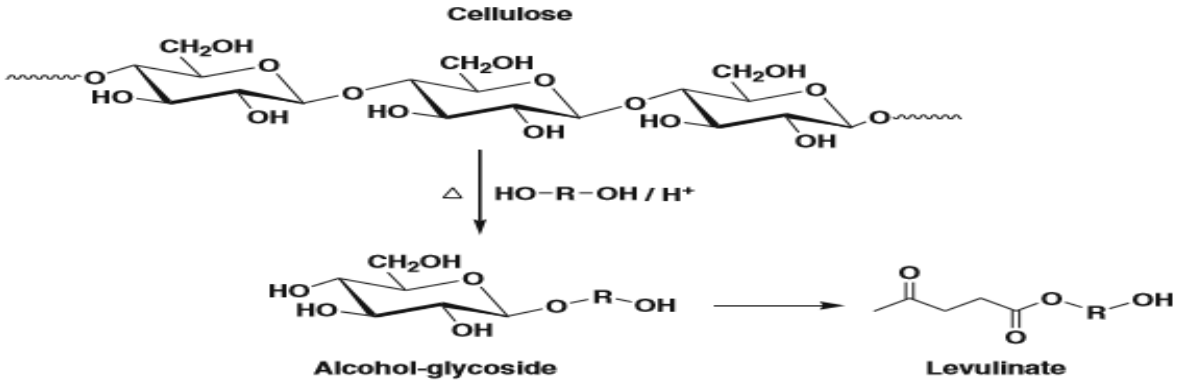

Figure 18: Reaction mechanism of acid-catalysed cellulose liquefaction in polyhydric alcohols [Li et al., 2015]

A large number of simultaneous competing reactions occur during liquefaction of lignocellulosic biomass. Recondensation reactions compete against the liquefaction reactions and decrease the process efficiency by forming more insoluble residues [Li et al., 2015]. Kobayashi et al. (2004) postulated that these recondensation reactions are due to reactions between depolymerized cellulose and degraded aromatic lignin derivatives. The most common way to decrease the menace of recondensation is to optimise the process parameters such as biomass to liquid ratio, solvent used, catalyst used, catalyst quantity, reaction time and temperature [Li et al., 2015].

The liquefaction products vary widely with the type of biomass used and the process parameters. As concluded by Zhang et al. (2007), the liquefied product from acid-catalysed bagasse liquefaction using ethylene glycol was composed of high molecular weight lignin degradation products, phenols, saccharides, alcohols, aldehydes, some acids and their esters while the liquefaction residue contained some lignin derivatives, undissolved cellulose and undissolved lignin.

1.5.1.2. Contemporary developments in biomass liquefaction:

The conversion of biomass to liquids started out with hydrothermal liquefaction processes which are carried out at high temperature and high pressure. To name a few, Pittsburgh Energy Research Centre (PERC) process, Bureau of Mines (BOM) process and Lawrence Berkeley Laboratory (LBL) process belong to this category of hydrothermal liquefaction [Elliott]. In BOM process, comminuted biomass was slurried using tar oil with 20 to 30% biomass in the slurry [Tarelho et al., 2011]. This slurry was then reacted with carbon monoxide and aqueous sodium carbonate in a reactor for 20 to 90 minutes at 300 to 370 °C and at high pressure of 2000 to 4000 psig [Elliott]. LBL process is carried out

under similar conditions as BOM process but the biomass is converted to aqueous slurry by acid hydrolysis without the need for pre-drying and comminution [Elliott]. Some processes use supercritical water or supercritical CO_2 as solvents to liquefy biomass. These hydrothermal liquefaction processes produce complex mixtures of biocrudes and it is an insurmountable task to upgrade and/or refine these crudes to pure chemicals [Zhang et al., 2007]. Also, the operational complexity and expense of these processes are quite high [Zhang et al., 2007]. Hence, mild liquefaction of biomass at low to moderate temperatures and atmospheric pressure is more interesting to convert biomass to liquid with significantly reduced operational complexity and costs [Zhang et al., 2007]. Ting Zhang et al. (2007) studied the sulphuric acid catalysed liquefaction of bagasse in ethylene glycol at 190 °C and atmospheric pressure and found that the process they used has a high potential to produce biofuels and some chemicals from biomass. Many similar liquefaction processes at similar range of temperatures and atmospheric pressure are found in scientific literature. The commonly used solvents are glycerol, ethylene glycol, diethylene glycol, 2-Ethyl hexanol and polyethylene glycol among other polyhydric alcohols [(Hu et al., 2013), (Mateus et al., 2015)]. Most of these processes are carried out at low biomass to solvent ratios of 1:3 to 1:5 [Li et al., 2015].

The solvent used and the lignocellulosic composition of the biomass highly influence the liquefaction efficiency. For instance, sulphuric acid catalysed liquefaction gave liquefaction rates in decreasing order from bagasse, cotton stalks to wheat straw [Li et al., 2015]. Biomass with high lignin and hemicellulose content show greater liquefaction rates due to the ease of accessibility of their amorphous structure by solvents. Using a mixture of 4:1 w/w PEG400 (MW. 400 g/mol) to glycerol as solvent showed high liquefaction efficiencies and decreased occurrence of recondensation reactions [Li et al., 2015]. Besides polyhydric alcohols, Ethylene carbonate and Propylene carbonate are also used as solvents with good efficiency in some cases [Yamada and Ono, 1999]. Hu et al. (2012) studied the use of crude glycerol from biodiesel production as a solvent and concluded that it is a potential alternative for expensive petroleum derived liquefaction solvents that are currently used.

The most common catalyst used in liquefaction processes is concentrated sulphuric acid and the catalyst loading of 1 to 3% sulphuric acid exhibits optimum liquefaction behaviour in most cases. Though there are base catalysed liquefaction reactions, these usually require higher temperatures than acid-catalysed liquefaction [Li et al., 2015]. There are studies about using several other catalysts. For instance, Tang et al. (2017) used 15 w. % of Zn supported on ZSM-5 as catalyst to liquefy oil palm empty fruit bunch. Besides these stand-alone liquefaction processes, there are investigations on ultrasonic, microwave and/or plasma aided liquefaction processes. The studies by Lu et al. (2016) concluded that microwave-ultrasonic assisted liquefaction of woody biomass intensified the heat & mass transfer, significantly reduced the liquefaction time and halved the solvent dosage. Xi et al. (2017) studied the application of plasma electrolysis in sulphuric acid catalysed liquefaction of sawdust using a mixture of PEG200 (MW. 200 g/mol) and glycerol as solvent. It was found that the liquefaction yield reached 99.08% in 5 minutes under optimal biomass to solvent ratio of 1:7 implicating the good potential of plasma electrolysis in fast biomass liquefaction.

Pinewood sawdust is the most studied lignocellulosic biomass in terms of liquefaction though liquefaction of several other biomasses such as cork, potato peels, eucalyptus bark and coffee

grounds have been studied and documented [(Mateus et al., 2016), (Mateus et al., 2017)]. Liquefaction of olive stone was studied by Cuevas et al. (2008) through autohydrolysis - enzymatic hydrolysis pathway and showed good potential for producing bioethanol through this process. However, there is hardly any research on direct solvolytic liquefaction of olive stones. Also, most documented research focus on optimising biomass liquefaction to produce polyurethane foams or to upgrade to bio-oils. Hardly any focus has been placed on investigating liquefaction in the context of a pre-treatment method before combustion in lieu of direct combustion of biomass.

1.5.2. Additives to reduce fine particle emissions:

There are three classes of additives related to combustion [Krause et al., 1977]. Class I additives are fuel-handling additives for improved storage and handling with stabilising agents, anti-icing agents, anti-static compounds and pour-point depressants as examples. Class II additives are combustion additives to improve combustion and reduce pollutants. Class III additives are post flame treatment additives such as soot removers, additives to control slag deposits, additives to enhance particulate collection in ESP, etc. Additives to reduce fine particle emissions belong to class II additives [Krause et al., 1977].

Combustion additives are commonly classified further, based on their chemical composition – specifically, their reactive component, into Calcium additives, Phosphorous additives, Aluminium additives, Aluminium-Silicate additives and Sulphur additives, with the first four possibly applicable for reduction of particle emissions [Bäfver et al., 2011]. Bauxite ore containing aluminium oxide or hydroxide is a prime example of Al-based combustion additives; Calcium carbonate and calcium hydroxide are examples of Ca-based combustion additives; Phosphoric acid, Calcium dihydrogen phosphate and phosphorous rich sewage sludge are examples of P-based combustion additives; Kaolin and bentonite are examples of Aluminium-silicates based additives. Bäfver et al. (2011) opine that Al-Si additives and P-based additives can decrease the PM emissions; Al-based additives are less effective than Al-Si based additives and Ca-based additives may decrease PM emissions from P-rich fuels such as oat grain, while they apparently have no effect on PM emissions from Si-rich fuels such as straw and woody biomass. The effects of additives, obviously, depend on their reactions with the problematic ash forming components during combustion.

As discussed in chapter 1.4.4, K is the main cause of PM in fly ash during combustion of most biomasses. PM emissions are controlled by additives either by chemical adsorption and interaction or by physical adsorption, with former being more common. Despite the complex nature of the reactions between additives and ash components and the seemingly impossible task of controlling their behaviour, there are several studies on the reaction mechanisms of additives with ash from different types of coals, biomasses and oils. Wang et al. (2012) summarize the main reactions between additives and K containing compounds formed during combustion, as shown below.

$Al_2O_3.xSiO_2 + 2\ KCl + H_2O \longrightarrow K_2O.\ Al_2O_3.xSiO_2 + 2\ HCl_{(g)}$ .....Equation (1)

$2\ KCl + H_2O_{(g)} + Al_2O_3 \longrightarrow 2\ KalO_2 + HCl_{(g)}$ .....Equation (2)

$2\ KCl + SiO_2 + H_2O \rightarrow K_2O.SiO_2 + 2\ HCl_{(g)}$ .....Equation (3)

$SO_2 + ½\ O_2 \rightarrow SO_3$ ……..Equation (4)

$(NH_4)_2SO_{4(l)} \rightarrow 2\ NH_{3(g)} + SO_{3(g)} + H_2O_{(g)}$ ……Equation (5)

$Fe_2(SO_4)_{3(l)} \rightarrow 3\ SO_3 + Fe_2O_3$ ……Equation (6)

$Al_2(SO_4)_{3(l)} \rightarrow 3\ SO_3 + Al_2O_3$ ……Equation (7)

$SO_3 + 2\ KCl + H_2O_{(g)} \rightarrow 2\ HCl_{(g)} + K_2SO_4$ ……Equation (8)

$KCl_{(g)} + CaHPO_4.2H_2O \rightarrow CaKPO_4 + 2\ H_2O + HCl_{(g)}$ .....Equation (9)

$K_2O.SiO_2 + 2\ CaCO_3 \rightarrow 2\ CaO.K_2O.SiO_2 + 2\ CO_2$ …….Equation (10)

In summary, PM emissions can be controlled by preventing the reaction of KCl with other ash components and/or capture the fine ash particles before their elutriation. The compounds resulting from the reactions between additive and ash should have a high melting point so as not to create slagging and agglomeration problems during blow down operation. This aspect is analysed by studying the phase diagrams of these compounds. Additives can be added either together with fuels or midway during combustion. When Davidsson et al. (2007) studied the combustion of forestry residues in a CFB boiler, they added kaolin to the particle seal of the boiler and found out that most of the kaolin was elutriated along with flue gas to the ESP indicating that pre-blending of kaolin with biomass could be tried to solve this elutriation problem. There are significantly more studies about additives to reduce slagging and corrosion from coal as well as biomass combustion than about additives to decrease PM emissions. However, there are some studies that address additives for PM emissions worth noting and the results of some of those are described in brief as follows. Höfer et al. (2016) concluded from their studies on additives during wood and straw combustion that the additives Al_2O_3, a blend of 46% Al_2O_3, 44% $CaCO_3$, 10% $CaHPO_4$, and another blend of 46% Al_2O_3, 44% $MgCO_3$,10% $MgHPO_4$ help to bind problematic species and reduce PM emissions. Fournel et al. (2015) studied combustion of reed canary grass blended with 50 w. % wood and 3 w. % fuel additives such as aluminium silicates (sewage sludge), calcium (limestone) and sulfur (lignosulfonate) based additives and found that combustion of these blends resulted in 17%–29% decrease of PM concentrations compared to pure reed canary grass. A report by Boman et al. (2012) indicates that kaolin has a good effect in decreasing PM emissions from combustion of many different types of biomass. Ninomiya et al. (2009) concluded that the use of Ca or Mg-based additives to coal combustion could result in the decrease of $PM_{2.5}$ and PM_1 emissions by improving the coalescence of fine particles. The effects of similar additives on PM from biomass combustion could be studied. There are more combustion additives than the common Al, Al-Si, Ca and P-based additives. For instance, Wiinikka et al. (2009) concluded from their study on straw combustion that the addition of an optimum amount of TiO_2 as additive reduced the vaporization of K by approximately 40 to 50% indicating its great potential in reduction of PM emissions. Besides their effect on combustion, additives are chosen having in mind the criteria such as absence of increased environmental toxicity due to adding it to combustion, stability of resultant compounds at high temperature and overhead cost of using the additives.

1.5.3. Downstream emissions reduction:

Even with state-of-the-art pre-combustion emission control methods, end of the pipe emission reduction is most often, if not always, needed to reach the target limits imposed by legislations. There are several equipment for post combustion particle capture and these can be broadly divided into two categories – wall collection devices and dividing collection devices based on their working principle and governing design equations, which will be explained in more detail in the following chapters [Nevers, 2000]. In all these equipment, the particles get collected by impaction with an obstacle, diffusion through the gas to a collection surface and interaction with other particles, and one or more of these mechanisms can be dominating. Some equipment belonging to the aforementioned categories are explained in brief as follows.

1.5.3.1. Wall collection devices

Wall collection devices capture particles by forcing them towards a wall leading to their agglomeration due to inertial forces acting on them and the particles settle down due to impact with the wall. Gravity settlers, cyclone separators and electrostatic precipitators are examples of these wall collection devices.

Figure 19 shows the schematic of a gravity settler for solids handling.

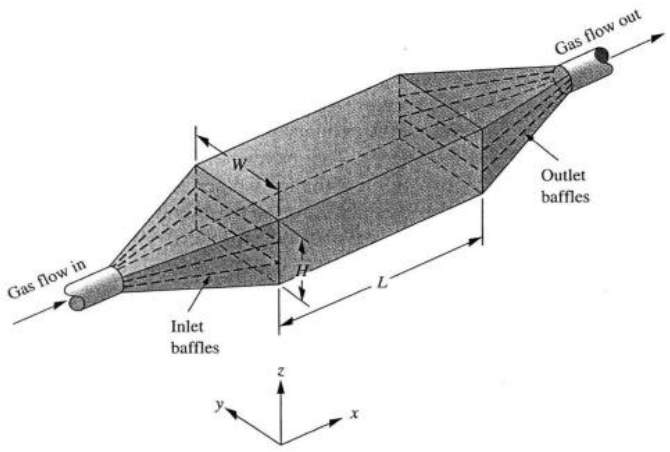

Figure 19: Schematic diagram of a gravity settler [Nevers, 2000]

Gravity settlers are the simplest type of collection devices that collect particles by impaction. The gas laden with particles is passed through one end of the tube and goes out cleaner through the other end. The velocity of gas decreases due to relatively huge volume in the middle compared to the end sections making large particles with high inertia to settle down. Often baffles are employed inside the chambers to equally distribute the flow of gas. Gravity settlers have a poor efficiency and are used only in operations where a very dirty gas with high particle loading has to be cleaned. Gravity settlers are ineffective for fine particles capture. Typically they have a cut diameter, D_{cut} (diameter of the particles removed with an efficiency of 50%) around 50 μm.

Cyclone separators use the same principle of forcing the gas towards a wall but they use the centrifugal force in addition to the gravitational force to cause this effect. The centrifugal force on any given particle inside a cyclone is at least two orders of magnitude greater than the gravitational force on the same particle indicating the cyclone's superiority over gravity settlers.

Torbel designs and sells cyclones and surface filters and so this equipment to control particles emissions will be described with more detail. Figure 20 shows the schematic of a cyclone separator.

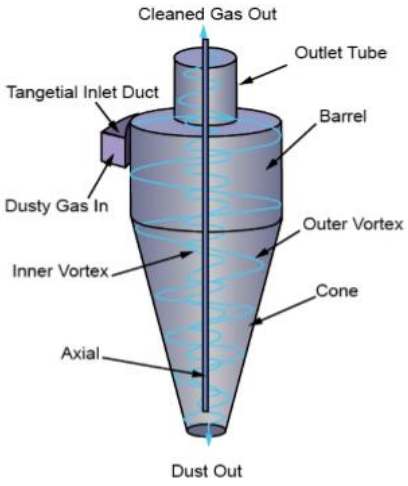

Figure 20: Schematic diagram of a cyclone separator showing the pathway of the gas [NPTEL]

A cyclone consists of a cylindrical body called barrel and a conical bottom called cone which serves as the outlet for the particles collected. The dirty gas enters the cyclone at the top through an inlet tangential to the barrel to make sure that it flows circumferentially near the wall inside the cyclone and not radially. The gas traverses a vortex till the bottom of the cyclone and then rises towards the top forming another vortex. During the outer vortex, the inertia of the particles which have difficulty in following the path of the vortex gives rise to the centrifugal forces acting on them and they hit the wall and fall down to the dust hopper at the bottom of the cyclone and the clean gas goes out through the top. The particles are collected only in the outer vortex formed by the gas and hence the particles which are not captured till then are carried out along with the gas through the inner vortex. There are three common configurations of cyclones based on the direction/position of the gas inlet, as shown in Figure 21.

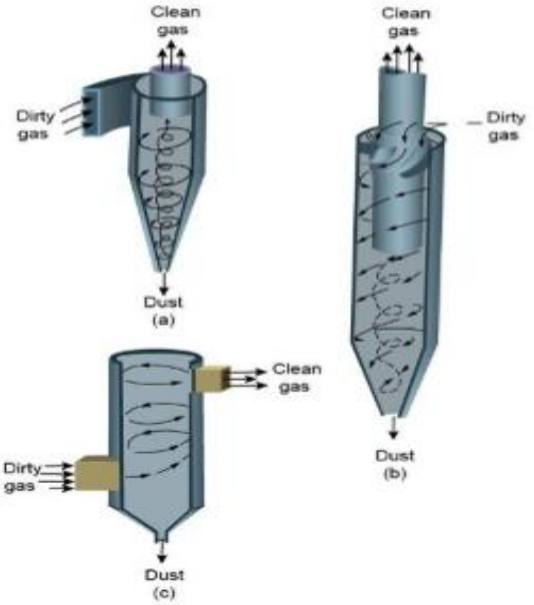

Figure 21: Three configurations of cyclones with gas inlet at different positions [NPTEL]

In Figure 21, (a) shows a cyclone with tangential inlet at the top, which are commonly used for PM capture in thermal power plants and cement industries; (b) shows a cyclone with gas inlet at the top parallel to the axis of cyclone which is often employed in multicyclones with high efficiency; (c) shows a cyclone with gas inlet at the bottom tangential to the axis of the cyclone which design is often used after wet scrubbers to effectively remove small liquid droplets. Cyclones are also categorised as high efficiency, conventional and high throughput cyclones. High efficiency cyclones have a high pressure drop while the high throughput cyclones have a lower pressure drop and high volumetric feed rate but low efficiency. The governing principle and equations are the same for these types but the dimensions of these cyclones vary. Unlike membranes and sieves, there is no fixed particle diameter at which the efficiency of cyclones will turn from 0 to 100. Hence, to define a clear relationship between the efficiency and particle size distribution of the collected solids the cut-diameter is used which is usually given by the Rosin-Rammler equation [55]. The equations for separation efficiency (η), pressure drop (ΔP), and cut diameter (D_{cut}), gas velocity (V_i) are given below [Nevers, 2000].

$$\eta = 1 - e^{-(\frac{\pi N V_c D^2 \rho_p}{9 W_i \mu})} \quad \rightarrow \text{Equation (11)}$$

$$\Delta P = K(\frac{\rho_g V_i^2}{2}) \quad \rightarrow \text{Equation (12)}$$

$$D_{cut} = (\frac{9 W_i \mu}{2\pi N V_c \rho_p})^{1/2} \quad \rightarrow \text{Equation (13)}$$

$$V_i = \frac{Q_i}{A_i} \quad \rightarrow \text{Equation (14)}$$

In the above equations, W_i is the gas inlet width, μ is the viscosity of gas, N is the number of revolutions the gas makes inside the cyclone, V_c is the gas velocity in the duct approaching the cyclone (usually about two-thirds of V_i), V_i is the velocity at the inlet to the cyclone, ρ_p is the particle density, ρ_g is the gas density, D is the cyclone body diameter, and K is a parametric property that has specific values for every cyclone system depending on the types of pipes and fittings used [Nevers, 2000]. For most industrial cyclones K is around 8 [Nevers, 2000]. Noel de Nevers (2000) states that there's no unanimously theoretically sound basis for calculating N and it is to be assumed as 5 for most industrial cyclones. According to Nevers (2000), it's an industrial rule of thumb to consider only cyclones if the size of the gas particles is above 5 μm since common cyclones are not efficient enough for particles below this size. From the aforementioned equations, it can be seen that, in order to increase the efficiency of cyclones for smaller particles, either the gas velocity needs to be increased or the inlet width has to be decreased since it's not possible to directly change the other factors that influence the efficiency. But, increasing the gas velocity will lead to high pressure drop causing increase in energy demand for this suction/blowing fan indicating the importance of optimising the cyclone to strike a balance between efficiency and pressure drop. . Since as shown in the efficiency increases with the decrease of the gas inlet, smaller particles are collected better in cyclones with a small inlet. Therefore, to treat a certain gas flow rate small inlet width cyclones together in arrangements called multicyclones are used as shown in Figure 22. Other than stand-alone and multicyclones, there are other modified designs of cyclones such as electrogasdynamically assisted cyclone systems, which use aerosol-charge carriers to charge fine particles in the gas stream to facilitate their collection inside cyclone due to electrostatic forces between the uncharged cyclone wall and charged particles in addition to the already existing centrifugal and gravitational forces [Kunsagi, 1983].

Figure 22: Multicyclone arrangements in industries [SRC]

Electrostatic precipitators are another alternative. They are more efficient in collecting even smaller particles than cyclones (D_{50} ten times lower) and they work on the same principle of wall collection but they use electrostatic force which is several orders of magnitude stronger than gravitational and centrifugal forces used in gravity settlers and cyclones. Figure 23 shows the schematic of an ESP. A typical ESP consists of parallel plates grounded and high voltage wires as electrodes between any two plates. These wires are connected to a high voltage AC source of about -40 kV to -60 kV. The wires

discharge a negative charge and hence the plates act as positive electrodes. One ESP has several pairs of plates and wires. Every plate and the wire next to it are separated by 4 to 6 inches space.

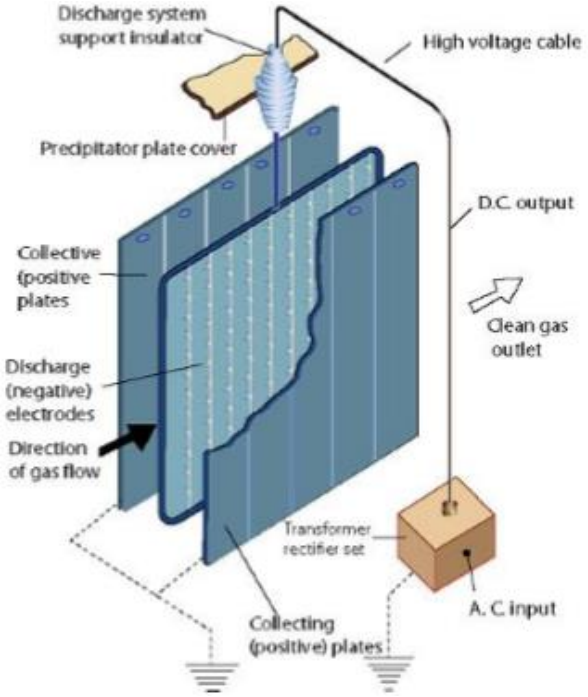

Figure 23: Schematic diagram of an ESP [55]

The gas enters the gap between the plates from the side of ESP through a diffuser and a distribution plate to ensure even distribution inside the ESP and leaves the ESP from the other side through another diffuser to form a narrow outlet stream of clean gas. The high potential difference between the electrodes ionises the incoming gas and causes the particles in the gas to get attracted to the plates and deposit on them. Solid cake deposited on the plates is removed by rapping the plates at regular time intervals using a device called a rapper which strikes a blow to the edge of the plates using mechanical or electromechanical means. During rapping, some particles from the plates are entrained back causing a decrease in efficiency. ESP is more efficient on particles with medium resistivity in the range of 10^7 mho to 2 x 10^7 mho [Nevers, 2000]. Lower resistivity of particles causes them to quickly lose charge on contacting the plate causing a low potential in the cake and makes it difficult for more particles to collect on the plate. This causes more particles to entrain. Higher resistivity particles cause a high potential gradient inside the cake and lower the potential near the wires causing an ineffective corona discharge at the wires. This also causes a back corona discharge inside the cake causing explosive entrainment of particles back to the gas. This problem can be alleviated to some extent by treating the gas at a higher temperature due to the decrease in resistivity of particles with increase in temperature. Due to this aspect, the sulphur content influences the collection efficiency with higher sulphur content resulting in higher collection efficiencies. However, above a certain limit of sulphur problems arise due to high resistivity. The ESP can either be single stage or two stages ESP. In single stage ESP both charging and collection are done at the same place whereas in two stages ESP charging and particle collection are done in two separate chambers. The collection efficiency of an ESP can be as high as 99%.

1.5.3.2. Dividing collection devices:

The dividing collection devices divide the flowing gas into several small flows to collect the particles. Filters and scrubbers are the prime examples of dividing collection devices. Filters can either be surface filters or depth filters. Surface filters collect the particles larger than the pore size of the filters and these collect particles only on their surfaces. Depth filters do not have a fixed pore size and they collect particles throughout them and not only on their surfaces. The particles collect on the surface of the surface filters and form a cake of particles on the filter. Then, the particles are further collected by the top layer of this cake and not by the filter. Hence, the cake grows bigger with time as shown in Figure 24.

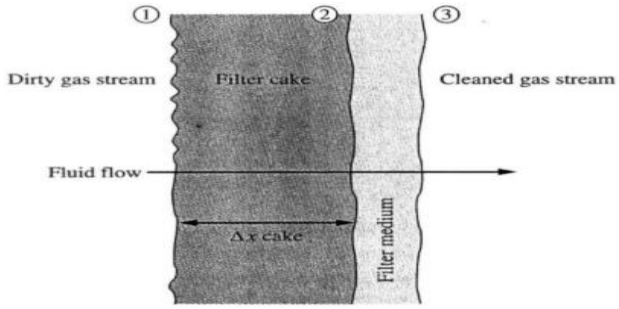

Figure 24: Flow through a surface filter showing formation of cake of particles [Nevers, 2000]

Due to collection of more particles on the cake layer, the pressure drop increases to a non-optimal value when cleaning of the filter becomes necessary. The cleaning is done by several ways such as shaking, passing a reverse jet of air, and passing a pulse-jet of air. The velocity of the gas flowing through filter is usually low and hence the laminar flow equations are the governing design equations.

The depth filters do not have a single uniform pore size. Instead, they have a plethora of randomly oriented fibres which collect particles. When the gas flows, it has to bend around these fibres and this makes the particles with high inertia unable to follow the trajectory of the gas and get attached to these fibres by electrostatic or Van der Waal's forces. The design of these filters is governed by Langmuir and Blodgett equations [Nevers, 2000]. Though these filters are used in small scale applications such as house chimneys, these are rarely used in post-combustion gas cleaning in industries. Hence, the depth filters will not be discussed further in detail due to their impertinence to large scale PM control in industries. The most commonly used design of surface filters in industries is the baghouse filter which is as shown in Figure 25.

Figure 25: Industrial baghouse filter [IAC]

Several design considerations need to be kept in mind while designing a baghouse filter. For instance, the gas inlet and particle discharge outlet should be situated on the opposite sides at the bottom else the incoming gas will entrain the collected particles. Likewise, situating the clean gas outlet at the top on the same side of the gas inlet at the bottom will cause channelling of the gas through the first few compartments due to powerful suction and hence, these should be located on opposite sides. The filter medium can be made of different materials such as cotton, wool, Dacron, Teflon, polypropylene, fibre glass, etc., depending on requirements such as temperature resistance, acid and/or alkali resistance and resistance to abrasion. The baghouses can have overall collection efficiency as high as 99.99%.

Scrubbers are devices which separate the incoming gas into smaller flows by means of an atomized spray of a liquid which washes out the particles from the gas. Scrubbers can collect particles sized as low as 0.5 µm. A scrubber has many components in one device as described by Noel de Nevers (2000) and a block diagram of these components is shown below in Figure 26.

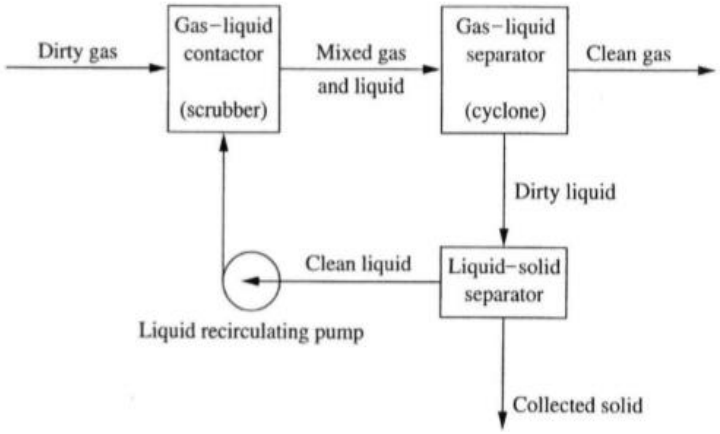

Figure 26: Block flow diagram of the components of a scrubber [Nevers, 2000]

The dirty gas is contacted with a liquid in the gas-liquid contactor where fine particles cling on to the liquid droplets. Then, the gas and liquid are separated in a gas-liquid separator which is similar in arrangement and working to a cyclone separator. Then the particles are separated from the liquid using a solid-liquid separator and the clean liquid is recirculated back to the scrubber. The scrubbers are commonly classified into co-current, counter-current and cross-current scrubbers based on the direction of flow of the liquid and the gas. The liquid and gas flow in the same direction in co-current scrubbers; opposite directions in counter-current scrubbers, and; in perpendicular directions in cross-current scrubbers. The cross-current and counter-current scrubbers have poor efficiencies while the design of co-current scrubbers can be modified to have high efficiencies [Nevers, 2000]. Based on the design, there are many types of scrubbers such as orifice, venturi, jet and dynamic scrubbers [NPETL]. Noel de Nevers (2000) opines that the venturi scrubber with co-current flow is the most economical to be used in industries. A venturi scrubber with co-current flow is as shown in Figure 27.

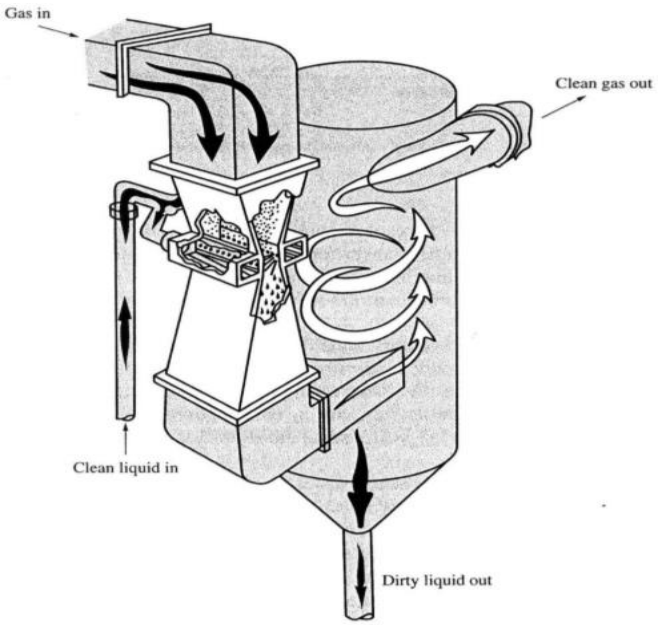

Figure 27: Schematic diagram of a venturi scrubber with co-current flow [Nevers, 2000]

Another type of scrubbers known as dry scrubbers is also used in industries. They work using the same principle as the wet scrubbers but instead of using a liquid, they use dry reagents which react with the incoming fluid to remove the target substance. However, these are used commonly in removing a harmful gas from a gaseous mixture and not in PM removal and are almost impertinent to removing fine particles from flue gases.

Collection devices are chosen based on several factors that combine to form the portfolio of specific industrial requirements. For example, adhesive particles are collected using wet scrubbers, wet-ESP or hydrocyclones but not using dry equipment; particles with low electrical resistivity cannot be collected using ESP and so, a cyclone or a scrubber has to be used; particles which have higher cohesion than adhesion can be collected easily using a bag house filter; non-adhesive particles of above 5 µm can be effectively collected using a cyclone; and scrubbers are best avoided for large flow rates since it ensues high pumping costs [Nevers, 2000]. Other than the technical parameters, if and when there's a chance to choose one or more equipment, a cost to benefit analysis is done for different possible portfolios of equipment to choose the best option.

1.5.4. Design and simulation of cyclone separators using Aspen Plus:

As mentioned in chapter 1.5.3.1, the cyclones can be categorised as high efficiency, conventional and high throughput cyclones based on their dimensions. There are several configurations of cyclones based on their dimensions. In the field of cyclone design, all cyclone dimensions are commonly normalized as a factor of the barrel diameter (D) of the cyclone as shown in Figure 28. The widely known configurations are Stairmand, Swift-High, Swift-General, Shepherd & Lapple and Peterson & Whitby cyclones [UF]. The normalized dimensions of these cyclones are as shown in Table 8. Here, in Figure 28, K_a, K_b, K_s, K_B, K_H, K_h, K_{D_e} are normalising factors for the respective parameters which are described in Table 8.

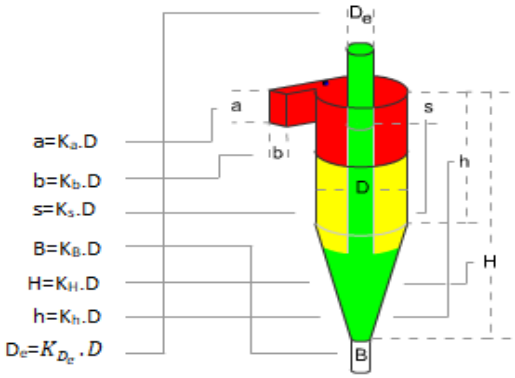

Figure 28: Normalised dimensions of a typical cyclone separator [UF]

Table 8: Normalised dimensions of common cyclone configurations [UF]

Symbol	Description	High efficiency		Conventional	High throughput	
		Stairmand	Swift-High	Shepherd & Lapple	Swift-General	Peterson & Whitby
a	Inlet height	0.5D	0.44D	0.5D	0.5D	0.583D
b	Inlet width	0.2D	0.21D	0.25D	0.25D	0.208D
s	Outlet length	0.5D	0.5D	0.625D	0.6D	0.583D
B	Dust outlet diameter	0.2D	0.21D	0.25D	0.25D	0.208D
H	Overall height	4D	3.9D	4D	3.75D	3.17D
h	Cylinder height	1.5D	1.4D	2D	1.75D	1.33D
D_e	Gas outlet diameter	0.5D	0.4D	0.5D	0.5D	0.5D

Pressure drop in a cyclone is an important parameter that is considered during the design. Pressure drop can be calculated fairly accurately using Stairmand's equation, as shown below, but it represents the pressure drop due to clean gas without particle loading and hence correction factor has to be applied for depending on the cyclone design [NPTEL].

$$\Delta P = \frac{\rho_g}{203}\{V_i^2\left[1 + 2\emptyset^2\left(\frac{2r_t}{r_e} - 1\right)\right] + 2V_o^2\} \quad \rightarrow \text{Equation (15)}$$

In the above equation, ρ_g is the gas density, V_i is the velocity of the gas at cyclone inlet, V_o is the velocity of the gas at cyclone gas outlet, r_t is the radius of circle to which the centre line of the inlet is

tangential, r_e is the radius of the cyclone gas outlet, and ϕ is cyclone pressure drop factor which is given by Equation (6) shown below [NPTEL].

$$\phi = f_c(^{A_s}/_{A_i}) \rightarrow \text{Equation (16)}$$

In the above equation, A_i is the area of cyclone inlet, and A_s is the surface area of cyclone that is exposed to the spinning gas inside the cyclone. Since, it is highly complex to theoretically compute A_s, it is taken to be equal to the surface area of an equivalent cylinder with same diameter as the cyclone body diameter and same height as the overall height of the cyclone [NPTEL].

As explained before, the collection efficiency of a cyclone is influenced by several parameters such as particle size, density, velocity of the gas, pressure drop in the cyclone, cyclone dimensions, surface characteristics of the material of the cyclone, particle loading in the gas, number of revolutions of the gas inside the cyclone, gas viscosity, leakage of air into the cyclone along with the gas, etc. In summary, the collection efficiency can be defined as a function of incoming gas properties, particle characteristics and cyclone design. There is no unified method of performing the design calculations for a cyclone separator and it is possible to use several approaches to explain the cyclone design calculations. Every method has its own merits and demerits depending on the process parameters and the cyclone design for which it is applied to. Some of these methods are modelled based on experimental results and some of these are derived theoretically based completely on empirical concepts. The most practical method is Muschelknautz method [Elsayed, 2011]. Besides theoretical methods, calculations can be performed on a case by case basis using numerical modelling and/or CFD software for more accurate results [Elsayed, 2011].

The simulation and/or design of cyclones to suit the needs of a specific process plant can be easily performed using a process simulation software package such as Aspen Plus, Chemcad, etc. The results from the simulation runs in Aspen can be exported to Microsoft Excel for further interpretation and presentation of results. In this thesis, Aspen Plus V8.4 is used for this purpose. Aspen Plus is a software package created by Aspen Tech to design, simulate and optimise process models to efficiently design and operate process plants. Simulation and design of cyclones and other end of pipe PM capture equipment can be done using the solids handling block of Aspen Plus. Aspen Plus provides two modes of solid handling which are design and simulation. Aspen Plus is versatile to a large extent and has a lot of simulation features. The pertinent steps involved are explained in brief as follows.

In simulation mode, the performance of a cyclone with known dimensions at predefined parameters can be evaluated whereas in design mode, Aspen Plus gives the design parameters of cyclone/multicyclone depending on the input conditions and required performance. The main steps in using Aspen solids handling by cyclones are setup, flowsheet, streams, blocks, and results. Setup is where the user can input the data regarding the unit system to be used, materials to be used in process streams, their properties, etc. Flowsheet is the core part where the process flow diagram is drawn. In the streams, the user has to define the materials, properties and process conditions of all the input and output streams. In blocks, the process parameters pertinent to all the process equipment

involved and the calculation method to be used are established. Then the simulation is run to get the results.

Aspen Plus contains several calculation methods for cyclone separators, namely, Muschelknautz, Leith-Licht, Shepherd & Lapple, modified Leith-Licht, Dietz, Mothes & Loffler and user-specified method. The design equations used by some of these methods are explained in brief as follows.

Leith-Licht model works under the assumptions that the gas flow is intermediate to free and forced vortex flow, the trajectories of gas inside the cyclone are circles, particle-gas slip velocity is only radial, Stoke's law, plug-flow and mixed-flow models govern the radial force on a particle and the particles have negligible radial acceleration [Clift et al., 1991]. Leith-Licht model gives the fractional efficiency (η_i) of a cyclone using the following equation [NPTEL]

$$\eta_i = 1 - \exp\left[-2(C\psi)^{\frac{1}{2n+2}}\right] \rightarrow \text{Equation (17)}$$

Here, C is the cyclone dimension factor which is a function of cyclone dimensions, n is the vortex component which is a function of cyclone barrel diameter and temperature, and ψ is the impaction parameter which is given by the equation:

$$\psi = \frac{\rho_p d_p^2 v_i}{18\mu D_c}(n+1) \rightarrow \text{Equation (18)}$$

Here, the product of ρ_p and v_i gives the initial momentum of the particle and D_c is the cut diameter.

Muschelknautz model is based on the main assumption that the pressure loss inside the cyclone is caused by wall friction and irreversible losses in the vortex with the latter dominating the former in most cases [Elsayed, 2011]. This model gives the cut diameter of a cyclone using the following expression.

$$D_c = \sqrt{\frac{9\mu(0.9Q)}{\pi(\rho_p - \rho_g)v_\theta^2(H_t - S)}} \rightarrow \text{Equation (19)}$$

Here, Q is the volumetric gas flow rate, ρ_g is the gas density, ρ_p is the particle density, v_θ is the tangential velocity of the gas, H_t is the overall height of cyclone and S is the length of vortex finder of the cyclone.

According to Dietz model, a cyclone comprises three regions – entrance, downflow and core [Dirgo and Leith, 1985]. The entrance region is the space around the gas outlet at the top; downflow is the region of vortex; and the core is the region formed from extension of the gas outlet to the bottom of cyclone. Dietz model assumes that the radial concentration profile of uncollected particles in each of these regions, created by turbulence, is uniform; and the exchange of particles between downflow and core regions exists [Dirgo and Leith, 1985].

The collection efficiency of cyclone is given by this model as a function of three parameters K_0, K_1, and K_2 which are functions of cyclone dimensions, particle properties and gas properties. These are expressed using following equations [Dirgo and Leith, 1985].

$K_0 = 0.5(1+\beta)$; $K_1 = 0.5(1-\beta)$; $K_2 = (D_e/D)^{2n}$ → Equation (20)

$$\beta = \left(\frac{D_e}{D}\right)^{2n}\left(1 + \frac{9\mu ab}{\pi\rho_p l d^2 v_i}\right) \quad \rightarrow \text{Equation (21)}$$

$$\eta = 1 - [K_0 - (K_1^2 + K_2^2)^{0.5}]exp\left[\frac{-\pi(2S-a)\rho_p d^2 v_i}{18\mu ab}\right] \quad \rightarrow \text{Equation (22)}$$

In the above equations, a is the cyclone inlet height, b is the cyclone inlet width, D is the cyclone barrel diameter, D_e is the gas outlet diameter, d is the particle diameter, v_i is the gas inlet velocity, S is the length of gas outlet, and l is the total height of cyclone.

2. Materials and Methods

2.1. Liquefaction

The biomass needed for liquefaction experiments – pinewood, olive stone, olive bagasse, and grape seeds were provided by Torbel whereas rice husk was procured from another source by Dr. Margarida Mateus. The pinewood here was the waste from forestry products; olive stones are the broken pits of olive fruits left after a second extraction of oil; olive bagasse is the same as olive stone but it contained fine powders from broken olive stones in addition to the olive stones itself; and grape seeds were the seeds left over from grapes after extraction and separation of the pulp in wineries. Except pinewood, all these other biomasses were used with the same size as received, in liquefaction experiments. Pinewood chips from Torbel were too big to be used in liquefaction and so, it was grinded to a particle size below 6 mm. Photographs of these biomasses are shown below in Figure 29.

Figure 29: Biomass raw materials: Top:- From left to right – Pinewood, olive stone, and olive bagasse all as received; Bottom:- From left to right – Pinewood grinded to below 6 mm, grape seeds, and rice husk as received.

In most of the liquefaction experiments, the solvent used was either 2-Ethyl hexanol (2EH) or a 1:1 w./w. mixture of 2EH and Diethylene Glycol (DEG) [this mixture is hereafter referred to as 'DEEH']. The catalyst used in all liquefaction experiments was p-Toluene Sulfonic acid (pTSA). In some experiments, Hydroquinone (HQ) was used as a stabilizer to test its effectiveness in preventing the occurrence of repolymerisation reactions. The sources of these reagents are as follows:

Acetone – LabChem, 99.6% purity; DEG – Resiquimica, p.a. grade (>99%); pTSOH – Resiquimica, reagent grade (98%); and 2EH – Sigma-Aldrich, food grade (>99%).

All the liquefaction experiments were carried out at 160 °C and ambient pressure. The procedure for this purpose was based on previous pinewood liquefaction studies at IST [Braz, 2015]. The catalyst quantity needed for pinewood liquefaction was calculated as 3% of the organic content of pinewood for the initial liquefaction experiments and then it was optimised in order to have a high biomass to solvent ratio closer to 1:1. Then, this optimised value was used as a basis for other liquefaction experiments and it was optimised further. For rice husk, 0.2:1 biomass/solvent was used as it has low density, in order to ensure that there was enough solvent for good stirring of the reaction mixture. Unless mentioned otherwise, the catalyst quantity is always mentioned in terms of weight percentage of total biomass feed, throughout this thesis. The biomass to be used in liquefaction experiment was

pre-treated by placing in a bag and spraying it with the solvent, enough to wet the biomass and then the biomass was placed in an oven at 80 °C for at least 30 minutes. This was done to soak the biomass with solvent and to reduce the thermal shock on the biomass when adding it to the reactor. Before some liquefaction experiments, the moisture from biomass was removed by heating it to 120 °C in an oven and keeping it at that temperature overnight. The account of these details for all the liquefaction experiments carried out is mentioned in Chapter 3.2. The experimental setup used for liquefaction is shown below in Figure 30.

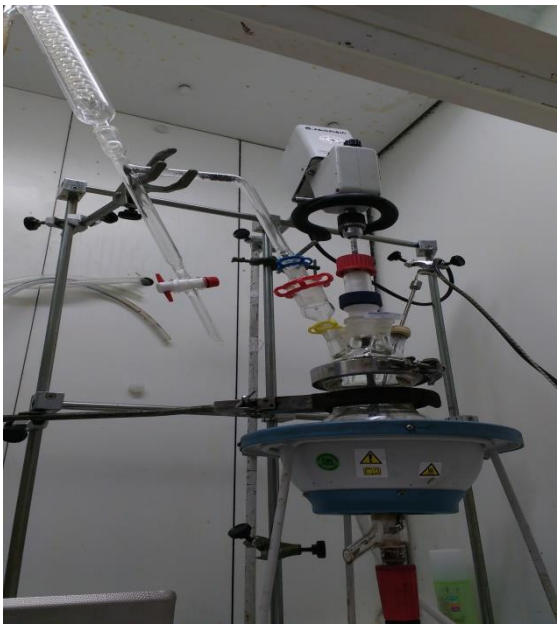

Figure 30: Experimental setup for liquefaction

This setup consists of a reactor with a bottom valve, mounted in a heating mantle supported by a tripod. The top end of the reactor was closed using a lid with 3 narrow and 1 wide inlet. One narrow inlet was used to insert a temperature sensor which was connected to a digital thermostat, into the reactor; the second narrow inlet was connected to a condenser through a dean stark. A metallic mesh was inserted into the neck of the dean stark to promote phase separation of the evaporated solvent and water mixture passing to the condenser. The third narrow inlet was used to feed the biomass into the reactor. The wide inlet was used to insert a stirrer into the reactor, which was driven by an electric motor. All the joints in this setup were hermetically sealed using high-temperature resistant grease. To start an experiment, a measured quantity of solvent was added to the reactor, the thermostat was set to 80 °C and the stirrer was switched on and set at a speed of around 180 rpm. When the temperature reached 80 °C, the pre-treated biomass was added to the reactor and the temperature in thermostat was set to 160 °C. When the reactor contents reach 160 °C, the measured quantity of catalyst was added to the reactor and the reaction timer was set to begin. After the planned reaction time, the heating and stirring are switched off and the contents of the reactor were allowed to cool down to ambient temperature. Then, one of the following two methods were used to separate the liquid from the solids. The first method was to simply separate the solids and liquid by filtration and then wash the solid residues using acetone to recuperate any bio-oil left; the filtrate was then distilled to remove the

acetone and then added back to the bio-oil obtained. The second method was to add acetone to the entire reaction contents, mix them up and then filter, separate the solids, and distil the filtrate to remove acetone and obtain the bio-oil. Using the second method, it was possible to remove finer solids from the bio-oils, which will be explained further in detail in Chapter 3.2. The solid residues obtained were heated to 80 °C to remove any acetone left and then cooled down in a desiccator before weighing. This weight was used to calculate the conversion of biomass in liquefaction experiments using the following formula.

$$\%\ Conversion = \left(\frac{Weight\ of\ biomass\ before\ liquefaction - Weight\ of\ residues\ obtained}{Weight\ of\ biomass\ before\ liquefaction}\right) * 100$$

2.2. Preliminary tests of additives to decrease fine particle emissions

In order to decrease the fine particles emission from biomass combustion, several additives are planned to be tested in a drop tube furnace at IST. For this purpose, the additives need to be screened initially. The additives selected for this initial screening phase were PentaErythritol Tetra Ester (hereafter referred to as 'TORR'), Kaolin, and TiO_2. TORR was selected due to its neopentane structure with ester chains on four end carbon atoms, which facilitates its use in multiple industrial applications such as lubricants, polymer cross-linking agents, etc. Hence, it was tested to determine if the four ester groups could trap smaller ash particles within its neopentane backbone. These additives were provided by a researcher from the research group 'CERENA' at IST. In order to test these additives, the biomass and additives were blended in a ball-mill for 15 minutes at 400 rpm. Two experiments were performed to test these blends. The first one was calcination in an oven (details described in Chapter 2.3.). The second experiment was preliminary lab-scale combustion to simulate a combustion environment as shown in Figure 31. In these tests, biomasses and biomass-additive blends (with 3% and 6% additives with respect to total biomass) were combusted in the presence of a Particulate Matter (PM) meter with the capability of measuring concentration of particle size as low as 1 µm. The apparatus used for this purpose was DUSTTRAK-II-Aerosol-Monitor-8530 and it operates by laser scattering to provide concentration values of different fractions. In these preliminary tests, the assembly shown in Figure 31 was used, in which the suction line was placed in the path of the flue gas released in the combustion, as visible. It should be noted that in the treatment of results, the background values and the values influenced by the flame of the torch used to ignite the biomass were discounted.

Figure 31: Experimental setup used for preliminary combustion tests of biomass-additives blends.

2.3. Characterisation techniques

The biomass feedstock used in liquefaction experiments, and preliminary combustion tests, the bio-oils and solid residues from liquefactions were characterised using Scanning Electron Microscopy (SEM), Energy Dispersive Spectroscopy (EDS), Calorimetry, Thermogravimetric analysis (TGA), Differential Thermogravimetric analysis (DTG), Calcination and Mid-Infrared Fourier Transform Infrared Spectroscopy (FTIR). Concerning calcination, the following programme was used. The samples were calcinated by heating from ambient temperature to 400 °C in 2 hours; then maintained at 400 °C for 3 hours; then heated up to 1000 °C in 3 hours; and finally maintained at 1000 °C for 3 hours. The calcinated samples were weighed after cooling down to ambient temperature from 1000 °C. The specifications of the characterisation equipment are as follows:

- **FTIR:** PerkinElmer, Spectrum Two, mid-Infrared spectrometer equipped with a Pike Technologies MIRacle® Attenuated Total Reflectance (ATR) accessory.
- **SEM-EDS:** Analytical FEG-SEM:JEOL 7001F with Oxford light elements EDS detector (point and area analysis)
- **Calorimetry:** LECO AC500 analyser.
- **Elemental analysis:** The chemical composition data concerning carbon, hydrogen, and nitrogen were obtained via elemental analysis using an LECO TruSpec CHN analyser instrument while for sulphur, the determination was carried out in an LECO CNS2000.
- **TGA:** NESTZSCH model STA 449 F5, Jupiter Deckel Al2O3 Ø7mm Crucibles, 85µl and respective covers Deckel Pt / Rh 80/20 Ø7mm, 85µl Crucibles and Lids, Type III nitrogen with a purity of 99.999%
- **Calcination:** Nabertherm P330 oven with temperature range of 30 to 3000 °C.

3. Results and discussion

3.1. Characterisation of biomass feedstock

The biomass feedstock used in liquefaction experiments, and preliminary combustion tests were characterised using Scanning Electron Microscopy (SEM), Energy Dispersive Spectroscopy (EDS), Calorimetry, Thermogravimetric analysis (TGA), Differential Thermogravimetric analysis (DTG), Calcination and Mid-Infrared Fourier Transform Infrared Spectroscopy (FTIR). Olive bagasse, olive stone, grape seeds, and rice husk are mostly homogeneous in appearance. Pinewood is inhomogeneous on both microscopic and macroscopic levels. This can be seen from the photograph and SEM images of pinewood as shown in Figure 32 and Figure 33.

Figure 32: Inhomogeneity of pinewood on macroscopic level: Photograph

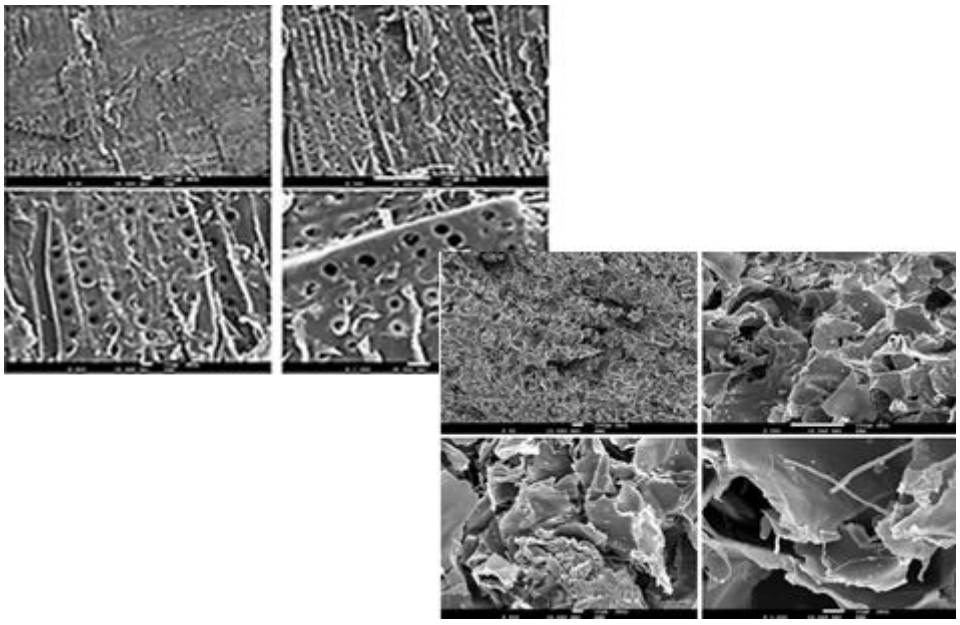

Figure 33: Inhomogeneity of pinewood on microscopic level: Different SEM images (left and right) of two random pinewood pieces, at same magnifications; Magnification in both left and right images are 50x, 250x, 500x, and 1000x from top left in counter-clockwise direction

The elemental composition and gross calorific values (GCV) of the biomass are tabulated in Table 9.

Table 9: Elemental composition and gross calorific value of biomass feedstock

Biomass / Component	Pinewood	Olive stone	Olive bagasse	Grape seeds	Rice husk
Carbon[*§]	51.00	50.20	50.40	53	34.87[£]
Hydrogen[*§]	5.84	5.82	6.02	5.78	4.23[£]
Nitrogen[*§]	<1.26	<1.26	<1.26	1.7	<0.5[£]
Sulphur[*§]	<0.11	<0.11	<0.11	<0.11	<2[£]
Moisture[§]	10.50	18.10	20.60	11.3	7.80
Ash[§]	0.30	0.82	2.15	2.64	15.11
GCV (J/g)	20150	20370	21180	21170	14200[#]

*** dry basis, § weight %, # [CFN], £ dry ash free basis**

It can be seen that the carbon content, hydrogen content, and GCV of the aforementioned biomass feedstock are closer to each other except rice husk which has significantly low carbon content leading to a lower GCV. All these biomass have low sulphur and nitrogen content. Olive stone and olive bagasse have high moisture content whereas rice husk has the lowest moisture content. Pinewood has the lowest ash content; olive stone ranks one position above the lowest; olive bagasse and grape seeds have similar ash content and; rice husk has the highest as content which is almost 15 times that of pinewood. This high ash of rice husk is due to the high Si content which can be seen from EDS results of the calcinated rice husk, as shown in Figure 34, in comparison to the EDS of calcinated pinewood, olive stone, and olive bagasse. This high Si content creates huge vitrification and agglomeration problems in direct combustion making it worthwhile to explore the feasibility of its liquefaction to produce a liquid fuel from rice husk with decreased ash content. On the other hand, olive stone and olive bagasse have high K content; and pinewood has high Ca content. Ca and K are known to be among the major precursors for formation of aerosols [Obernberger]. As discussed in the chapter ‘Materials and Methods’, olive stone and olive bagasse are essentially the same material with the only difference that olive bagasse contains both olive stones and fine powder from comminution of olive stones. However, they have a big difference in inorganic content. This may be due to the inhomogeneous distribution of inorganic components throughout the structure of olive stone before comminution and the inhomogeneous distribution of these inorganic components between crushed and uncrushed olive stones post comminution.

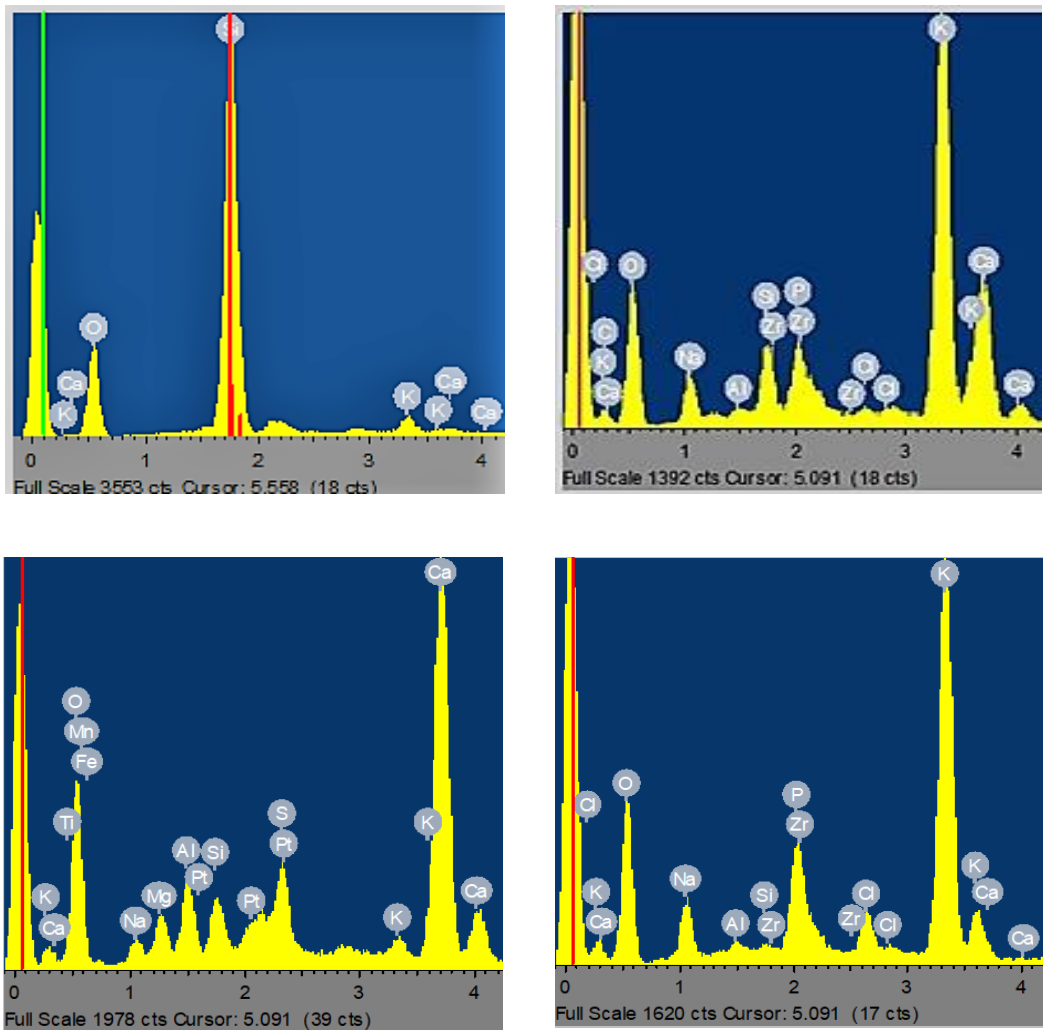

Figure 34: EDS of calcinated rice husk, calcinated olive stone, calcinated olive bagasse, and calcinated pinewood (starting from top-left in clockwise direction)

Figure 35 presents the TGA and DTG analyses of pinewood and olive stone between 0 and 600ºC. The TGA curves present the remaining weight as a function of the temperature whereas the DTG curves present the rate of fractional conversion. After the peak at temperatures below 100ºC due to the moisture loss, the DTG curve for pinewood shows that its decomposition occurs between 150 ºC and 600ºC with two small peaks at 150ºC and 500ºC and with a large decomposition peak at 350ºC. Olive stone decomposes between 200 and 600ºC with and important peak at 300ºC slightly below the decomposition peak of pinewood. According to Jin et al. (2012), the peak temperature for cellulose decomposition occurs in the temperature range of 300 °C to 400 °C with a large decomposition peak at 340 °C; hemicellulose gets decomposed in the temperature range of 150 °C to 400 °C with a large decomposition peak at 200 °C; and the degradation of lignin occurred in the temperature range of 100 °C to 700 °C with a small degradation peak at 340 °C. It is worth noting that depending on the crystallinity of the samples, the decomposition peaks can vary significantly.

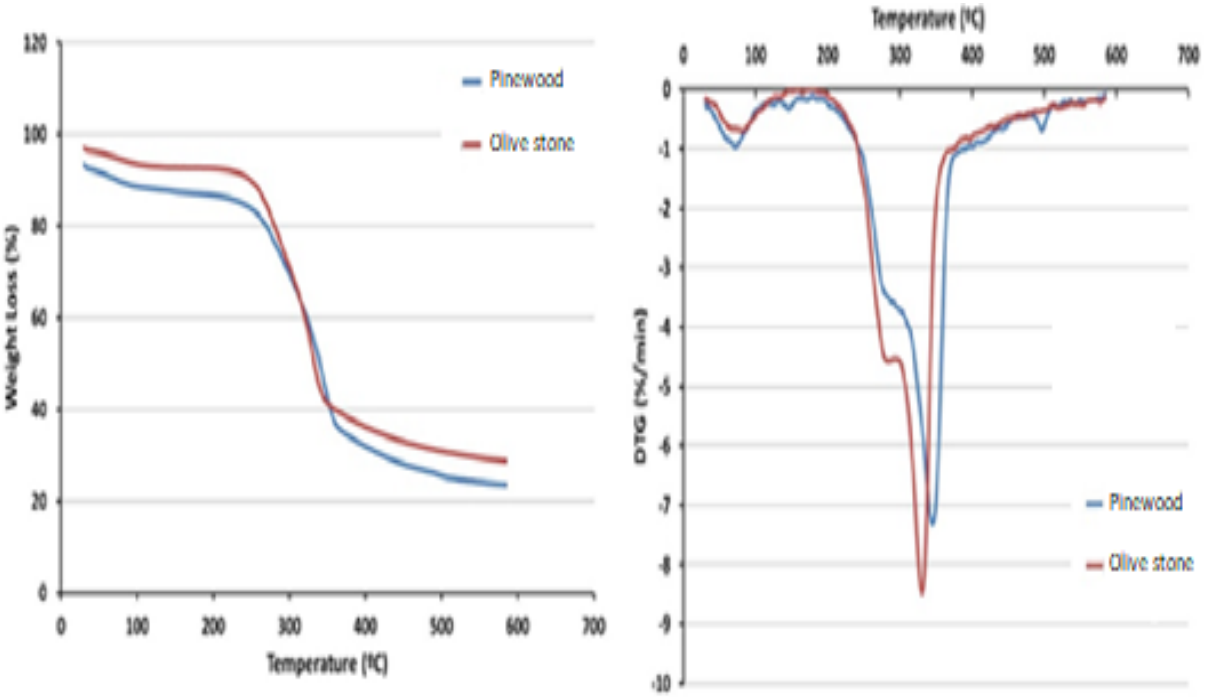

Figure 35: TGA (left) and DTG (left) analyses of pinewood and olive stone

Figure 36 presents the FTIR spectra of the biomass feedstock which can be analysed to interpret the functional groups present indicated by the characteristic absorption peaks as tabulated in Table 10 [(Zou et al., 2009 cited by Braz, A., 2015), (Sills & Gossett, 2011), (Adapa et al., 2011)].

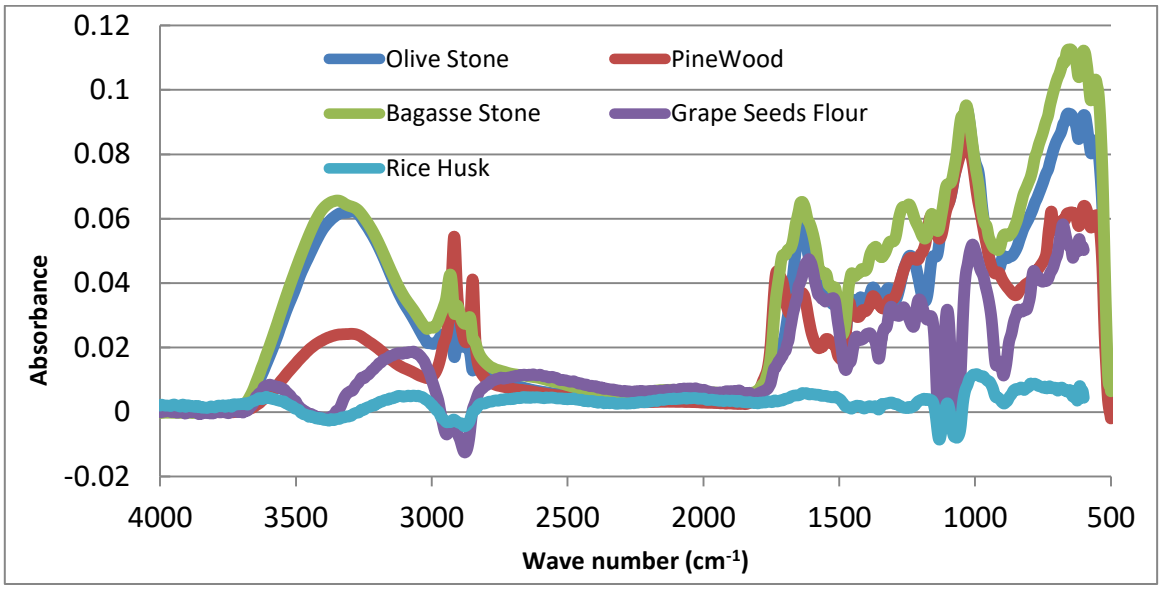

Figure 36: FTIR spectra of biomass feedstock

Table 10: Characteristic FTIR absorption bands of specific functional groups

Wave number (cm^{-1})	Functional grupos
3700-3200	O-H stretching indicating hydroxyl groups from lignin
3000-2800	C-H stretching corresponding to lignin
1730	Carbonyl C=O stretching indicating ketones and aldehydes from hemicellulose
1600, 1500	Aromatic ring vibration corresponding to lignin
1470-1430	C-O stretching in $O-CH_3$
1234	C-O-C stretching of the aromatic alkyl groups
1157	C-O-C asymmetrical stretching corresponding to cellulose, and hemicellulose
1057	C-O stretching could indicate β(1-3) polysaccharides from lignin
1033	C-O, C=C, C-C-O stretching of cellulose, hemicellulose, and lignin
930	Glycosidic linkage of cellulose and hemicellulose
875	Glycosidic linkage of hemicellulose

As seen in Figure 36, all the spectra exhibit peaks at the similar wavelengths but with different heights. Actually, the spectra have the typical bands of cellulosic biomasses such as at 3200 - 3500 cm^{-1} due to the stretching vibration of hydroxyl groups [Zou, et al., 2009], at 2800-3000 cm^{-1} which corresponds to the C-H stretching [(Grilc et al., 2015), (Bui et al., 2015)], the peaks at 1510-1600 cm^{-1} that may be related to the lignin's aromatic rings stretching [(Chen & Lu, 2009), (Zou, et al., 2009)] and at 1000-1200 cm^{-1} due to C-O stretching of the cellulose [(Zhang et al., 2012), (Bui et al., 2015)].

3.2. Liquefaction experiments

The reaction conditions and the obtained conversions for the experiments carried out are tabulated as follows in Table 11.

Table 11: Reaction conditions and conversions for liquefaction experiments

No.	Biomass	Solvent	Biomass to Solvent	Stages	Reaction time (hours)	HQ (%)	Catalyst (%)	Conversion (%)	Remarks
1	PW	2EH	1.0	1	3.00	0.0	5.6	54	**1**
2	PW	2EH	1.0	1	3.00	1.0	5.6	48	**1**
3	PW	2EH	1.0	1	3.00	5.0	5.6	26	**1**
4	PW	2EH	1.0	1	5.00	0.0	5.6	77	**2**
5	PW	2EH	1.0	1	5.00	1.0	5.6	67	**2**
6	PW	2EH	1.0	1	5.00	0.0	5.6	51	**1**
7	PW	2EH	0.7	6	24.25	0.0	5.6	72	**2**
8	OS	2EH	1.0	1	4.00	0.0	6.0	58	**1**
9	OS	2EH	1.0	1	4.00	0.0	4.5	57	**1**
10	OS	2EH	1.0	1	4.00	0.0	3.0	42	**1**
11	OS	DEEH	1.0	1	4.00	0.0	4.5	56	**1**
12	OS	2EH	1.0	1	8.00	0.0	4.5	51	**1**
13	OS	2EH	1.0	1	4.00	0.0	4.5	49	**1, 4**
14	OS	2EH	1.6	8	6.40	0.0	4.5	37	**1, 3, 5**
15	OS	2EH	1.6	8	6.40	0.0	4.5	31	**1**
16	OS	2EH	1.2	8	22.00	0.0	4.5	79	**2,3**
17	OS	2EH	0.7	1	3.00	0.8	4.5	61	**2,3**
18	OS	2EH	1.6	1	6.00	0.7	4.5	31	**2,3**
19	OS	2EH	0.8	1	3.00	0.0	4.5	69	**2,3**
20	OB	2EH	1.0	1	1.00	0.0	4.5	19	**1**
21	OB	2EH	1.0	1	2.00	0.0	4.5	29	**1**
22	OB	2EH	1.0	1	3.00	0.0	4.5	22	**1**
23	OB	2EH	1.0	1	4.00	0.0	4.5	25	**1**
24	GS	2EH	1.0	1	3.75	0.0	4.5	8	**1**
25	GS	2EH	1.0	1	6.00	0.0	4.5	7	**1, 3**
26	RH	2EH	0.2	1	5.00	0.0	4.5	58	**1**
27	RH	**6**	0.2	1	5.00	0.0	4.5	23	**1**

1 Acetone extraction of liquefied to facilitate the separation of the unreacted biomass from the bio-oil, 2 No acetone extraction of liquefied, 3 Moisture of biomass removed before liquefaction, 4 Scaled up reaction with 1500g:1500g B/S, 5 Half of catalyst added in 1st stage and remaining in 5th stage, 6 Liquefied product from no. 26

It is worth noting that the results presented in Table 11 clearly indicate that when the liquefied products were washed with acetone to extract the organic fraction and to improve the separation of the solids, it leads to the increase of amount of residue obtained, thus lowering the conversion.
The SEM images of pinewood and olive stone before and after liquefaction, as shown in Figure 37 and Figure 38, are visual indicators of the degradation of the biomasses during liquefaction.

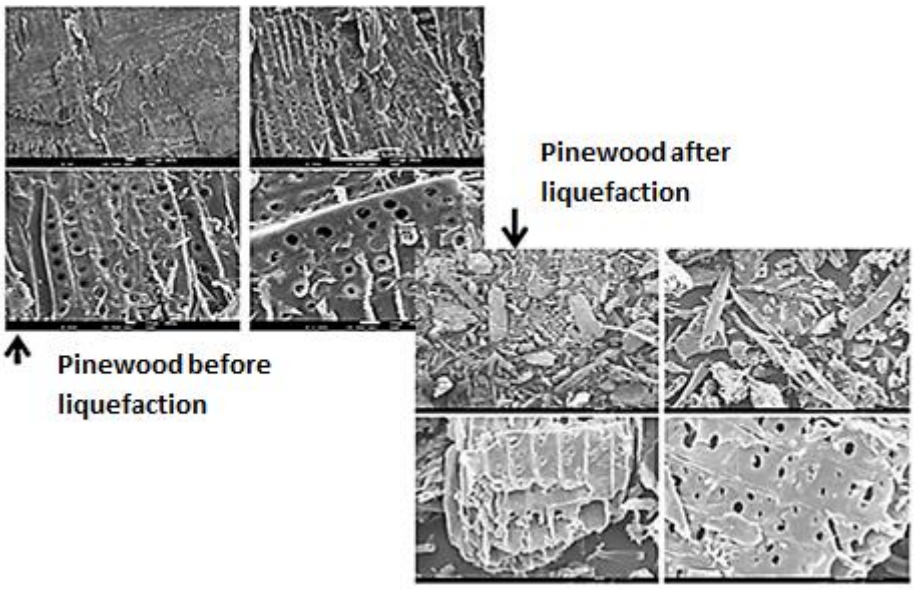

Figure 37: SEM images of pinewood before (left) and after liquefaction (right); Magnification in both left and right images are 50x, 250x, 500x, and 1000x from top left in counter-clockwise direction; Conditions: 0.7:1 B/S, 6 stages, 5.6% catalyst, 24.25 hours reaction time.

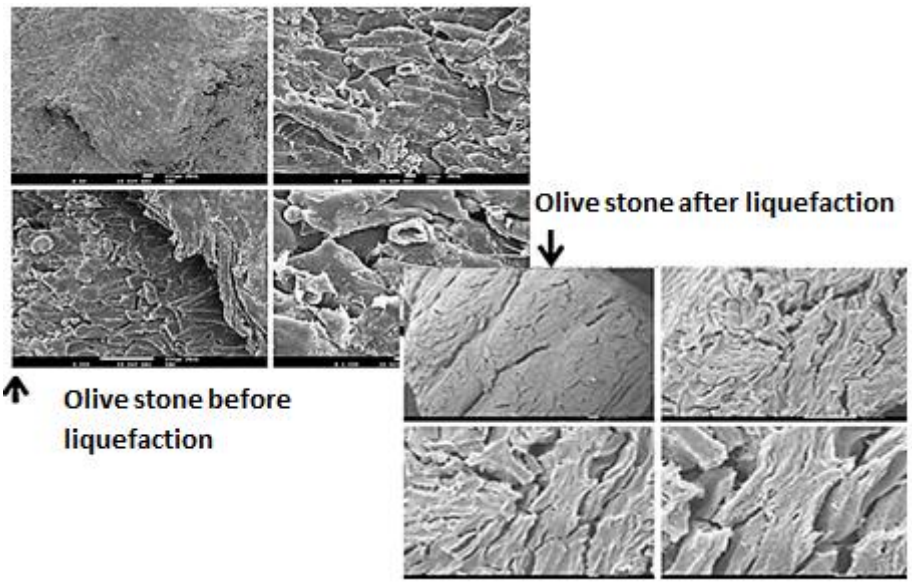

Figure 38: SEM images of pinewood before (left) and after liquefaction (right); Magnification in both left and right images are 50x, 250x, 500x, and 1000x from top left in counter-clockwise direction; Conditions: 0.8:1 B/S, 4.5% catalyst, 3 hours reaction time.

3.2.1. Effect of multi-staged reactions on conversion and viscosity of bio-oils

Having in mind the economic viability of scaling up the biomass liquefaction to an industrial scale, it is crucial to use high values of the biomass to solvent ratio. However, it is also necessary to have a certain minimum amount of liquid in the reactor to ensure the continuation of reaction, proper stirring of the reaction mixture, and prevention of bio-oils from becoming too viscous. Therefore, in some of the experiments the addition of the biomass was carried out in several stages to increase the biomass to solvent ratio as much as possible (experiment numbers 7, 14, 15, and 16 in Table 3.2.-1). Figure 39 presents the conversion results of multi-staged experiments in comparison to those of single stage experiments.

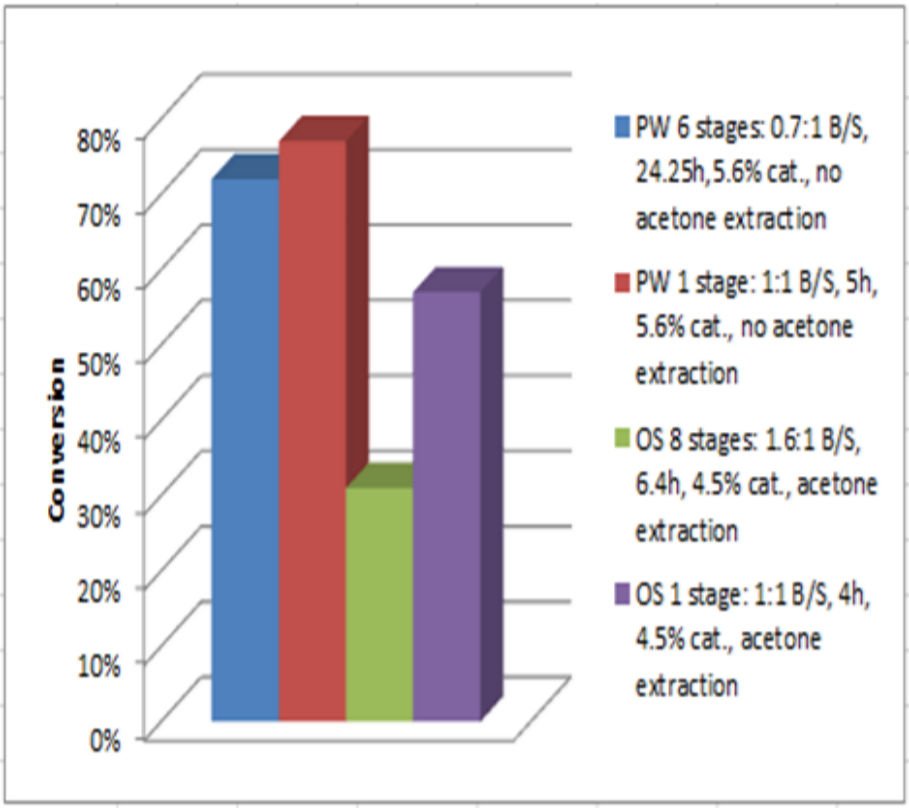

Figure 39: Conversion of liquefaction experiments in several vs. single stages

However, carrying out liquefaction in incremental stages takes more time to produce similar conversions as that of single stage reactions and if carried out with less reaction time, the conversion is much lower than that of single stage reactions.

The viscosities of liquefied products, at 25 °C, from different stages of liquefaction were measured for experiment 7 and experiment 16. However, the viscosity for 5th stage product of reaction 7 was not measured as the product was too viscous to collect through the reactor outlet. These results are shown in Figure 40. It can be seen from this figure that the viscosity of liquefied products increased with the increase in number of stages, which was slow till third stage for pinewood and fifth stage for olive stone. After these stages, the increase in viscosity is rapid. This augment of viscosity may be due to the occurrence of re-polymerisation reactions and/or due to more solids getting suspended in the

liquid. However, viscosity of the final liquefaction products from these experiments after washing with acetone to remove, as completely as possible, the solids from bio-oils, was around 0.3 P between 25 to 50 °C and decreased below 0.1 P above 50 °C. The viscosity of these bio-oils is comparable to that of Heavy gas oil from North Sea light crude (0.07 P at 99 °C) and that of Heavy gas oil from the Alaskan North slope crude (0.13 P at 37 °C) [ABS, 1984] These heavy gas oils are used as liquid fuel in many thermal power plants in the USA, Canada, and many European countries [ABS, 1984]. It can be inferred from these data that the viscosities of these bio-oils are in the suitable range for industrial applications.

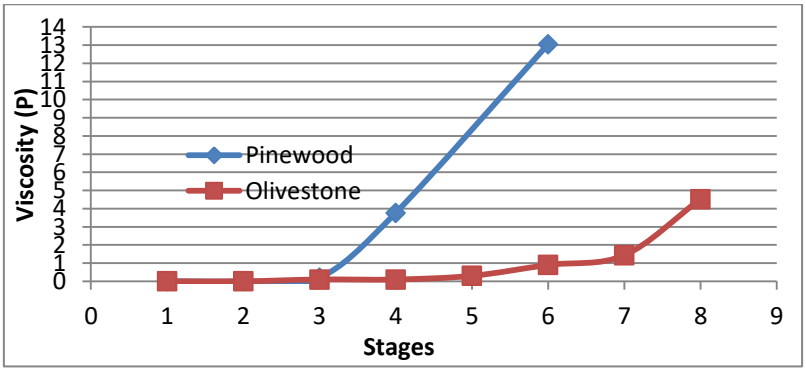

Figure 40: Viscosity of liquefied products from pinewood and olive stone at different stages of reaction; Conditions: PW – 0.72:1 B/S, 24.25 hours reaction time, 5.58% catalyst (total biomass basis), OS – 1.19:1 B/S, 22 hours reaction time, 4.5% catalyst (total biomass basis)

The observed increase of viscosity during the liquefaction reaction and/or during storage of the bio-oils may be due to the occurrence of re-polymerisation reactions. Therefore, the effect of the addition of hydroquinone (HQ) was studied based on a hypothesis that this compound can hinder these reactions by acting as a radical scavenger, thus stabilizing the polymerization initiators.

3.2.2. Effect of HQ on conversion

The following Figure 41 shows the relationship between pinewood liquefaction conversion and the quantity of the stabilizer hydroquinone added.

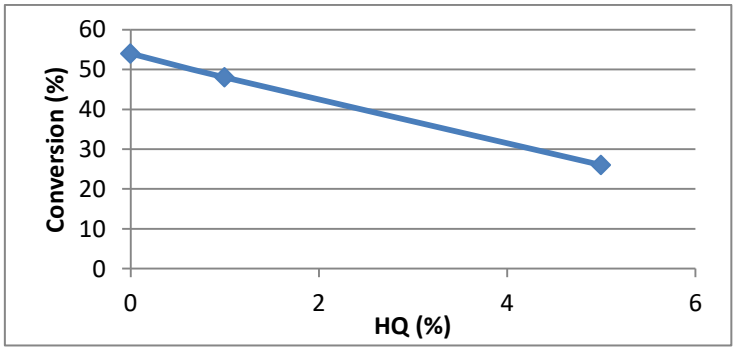

Figure 41: Effect of HQ quantity on conversion of pinewood liquefaction; Conditions: 1:1 B/S, 5.6% catalyst (total biomass basis), 3 hours reaction time

It can be inferred from Figure 41 that the conversion decreases almost linearly with the increase in HQ used in the reaction irrespective of the reaction time. From experiments 17 and 19, it can be seen that the conversion drops with increase in use of HQ for olive stone liquefaction, though it must be noted that these reactions have different biomass to solvent ratios (0.7 and 0.8). It can be concluded that using HQ as a stabiliser for liquefaction considerably decreases the conversion.

3.2.3. Effect of catalyst concentration on conversion

As mentioned in the chapter 'Materials and Methods', the catalyst quantity of 3% by weight of the organic content of the biomass was used initially to carry out liquefaction experiments, based on previous studies conducted on pinewood liquefaction. However, for pinewood liquefaction, the use of catalyst in any quantity less than 5% of the organic content of pinewood (which is 5.6% of the total biomass) always led to a conversion less than 10%, irrespective of other reaction parameters such as reaction time and biomass/solvent ratio. However, since no reactions were carried out using a catalyst concentration higher than 5.6% the optimum catalyst amount could be equal to or more than 5.6% of the biomass fed. Also, it must be emphasized that increase in catalyst quantity leads to increase in cost of liquefaction. Concerning olive stone liquefaction, catalyst quantities below 2.4% of the organic content of olive stone (3% of the total biomass) led to incredibly low conversions independent of other reaction parameters. The conversion increased steeply from 3% catalyst to 4.5% catalyst, after which it plateaued. This is illustrated in Figure 42.

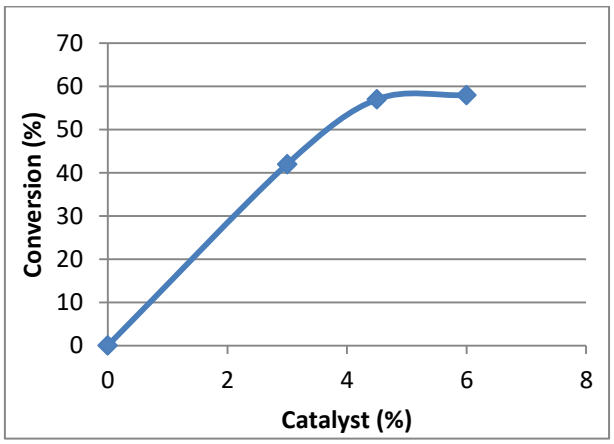

Figure 42: Conversion of olive stone liquefaction at different catalyst quantities; Conditions: 1:1 B/S, 4 hours reaction time.

Also, when olive stone liquefaction was scaled up from 50g:50g of biomass/solvent to 1500g:1500g biomass/solvent, with 4.5% catalyst, it resulted in 49% conversion, around 8% less than that of its smaller scale counterpart, which is not much of a loss for a scaled up reaction. Hence, the optimum amount of catalyst for olive stone liquefaction is 4.5% of the biomass fed. From reaction 11, it can be seen that using DEEH as solvent gives a conversion similar to that of using 2EH as solvent, with same values for all other parameters. The same 4.5% catalyst was used for liquefaction experiments of grape seeds and rice husk.

3.2.4. Effect of reaction time on conversion

The reaction time is an important variable and previous results have shown that increasing the time does not necessary lead to a higher conversion [Braz, A., 2015]. In fact, for example, an increase in the reaction time can favour the re-polymerisation reaction. Hence, this variable was studied. For pinewood, the optimum reaction time was found to be between 3 and 5 hours whereas it was 4 hours for olive stone. The conversion vs. reaction time for olive bagasse shown in Figure 43 indicates that the conversion increases with time and above 2 hours, the conversion values are in the same range. The conversion is almost half of that obtained for pinewood and olive stone liquefactions. Hence, olive bagasse liquefaction has to be optimized further by changing biomass/solvent ratio and catalyst quantity.

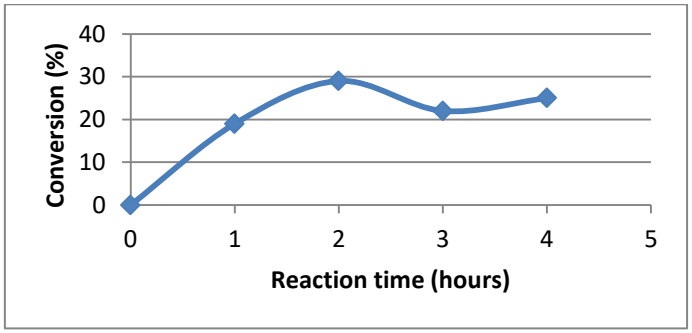

Figure 43: Conversion vs. Reaction time for olive bagasse liquefaction
Conditions: 1:1 B/S, 4.5% catalyst (total biomass basis)

3.2.5. Effect of Biomass to Solvent ratio on conversion

As explained in chapter 3.2.1, the quantity of catalyst and reaction time of liquefaction reactions were optimised while trying to maintain a high biomass to solvent ratio. No firm conclusions can be derived from the obtained results, as to the effect of biomass to solvent ratio on conversion of pinewood and olive stone liquefaction. However, it can be inferred from rice husk liquefaction results that lower biomass to solvent ratio (5 times lower) had to be used to obtain conversions similar to that of pinewood and olive stone liquefaction. Also, using the same biomass to solvent ratio (1:1) for olive bagasse gives significantly lower conversions while it is almost negligible for grape seeds. This could be due to the higher inorganic content of olive bagasse and grape seeds compared to that of pinewood and olive stone. From these results, it can be hypothesised that it is necessary to decrease biomass to solvent ratio for biomass with high inorganic content, in order to achieve higher conversions.

3.2.6. Behaviour of different biomasses

Liquefaction of olive bagasse exhibited much lower conversion than pinewood and olive stone liquefaction as discussed earlier. Liquefaction of grape seeds with 4.5% catalyst and 1:1 biomass/solvent ratio led to a low conversion of 8% irrespective of increasing the reaction time till 6 hours. Also, concerning rice husk, the conversion was 58%, with 0.2:1 biomass/solvent ratio, 5 hours reaction time and 4.5% catalyst. When the liquefied product from this reaction was used as solvent in another reaction with same reaction parameters, the conversion dropped to 23%. So, the overall conversion for an overall biomass/solvent ratio of 0.4:1 and overall reaction time of 10 hours was 40%. Notwithstanding the fact that the elemental compositions of olive bagasse and grape seeds are not so different from olive stone and pinewood, it must also be taken into account that olive bagasse and grape seeds have inorganic content more than twice that of pinewood and olive stone whereas rice husk has about 15 times more inorganic content than pinewood and olive stone. Considering these aspects, the liquefactions of these biomasses need to be investigated and optimised further by changing biomass/solvent ratio, catalyst quantity, and reaction time.

3.2.7. Calorific value of bio-oils

In order to estimate the calorific value of bio-oils from different biomass, representative samples were made by mixing products from different experiments in proportions as tabulated in Table 12, due to inadequate quantity of any one sample. Table 12 gives the gross calorific values of liquefied products in comparison to that of some common fuels [(NPL), (Oliveira, 2013)].

Table 12: Calorific values of liquefied products in comparison to some common fuels

No.	Biomass	Sample description	Gross calorific value of samples (J/g)	Gross calorific value of common fuels (J/g)
C1	PW	Liquefied products from experiments 7 and 1, 0.94:1	35295	**Biodiesel** 39000-41000
C2	OS	Liquefied products from experiments 8 and 9, 0.98:1	35550	**Ethanol** 30000
C3	GS	Liquefied products from experiments 24 and 25, 0.88:1	22805	**Anthracite(4%H_2O)** 36000
C4	RH	Liquefied product from experiment 27	38375	**Heavy fuel oil** 43000

The GCV of bio-oils are significantly higher than that of their biomass feedstock. Also, the GCV of bio-oils from PW, OS and RH are higher than that of Ethanol and comparable to that of anthracite with 4% water while these are lower than the GCV of biodiesel and heavy fuel oil. It may be hypothesised that the high GCV of C1 and C2 may be suspected to be due to high amounts of unreacted solvent since their GCV are closer to GCV of 2EH [BASF]. But, the lower GCV of C3 which had insignificantly low conversion and consequently high amounts of unreacted 2EH disproves this hypothesis.

3.2.8. Composition of bio-oils

The elemental analyses of the bio-oils C1 to C4 are presented below in Table 13.

Table 13: Elemental analyses of liquefied products C1, C2, C3, C4

Component	C1	C2	C3	C4
Carbon[*§]	68.13	70.385	69.6	70.335
Hydrogen[*§]	11.15	11.05	12.45	12.5
Nitrogen[*§]	<0.89	<0.83	<0.89	<0.84
Sulphur[*§]	<0.33	<0.36	<0.3	<0.32
Moisture[§]	2	0.9	1.8	0.5

***on dry basis, [§]weight %**

Comparing with the results presented in Table 9, the higher carbon and hydrogen content of the bio-oils from PW and OS can indicate that the bio-oils are better fuels than their feedstock. However, it must be taken into account that a part of this increase may be due to contribution of some carbon and hydrogen from the solvent. FTIR spectroscopy was performed for the bio-oils from different biomass feedstock. These FTIR spectra are shown in Figure 44.

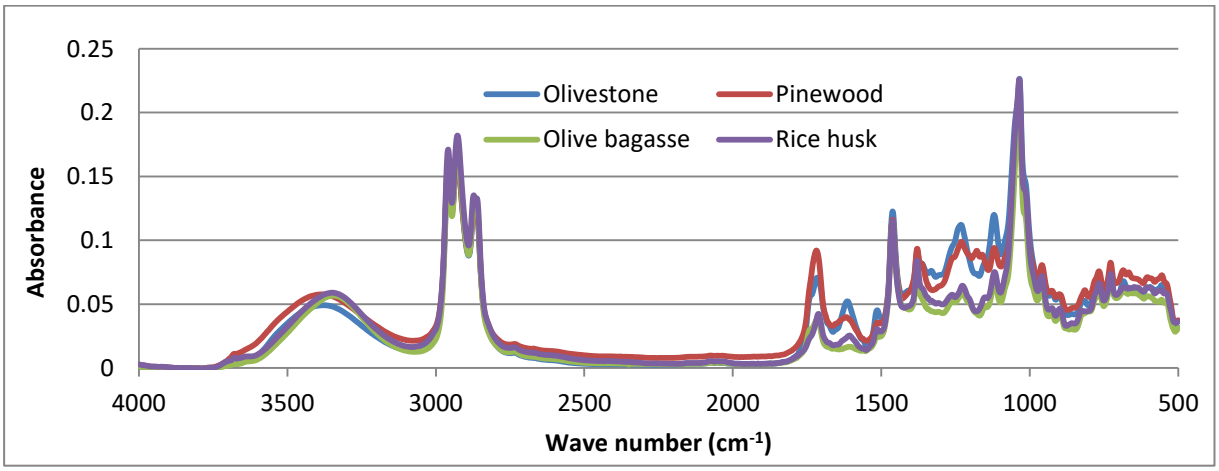

Figure 44: FTIR spectra of liquefied products from OS, PW, OB, and RH; Conditions: OS – 1:1 B/S, 4 hours reaction time, 4.5% catalyst (total biomass basis), OB - 1:1 B/S, 3 hours reaction time, 4.5% catalyst (total biomass basis), PW - 1:1 B/S, 5 hours reaction time, 5.6% catalyst (total biomass basis), RH - 0.2:1 B/S, 5 hours reaction time, 4.5% catalyst (total biomass basis)

Though FTIR analysis of liquefied products is not as pertinent as measurements such as viscosity, calorific value, inorganic content, and proximate analysis, to using liquefied products in direct industrial combustion, the following qualitative inferences from the above FTIR spectra could be useful in further research in optimising the liquefaction reactions to produce specific chemical products. The peak at 3422 cm^{-1} is the characteristic O-H stretch indicating the presence of alcohol groups. However, it must be taken into account that this also includes the alcohol groups from the unreacted solvent since it was not removed before the measurement of these spectra. The peak in the characteristic C-H stretching region from 2800 to 3000 cm^{-1} indicates the presence of aromatic groups, a part of which maybe due to the catalyst. The spectral region with the C=O stretching peak at 1730 cm^{-1} indicates the presence of aldehyde and ketone groups. The peak at 1466 cm^{-1} indicates the presence of compounds formed by C-H deformation of lignin. The absence of any prominent peak in the region 875 to 930 cm^{-1} which is the characteristic of glycosidic linkages of cellulose, hemicellulose, and lignin indicates that the breakage of glycosidic bonds between the monomeric units of the biomasses is complete. Further analysis using FTIR or other methods such as GC-MS is needed to firmly substantiate any more claims as to the qualitative and quantitative analysis of the liquefied products.

3.2.9. Analysis of liquefaction residues

The amount and composition of the inorganic fraction of the bio-oils is also an important issue. Therefore, the ash content of residues from different bio-oils was measured in order to determine the ash content that is still left in the bio-oils. But, neither the composition of the ash content of the residues nor the bio-oils have been determined yet. Table 14 presents the inorganic content of liquefaction residues from some reactions.

Table 14: Inorganic content of liquefaction residues

Reaction number	Biomass feed	Inorganic content of liquefaction residue (%)
1	PW	0.50
4	PW	0.42
6	PW	0.44
7	PW	0.54
8	OS	1.53
9	OS	1.63
10	OS	1.17
11	OS	0.68
13*	OS	0.87
13$	OS	0.83
13§	OS	1.25
13#	OS	0.93
26	RH	24.93
27	RH	22.71

***,$,§ - Fractions with particle size: >1000 µm, 100-1000 µm, and between 5 & 100 µm respectively. # - Total residue with overall particle size > 5 µm**

From Table 14, it can be concluded that liquefaction helps in decreasing the inorganic content of biomass by a considerably high extent. It was calculated that 72% of the inorganic content of pinewood feed was found in the residue while the remaining 28% was in the liquefied product; for olive stone, this share was 60% in residue and 40% in liquefied product; and for rice husk, this was 70% in residue and 30% in liquefied product. From the data for reaction 11 in this table, it can be inferred that using 2EH as solvent is far more effective in removing the inorganic content of the biomass. Also, the inorganic content of fine particles fraction is far more than that of the other fractions from reaction 13. Hence, it is worthwhile removing this fraction from the liquefied product by washing it with acetone. The remaining inorganic content in the liquefied products may be due to two reasons: the inorganic particles are less than 5 to 13 µm in size and/or they are trapped between bigger polymeric compounds in the liquefied product. If this smaller particle size is the sole reason, then it should be possible to produce a liquefied product that is completely free of inorganic content by methods such as ultra-filtration although it finally boils down to economic feasibility of such filtration processes. As for the inorganic particles that could be trapped between the polymeric components, ultrasonic agitation combined with solvent extraction could be a plausible solution.

3.3. Preliminary tests on the use of additives to decrease fine particles emission

To evaluate the effect of different additives on the inorganic content present after calcination of olive stone and pinewood, several tests were carried out according to the procedure described in Chapter 2 that led to the results shown in Table 15. However, these results were inconclusive and indicate that this is not the ideal method to analyse the effect of these additives on the amount of ash produced from biomass combustion. The TGA of the biomasses with and without additives will have to be carried out to plan further experiments.

Table 15: Calcination of biomass with and without additives

Sample	Additive	Additive content	Inorganic content (%)
OS	-	-	0.815
OS	Kaolin	3	2.98
OS	TiO_2	3	3.13
OS	TORR	3	0.72
OS	TiO_2	6	4.75
OS	TORR	6	0.45
PW	-	-	0.30
PW	Kaolin	3	1.12
PW	TiO_2	3	2.57
PW	TORR	3	0.20
PW	TiO_2	6	2.23
PW	TORR	6	-0.34

Besides the calcination results presented above, the results obtained from the preliminary combustion tests described in chapter 2 are shown below in Figure 45 and Figure 46.

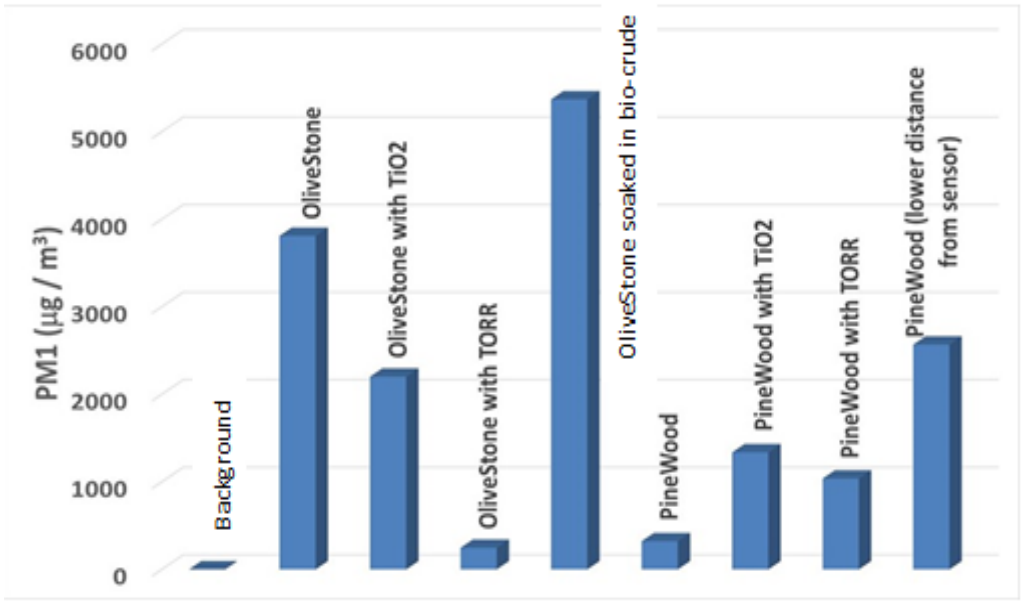

Figure 45: PM_1 emission in the preliminary combustion of pinewood and olive stone biomasses with and without additives

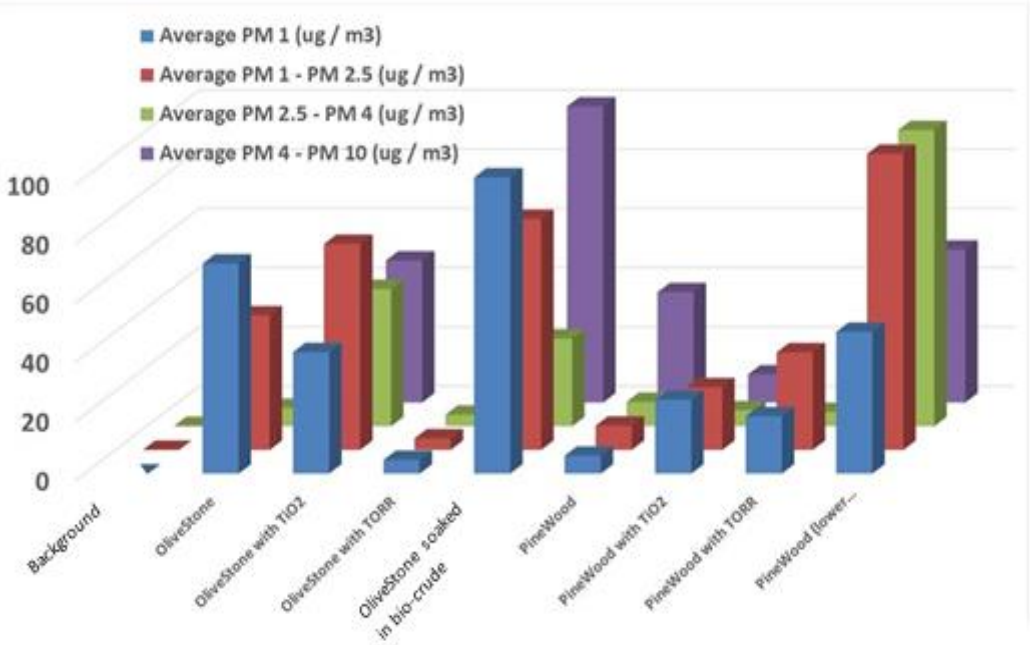

Figure 46: PM_1, $PM_{2.5}$, PM_4 and PM_{10} emissions in the preliminary combustion of pinewood and olive stone biomasses with and without additives

Despite the limitations of the experimental setup, some differences in the behaviour of biomasses with and without additives were apparent. With respect to olive stone, Figure 45 seems to indicate that TiO_2 decreases the amount of total particulate matter and Figure 46 shows that PM_1 decreases at the expense of the increase in $PM_{2.5}$ and PM_4 emissions. This could indicate the effectiveness of TiO_2 in increasing the granule size of ash particles from biomass combustion. The combustion emissions of the biomass added with the TORR are much lower than those obtained in the other tests. However, this decrease is certainly related to the combustion problems since the flame got extinguished several times due to the flame retardant property of TORR. The results with respect to pinewood seem to indicate that TiO_2 increases the PM emissions. However, in this case, it was observed during the firing that very fine pieces of biomass were ejected into the air (probably due to undetected drafts in the room) along with flue gas which has enough ground to invalidate the result from this particular case.

Although these results do not provide much insight into the efficacy of additives in decreasing the PM emissions, it can be seen that TiO_2 has a good potential to decrease fine PM emissions from biomass combustion. Also, it is worth noting that these tests have facilitated Torbel to construct a new laboratory scale installation in order to further proceed with these tests in a more controlled environment.

3.4. Aspen results

3.4.1. Input values of simulation parameters

The values of typical input parameters, provided by Torbel, for cyclone design/simulation are shown in Table 16.

.

Table 16: Input parameters provided by Torbel for cyclone design/simulation

Parameter	Value	Unit
Flue gas inlet flow	4500	m^3/h
Temperature	200	°C
Pressure	1	atm
Maximum allowed pressure drop	150	mm-water

The flue gas composition is unknown and hence a reasonable composition was assumed based on data from literature [(Xu et al., 2003), (Liu et al., 2010)]. These values are as shown in Table 17.

Table 17: Flue gas composition used for cyclone design/simulation

Component	Mole %
H_2O	6.20%
NO_2	0.03%
O_2	4.40%
N_2	76.81%
NO	0.01%
SO_2	0.04%
CO	0.01%
CO_2	12.50%

The ash loading in the flue gas was assumed to be 150 mg/Nm^3 based on data from literature for woody biomass combustion [Hasler et al., 1998]. However, to evaluate the influence of this parameter on efficiency, a value of 1500 $mg//Nm^3$ was also used to simulate multicyclones. Simulations were performed for three types of Torbel's cyclones – Helical cyclone, spiral cyclone, and multicyclones. The dimensions of these cyclones are confidential and hence not shown here.

The length of vortex finder for Torbel's helical and spiral cyclones were not given. Hence, values which were optimised using Aspen to give maximum efficiencies were used to run simulations. Also, the inlet angle for spiral cyclone was not given. Hence, it was assumed to be 0° since it gave the maximum efficiency.

The real PSD of the flue gas is also unknown. Hence, the PSD used to perform the simulations were based on a literature survey and is presented in Table 18.

Table 18: PSD of flue gas used to perform simulations

Lower limit (µm)	Upper limit (µm)	Mass fraction	Cumulative mass
0.05	0.15	0.01	0.01
0.15	0.25	0.03	0.04
0.25	0.75	0.04	0.08
0.75	2.25	0.04	0.12
2.25	7.75	0.15	0.27
7.75	12.25	0.40	0.67
12.25	37.75	0.20	0.87
37.75	82.25	0.10	0.97
82.25	277.75	0.03	1.00
SMD (µm) 2.29			
D_{50} (µm)10.34			

The block flow diagram of the cyclone used to perform simulations is shown in Figure 47. The block named 'CYCLONE' represents the cyclone separator and the streams 'GAS-IN', 'GAS-OUT' and 'DUST' represent the inlet flue gas stream, outlet flue gas stream, and particulates collected by the cyclone respectively.

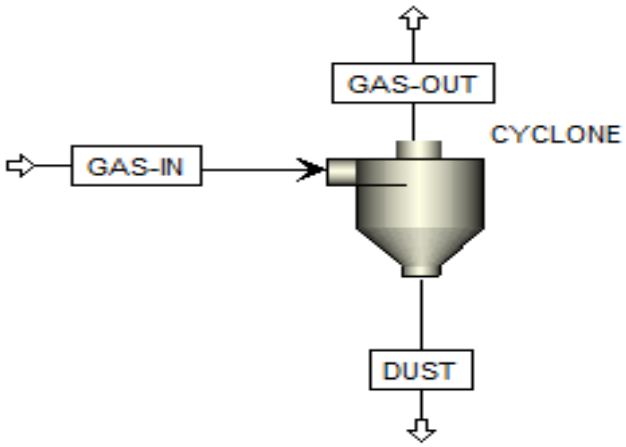

Figure 47: Block Flow diagram of cyclone system used to run Aspen simulations

3.4.2. Optimization of Torbel´s multicyclones

Aspen recommends the use of Muschelknautz (MU) model to test the performance of cyclones with known dimensions [Aspen]. However, for multicyclones, Aspen assumes an axial inlet configuration. But, Torbel's multicyclones have tangential inlets. Hence, MU model cannot be used for Torbel's multicyclones due to non-convergence of results although it gives the same results as that of Mothes-Loffler model. However, Mothes-Loffler (ML) model was used since it gives more realistic results due to more accurate turbulence and particle diffusion calculations [Aspen]. Shepherd & Lapple model (SL) was also used to determine the effect of changing the inlet length inside the cyclones. Both SL

and ML gave similar results for the separation efficiencies, with up to 0.01% difference for 150 mg/Nm^3 ash loading and up to 5% difference for 1500 mg/Nm^3 ash loading. The results from SL model are tabulated in Table 19 and Table 20.

Table 19: Results for simulation of Torbel's multicyclones using Shepherd & Lapple (SL) model for an ash loading of 150 mg/Nm^3

No.	Vane constant	No. of cyclones	ΔP (mm-water)	Separation efficiency η (%)	PM emissions (mg/Nm3)	Inlet velocity (m/s)	Cut Diameter (D_{cut}) (µm)
1	16	T	31	97.7	3.44	9.50	3.39
2	7.5	T	15	97.7	3.45	9.50	
3	16	2T/3	70	98.2	2.69	14.25	3.13
4	7.5	2T/3	33	98.2	2.70	14.25	
5	16	T/3	280	98.8	1.82	28.50	3.02
6	7.5	T/3	131	98.8	1.84	28.50	

T – Number of multicyclones prescribed in Torbel's design, as mentioned in Annex in Table 24

Table 20: Results for simulation of Torbel's multicyclones using Shepherd & Lapple (SL) model for an ash loading of 1500 mg/Nm^3

No.	Vane constant	No. of cyclones	ΔP (mm-water)	Separation efficiency η (%)	PM emissions (mg/Nm3)	Inlet velocity (m/s)	Cut Diameter (D_{cut}) (µm)
1	16	T	31	80	293.11	9.50	3.79
2	7.5	T	15	80	293.58	9.50	
3	16	2T/3	70	84	246.73	14.25	3.26
4	7.5	2T/3	33	84	247.63	14.25	
5	16	T/3	280	87	187.88	28.50	2.34
6	7.5	T/3	131	87	190.66	28.50	

T – Number of multicyclones prescribed in Torbel's design, as mentioned in Annex in Table 24

The vane constant is a measure of the length to which the gas inlet of the cyclone extends inside the cyclone [Aspen]. When the vane constant is 16, the inlet does not extend beyond the wall of the cyclone whereas when it is 7.5, the inlet extends inside the cyclone till the axis [Aspen].

The simulation results presented in Tables 19 and 20 allow concluding that decreasing the vane constant from 16 to 7.5 causes a 53% decrease in pressure drop, independent of the number of cyclones used and of the ash loading. Hence, using an inlet vane, to extend the gas inlet till the axis of the cyclone, can reduce the pressure drop by half in Torbel's multicyclones system. However, changing the vane constant has no effect on separation efficiency and PM emissions. As expected, due to the reduction of the velocity, the pressure drop significantly decreases with increase in the number of cyclones. However, even for a multicyclone system with T number of cyclones, as prescribed by Torbel (value of T is confidential and hence not shown), with Torbel dimensions, the pressure drop is far below 150 mm-water, which is Torbel's limit.

Concerning multicyclones, simulations were performed using the number of cyclones prescribed by Torbel (T) and also different numbers of cyclones. Systems with less than T/3 cyclones led to an inlet velocity more than 30 m/s, which is the highest allowable limit in Aspen.

The overall separation efficiency is a critical evaluator of the performance of a cyclone. However, parameters such as fractional efficiency curve, Sauter Mean Diameter (SMD), D_{50}, Cut diameter and Particle Size Distribution (PSD) of the outlet flue gas of the cyclones are needed to more holistically define the performance of a cyclone system [Nevers, 2000]. Fractional efficiency curve represents the separation efficiency of a cyclone system for several particle sizes [Nevers, 2000]. SMD and D_{50} give a measure of the overall particle size of the flue gas stream. SMD, commonly denoted as D_{32}, of a particle represents the diameter of a sphere that has the same volume/area ratio as the particle and the median D_{50}, calculated from the cumulative mass distribution curve, is defined as the diameter of the particle larger/smaller than 50% of the particles (by mass) in the PSD. It must be noted that D_{50} can also be calculated based on number and volume of particles. Aspen calculates D_{50} based on mass of the particles. Also, one must be cautious while using the SMD and D_{50} values of inlet flue gas given by Aspen. Because, Aspen makes use of the user-specified PSD to create a mathematical distribution function; and SMD, and D_{50} are calculated from the inlet PSD which is normalised with respect to the Aspen-generated PSD for outlet streams. Hence, SMD and D_{50} values generated by Aspen need to be considered accurate only when the particle size intervals of the output streams match those mentioned by the user as input. However, the SMD and D_{50} values generated by Aspen for the output streams seem to be accurate and credible. SMD and D_{50} for outlet streams of the simulated multicyclone systems are presented in Figure 48.

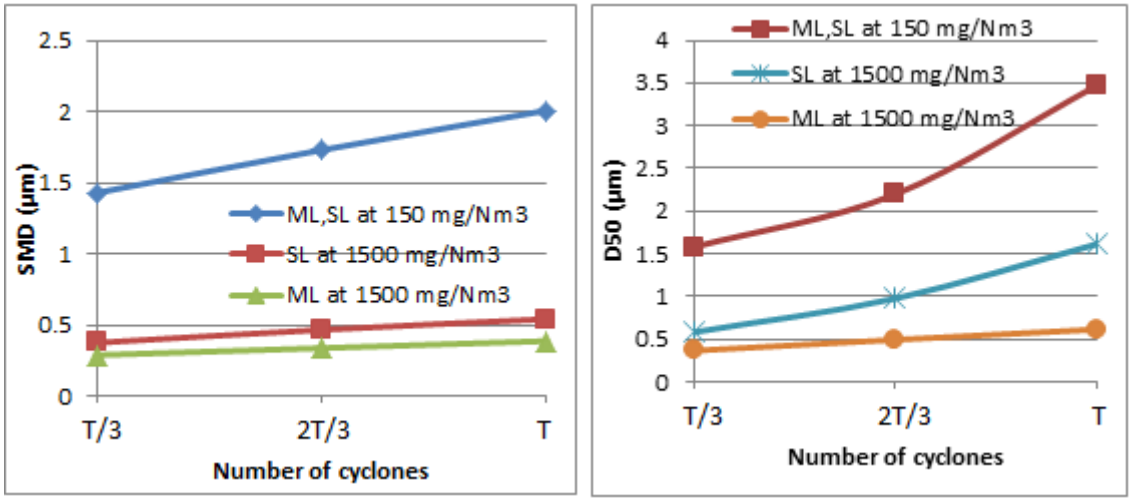

Figure 48: SMD (left) and D_{50} (right) vs. Number of cyclones for Torbel's multicyclone systems; ML: Mothes - Loffler model, SL: Shepherd & Lapple model

From above Figure 48, it can be seen that SMD and D_{50} slightly increase with increase in number of cyclones indicating that the multicyclone systems with lesser number of cyclones are better at removing finer particles than systems with more cyclones. The reason behind this increase is yet to be determined by performing more simulations with different PSD. However, this influence decreased

considerably with increase in ash loading by one order of magnitude indicating that at high values of ash loading, the number of cyclones in a multicyclone system does not influence the SMD and D_{50} of output streams.

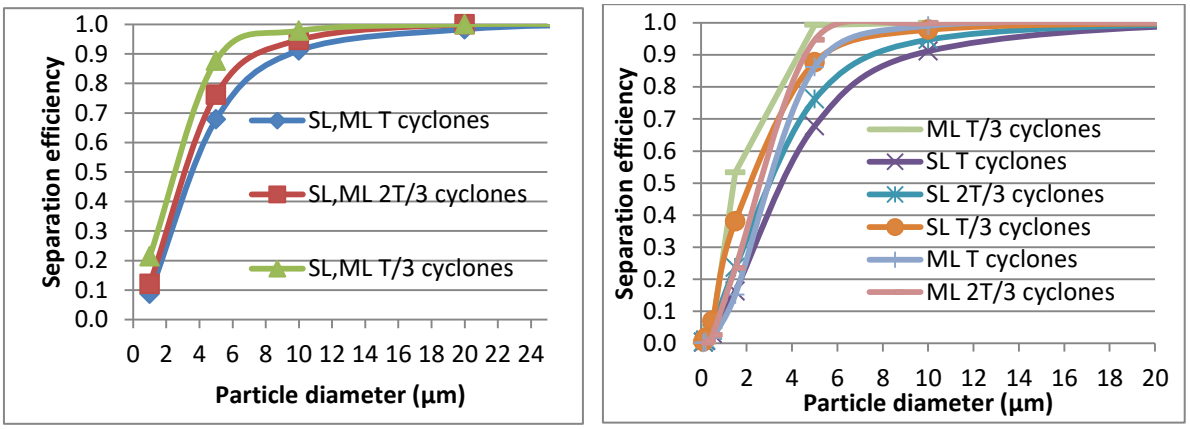

Figure 49: Fractional efficiency curves for Torbel's multicyclone systems at ash loading of 150 mg/Nm^3 (left) and 1500 mg/Nm^3; ML: Mothes - Loffler model, SL: Shepherd & Lapple model.

The above Figure 49 indicates that, separation efficiencies of the simulated multicyclones for particles smaller than 20 µm increase significantly with decrease in number of cyclones. For instance, when using 2T/3 cyclones instead of T, there is 97% removal of PM_5. This influence is observed at an ash loading of 1500 mg/Nm^3 as well. It can be surmised that one of the reasons for this increase is the higher inlet gas velocity, but the exact set of causes for this influence is yet to be determined. This result is further emphasized by the increase in D_{cut} - the cut diameter with increase in the number of cyclones, as shown in Figure 50.

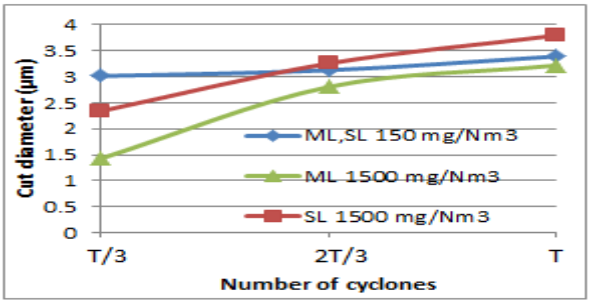

Figure 50: D_{cut} vs. Number of cyclones for Torbel's multicyclone systems; ML: Mothes - Loffler model, SL: Shepherd & Lapple model

The fractional efficiency increases with increase in ash loading despite the decrease in the overall separation efficiency. At 1500 mg/Nm^3 ash loading, the separation efficiency of the multicyclone system can reach as high as 90% when using T/3 cyclones. When the ash loading is 150 mg/Nm^3, the PM emissions are well below Torbel's target 50 mg/Nm^3. But, it is always above 140 mg/Nm^3 for all the simulations at ash loading of 1500 mg/Nm^3. This is far higher than the target and more post cyclone emission control equipment need to be installed in order to reach the target limit.

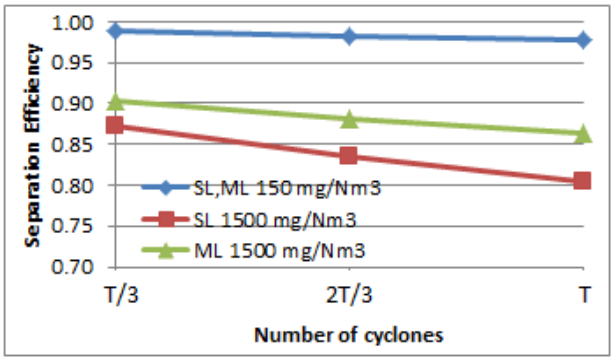

Figure 51: Efficiency vs. Number of cyclones for Torbel's multicyclone systems; ML: Mothes - Loffler model, SL: Shepherd & Lapple model

As seen in Figure 51, the separation efficiencies slightly decrease (less than 7% decrease for both the ash loadings) with the increase in number of cyclones. While this effect is almost insignificant for ash loading of 150 mg/Nm^3 (1.1% efficiency loss), it becomes more influential when ash loading is increased by one order of magnitude (7% efficiency loss). It is worth mentioning that due to the changes in the velocity of the gas, increasing the number of cyclones from T/3 to 2T/3 causes a 75% decrease in pressure drop, whereas increasing from 2T/3 to T causes only 55% decrease in pressure drop. Inlet gas velocity is quite high for the T cyclone system (28 m/s) whereas it is within the optimum interval for T/2 to T cyclones (19 m/s to 9.5 m/s).

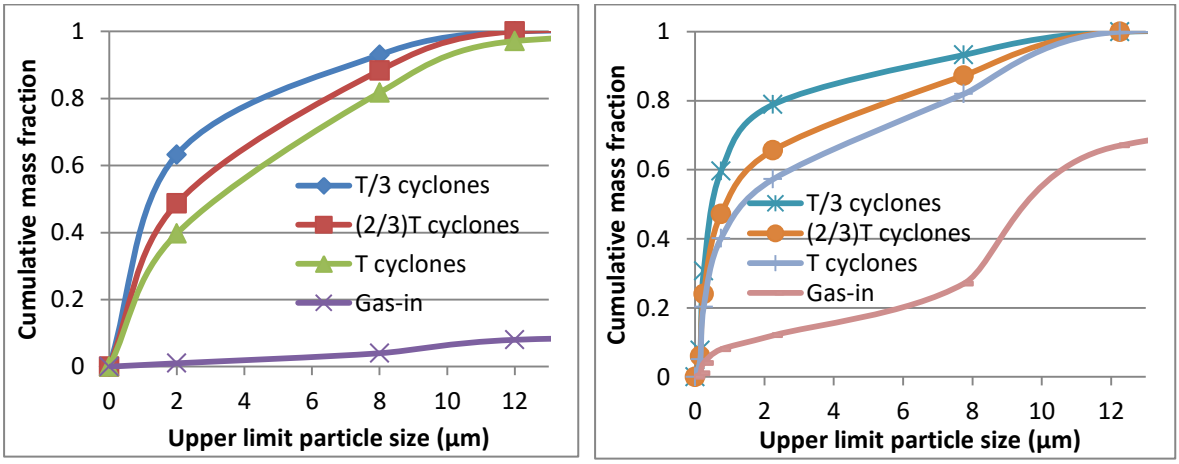

Figure 52: Cumulative PSD of Torbel's multicyclone systems for ash loading of 150 mg/Nm^3 (left) and 1500 mg/Nm^3 (right) (calculated by Shepherd & Lapple model)

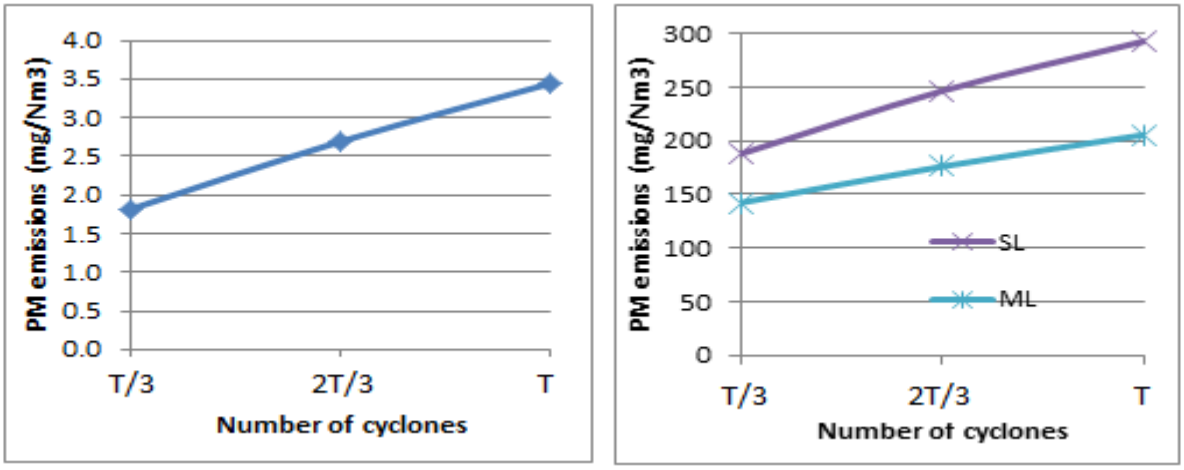

Figure 53: PM emissions vs. Number of cyclones for Torbel's multicyclone systems for ash loading of 150 mg/Nm^3 (left) and 1500 mg/Nm^3 (right);
ML: Mothes - Loffler model, SL: Shepherd & Lapple model.

As seen in Figure 53, PM emissions decrease with decrease in the number of cyclones. This supplements the results for fractional efficiency and overall efficiency which increase with the decrease in number of cyclones. In conclusion, for the given input parameters under the assumptions made, optimum design would be to use the current Torbel multicyclone dimensions with an inlet vane so that the vane constant is 7.5 (extending from the tangential inlet till the axis of cyclone) and to choose the number of cyclones between T/3 and T based on several factors such as ash loading, aerosol concentration in fly ash, pressure drop vs. energy consumption data, cost of installation of more cyclones, space limitations, etc. If the ash loading varies widely, it is prudent to use T/3 cyclones instead of the T cyclones system proposed by Torbel. Also, in case of a ash loading of 1500 mg/Nm^3, it is necessary to use anew more emission control equipment on the downstream of this multicyclone system in order to reach Torbel's target value. For this purpose, cyclones cannot be used due to very low ash loading with a major fraction below PM_5 and high volumetric flow rate. All Aspen simulations using Torbel's cyclone designs led to efficiencies below 5% and even modified designs of microcyclones could reach only till 30% efficiency but couldn't bring down the PM emissions to below 50 mg/Nm^3. Hence, when the ash loading is very high, it is a wise choice to use an ESP or a fabric filter downstream of the cyclones.

3.4.3. Simulation of Torbel´s helical and spiral cyclones

The next study was to use Muschelknautz model to simulate Torbel's spiral and helical cyclones. According to the Aspen manual, it is recommended to use this model for simulating cyclone systems with known dimensions. The first two rows of Table 21, respectively, present the results of simulations for Torbel's helical and spiral cyclones; the third row presents the results for a simulation run for Torbel's spiral cyclone using inlet height decreased by 12.5% and inlet width decreased by 35%, while keeping the Torbel dimensions for other parameters. Also, the same input conditions were used to run iterations in Aspen's design mode (fourth row of Table 21) to determine the optimum cyclone dimensions for a Stairmand High Efficiency cyclone instead of Torbel's helical and spiral cyclone designs.

Table 21: Results from simulation of Torbel's helical and spiral cyclones using Muschelknautz model

No.	D (m)	ΔP (mm-water)	Separation efficiency η (%)	PM emissions (mg/Nm3)	Inlet velocity (m/s)	Cut Diameter (D_{cut}) (μm)
1	DT_H	81	90	14.79	13.9	0.10
2	DT_S	47	81	29.04	15.6	3.83
3	DT_S	107	93	10.51	27.5	0.08
4	0.626	319	97	4.72	17.0	0.07

DT_H and DT_S are diameters of Torbel's helical and spiral cyclones, as mentioned in Annex in Table 24

It can be seen that the cyclone model proposed by Aspen in the last raw gives the highest separation efficiency and the lowest cut diameter, despite the lower velocity. However, the pressure drop of the Aspen cyclone is the highest of the below. The dimensions given by Aspen for this Stairmand High Efficiency cyclone are shown in Table 22.

Table 22: Dimensions of the Stairmand High Efficiency cyclone proposed by Aspen

Cyclone Type		Stairmand HE	
Parameter	**Notation**	**Value (mm)**	**Ratios with respect to D**
Inlet height	a	313	0.50000
Inlet width	b	234.8	0.37508
Cyclone body diameter	D	626	1.00000
Underflow diameter	B	234.8	0.37508
Overall height of cyclone	H	939	1.50000
Height of cylinder	h	1565.1	2.50016
Vortex finder height	s	313	0.50000
Overflow diameter	D_e	313	0.50000

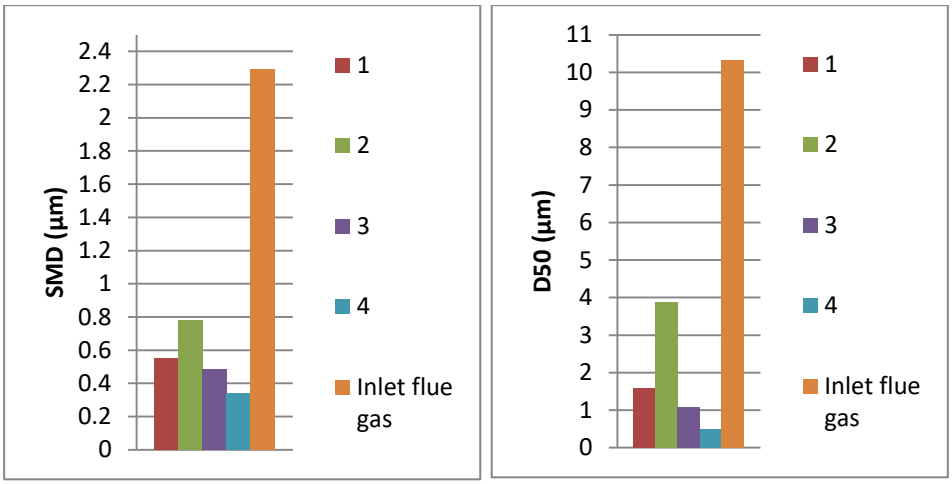

Figure 54: SMD (left) and D_{50} (right) of helical, spiral and aspen-proposed cyclones; 1, 2, 3, and 4 are respectively Torbel's helical, spiral, spiral with reduced inlet dimensions, and Aspen-proposed Stairmand High Efficiency cyclones.

From Figure 54, it can be seen that the Aspen-proposed cyclone gives the lowest SMD and D_{50} whereas Torbel's spiral cyclone design gives the highest SMD and D_{50}. This is further supplemented by the lowest emissions given by Aspen-proposed cyclone and the highest emissions from Torbel's spiral cyclone, as shown below in Figure 55.

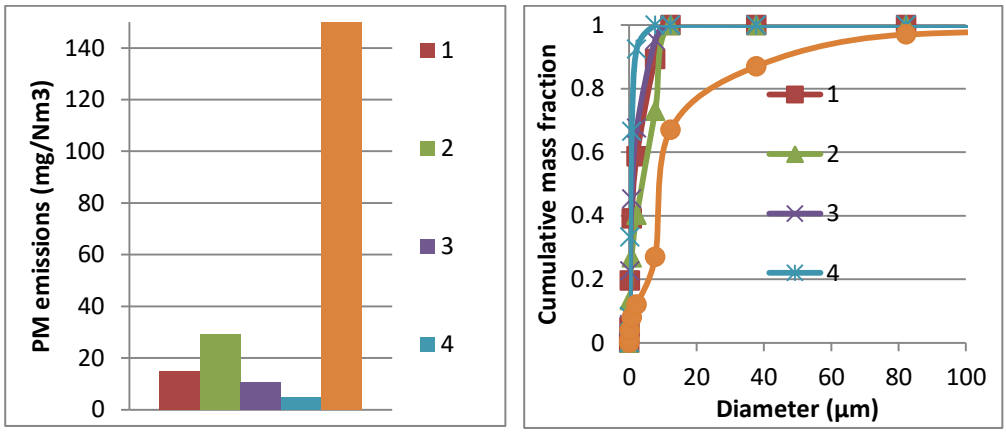

Figure 55: PM emissions and cumulative PSD for helical, spiral, and aspen-proposed cyclones; 1, 2, 3, and 4 are respectively Torbel's helical, spiral, spiral with reduced inlet dimensions, and Aspen-proposed Stairmand High Efficiency cyclones.

Furthermore, among the aforementioned four simulated cases, Aspen-proposed cyclone has superior separation efficiency characteristics while Torbel's spiral cyclone has the lowest separation efficiency. This is illustrated below in Figure 56.

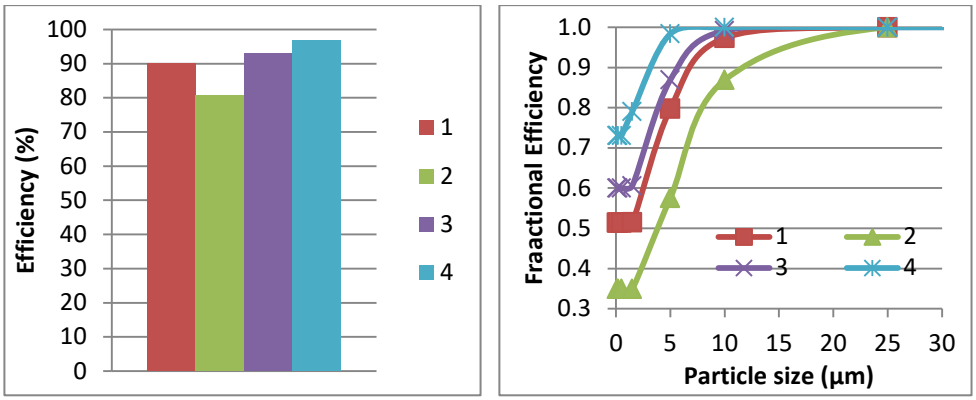

Figure 56: Overall efficiency (left) and fractional efficiency curves (right) of helical, spiral, and aspen-proposed cyclones; 1, 2, 3, and 4 are respectively Torbel's helical, spiral, spiral with reduced inlet dimensions, and Aspen-proposed Stairmand High Efficiency cyclones.

The helical cyclones analysed here perform better than spiral cyclones in all the above scenarios with higher overall separation efficiencies and higher fractional efficiencies. However, the efficiency of spiral cyclones can be improved further by decreasing the inlet height and width thus increasing the inlet velocity till 28 m/s, which is Torbel's limit for spiral cyclones. The cut diameters and SMD of the spiral cyclone are higher than those of helical cyclones but this reverses when the inlet height and width of spiral cyclone are decreased such that the inlet velocity is closer to 28 m/s. For the given process conditions, Aspen gives an optimised design of Stairmand High Efficiency cyclone, which has better overall separation efficiency, fractional efficiencies, smaller cut diameter and SMD. Hence, for the given process conditions and assumed parameters, the order of preference of cyclones is as follows: Torbel's multicyclone system with T/3 cyclones and vane constant 7.5 > Torbel's multicyclone system with T cyclones > Stairmand HE proposed by Aspen > Torbel's Helical cyclone > Torbel's spiral cyclone with reduced inlet height and width > Torbel's spiral cyclone.

4. Conclusions

To summarise, in this work, liquefaction of the biomasses – pinewood, olive stone, olive bagasse, grape seed, and rice husk was investigated as a pre-treatment before combustion in order to: i) decrease fine particles emission from biomass combustion and ii) produce a liquid biofuel that can be easily burned. The liquefaction conditions for pinewood and olive stone were optimized to use high biomass to solvent ratio of 1:1 (w/w). The solvent used was 2-Ethylhexanol and at this ratio pinewood and olive stone yielded around 55% conversion of the initial biomass. To achieve this conversion, the required reaction time at 160ºC is between 3 to 5 hours for pinewood whereas it is 4 hours for olive stone. The catalyst used was p-Toluene sulfonic acid and the concentration needed for this conversion is 5.6% for pinewood and 4.5% for olive stone. The liquefaction of olive stone was successfully scaled up to use 15 times more biomass feed than the optimised experiments proving its potential to be scaled up further. Olive bagasse gave low conversions of around 20% with the same conditions as olive stone whereas grape seeds gave insignificant conversions. Therefore, olive bagasse and grape seeds need to be investigated further to establish optimum liquefaction conditions. Rice husk gave similar conversions of around 55% as pinewood or olive stone but with a less biomass to solvent ratio (0.2:1) because of its low density. This behaviour of rice husk may be due to its high inorganic content which is 15 times higher than that of pinewood and olive stone. Thus, rice husk liquefaction is promising and has to be studied further using different conditions.

Concerning the calcination of the liquefaction residues the results showed that 60 to 70% of the inorganic content of the biomass was removed by liquefaction. It is important to note that the solids left in the bio-oils may be due to the presence of solids in suspension due to an inefficient solid-liquid separation and/or due to the particles caught up between large molecules in the bio-oils.

The higher heating values of the bio-oils from pinewood and olive stone liquefaction were 35.3 and 35.6 MJ/kg which is closer to that of anthracite with 4% H_2O (36 MJ/kg) and biodiesel (39-41 MJ/kg) and less than the higher heating value of heavy fuel oil (43 MJ/kg). Their viscosities (~0.3 P at 25 °C and <0.1 P above 50°C) were closer to that of heavy gas oil fractions obtained from Alaskan North Slope (0.13 P at 37 °C) and North Sea Light crudes (0.07 P at 99 °C). These results indicate the suitability of these bio-oils to be used in industrial combustion applications.

Preliminary tests were performed to evaluate the efficacy of the additives, PentaErythritol Tetra Ester, Kaolin and Titanium dioxide, to reduce fine particle emissions from biomass combustion. The first attempt was to evaluate their effect in the amount of inorganic residue obtained after calcination. However, the tests performed for this purpose turned out to be inconclusive, proving this method is not effective. TGA analyses will be also carried out as soon as possible. The preliminary lab-scale combustion tests performed with these additives proved that TiO_2 can be a promising additive to decrease particulate emissions in flue gases, especially PM_1 emissions. The decrease of PM1 emissions was accompanied by an increase of $PM_{2.5}$ and PM_4 which may be an indication of the formation of aggregates. On the other hand, these combustion tests turned out to be a useful basis that was given to Torbel to set up a laboratory scale installation to test the performance of these additives in more controlled environment.

Finally, Aspen Plus V8.4 was used to rate the performance of Torbel's multicyclone system, spiral cyclone and helical cyclone designs at given process conditions and under reasonable assumptions for unknown parameters. It was found that Torbel's multicyclones performed better for removing PM emissions in flue gas than helical cyclone, which in turn performed better than Torbel's spiral cyclone. Decreasing the number of cyclones in the multicyclones system from Torbel, specified value identified as T, to T/3 resulted in an increase in the efficiency. Even though this increase was small (1.1%) at an ash loading of 150 mg/Nm^3, it increased further to 7% when the ash loading was increased by one order of magnitude. This indicates that decreasing the number of cyclones from T to T/3 has significant advantage at high ash loading of flue gas. Also, adding an inlet vane to cyclones extending from the point of intersection of gas inlet and cyclone wall till the axis of cyclone (vane constant is 7.5) reduced the pressure drop by half. Concerning Torbel's spiral cyclone, it was possible to improve its performance by decreasing the inlet height by 12.5% and inlet width by 35%. This change resulted in 12% increase in overall separation efficiency and 64% decrease in PM emissions when compared to the spiral cyclone with Torbel's dimensions. A set of iterations were performed in design mode with the same input parameters in order to determine the optimum cyclone dimensions suggested by Aspen. Aspen suggested the use of a Stairmand High Efficiency cyclone instead of Torbel's spiral and helical cyclones. This cyclone showed 7% higher efficiency than Torbel's helical cyclone and 16% more efficiency than Torbel's spiral cyclone. Also, at an ash loading of 150 mg/Nm^3, the PM emissions from all these cyclones were less than 50 mg/Nm^3, which is Torbel's target. However, at an ash loading of 1500 mg/Nm^3, the minimum possible PM emissions achievable was 142 mg/Nm^3.Since the output gas stream downstream of this cyclone has a high volumetric flow rate and more aerosols, cyclones cannot be used to decrease the PM emissions further from 142 to 50 mg/Nm^3 and hence other equipment such as small bags filter or ESP is needed for this purpose.

To conclude, for the given process conditions and for the studied particles loadings, the order of preference of the cyclone separators is as follows: Torbel's multicyclones system with T/3 cyclones and vane constant 7.5 > Torbel's multicyclone system with T cyclones > Stairmand HE proposed by Aspen > Torbel's Helical cyclone > Torbel's spiral cyclone with reduced inlet height and width > Torbel's spiral cyclone.

5. Future work

Liquefaction of olive bagasse, grape seeds and rice husk need to be studied further and optimised. Although literature indicates the occurrence of reactions between the solvent and lignocellulosic biomasses, the exact nature of these reactions, for instance, kinetics, extent and mechanism are unknown [Li et al., 2015]. These need to be studied in order to develop methods to recover the unreacted solvent, if any, from the bio-oils in order to reuse it.

On the other hand, the composition of bio-oils needs to be studied in more detail. The optimization of sugars extraction and further characterization and the study of potential applications is also important. Also, the characterization of the remaining fraction of the bio-oil to explore the possibilities of upgrading should also be considered.

Concerning the use of additives, the selected additives need to be tested in more controlled environments and then in the drop tube furnace at IST to determine their effectiveness in increasing the granule size of ash in order to decrease the fine particles emission in fly ash. The survey/test for new additives should be also considered

The PSD, ash loading, and flue gas composition in Torbel should be measured in order to allow a better evaluation and optimization of the cyclone separators and also custom design. Post cyclone systems need to be studied further to reach Torbel's target of 50 mg/Nm^3 at high ash loading. Furthermore, heat and mass analysis of cyclones using numerical and/or CFD simulations need to be performed to further optimise these cyclone designs.

6. Bibliography:

6.1. Scientific articles, publications and books

Adapa, P. K.; Schonenau, L. G.; Canam, Thomas; and Dumonceaux, T., 2011, 'Quantitative Analysis of Lignocellulosic Components of Non-Treated and Steam Exploded Barley, Canola, Oat and Wheat Straw Using Fourier Transform Infrared Spectroscopy', Faculty Research & Creative Activity. 107.

Aro, E.M., 2016, 'From first generation biofuels to advanced solar biofuels', Ambio. 45(1): 24-31.

Bäfver, L.; Boman, C.; and Rönnbäck, M., 2011, 'Reduction of particle emissions by using additives', Central European Biomass Conference, Graz, Austria.

Bajpai, P., 2016, 'Pretreatment of Lignocellulosic Biomass for Biofuel Production', Chapter 2: 7.

Banoub, J.H.; and Delmas, M., 2003, 'Structural elucidation of the wheat straw lignin polymer by atmospheric pressure chemical ionization tandem mass spectrometry and matrix-assisted laser desorption/ionization time-of-flight mass spectrometry', Journal of Mass Spectrometry 38(8): 900-903.

Barros, J.; Serrani-Yarce J.C.; Chen, F.; Baxter, D.; Venables, B.J.; Dixon, R.A., 2016, 'Role of bifunctional ammonia-lyase in grass cell wall biosynthesis', Nature Plants 2, Article number: 16050

Brandt, A.; Gräsvik, J.; Hallett, J.P.; and Welton, T., 2013, 'Deconstruction of lignocellulosic biomass with ionic liquids', Green Chem 15: 550.

Braz, A., 2015, 'Liquefacção de Madeira de Pinho', Dissertation for Master's in Chemical Engineering, Instituto Superiro Técnico.

Brunner, T.; Joeller, M.; Obernberger, I.; and Frandsen, F., 2002, 'Aerosol and fly ash formation in fixed bed biomass combustion using woody biofuels', 12th European Conference and Technology Exhibition on Biomass for Energy, Industry and Climate Protection, 17-21 June 2002, Amsterdam.

Bui, N.Q.; Fongarland, P.; Rataboul, F.; Dartiguelongue, C.; Charon, N.; Vallée, C.; and Essayem, N., 2015, 'FTIR as a simple tool to quantify unconverted lignin from chars in biomass liquefaction process: Application to SC ethanol liquefaction of pine wood', Fuel Processing Technology 134: 378-386.

Carvalho D.M.D., 2015, 'Study on the structure and properties of xylan extracted from eucalyptus, sugarcane bagasse and sugarcane straw', Licentiate thesis in Fibre and Polymer Science: 39, KTH Royal Institute of Technology, Stockholm.

Chen, F.; and Lu, Z., 2009, 'Liquefaction of wheat straw and preparation of rigid polyurethane foam from the liquefaction products', Journal of Applied Polymer Science 111(1): 508–516

Chew, J.J.; and Doshi, V., 2011, 'Recent advances in biomass pretreatment – Torrefaction fundamentals and technology', Renewable and Sustainable Energy Reviews 15(8): 4212-4222.

Clift, R.; Ghadiri, M.; and Hoffman, A.C., 1991, 'A critique of two models for cyclone performance', AIChE Journal 37(2): 285-289.

Cuevas, M.; Sánchez, S.; Bravo, V.; Cruz, N.; and García, J.F., 2009, 'Fermentation of enzymatic hydrolysates from olive stones by *Pachysolen tannophilus*', J. Chem. Technol. Biotechnol. 84: 461–467

Davidsson, K.O.; Steenari, B.M.; and Eskilsson, D., 2007, 'Kaolin Addition during Biomass Combustion in a 35 MW Circulating Fluidized-Bed Boiler', Energy Fuels 21(4): 1959–1966

Dirgo, J.; and Leith, D., 1985, 'Cyclone Collection Efficiency: Comparison of Experimental Results with Theoretical Predictions', Aerosol Science and Technology 4(4): 401-415.

Elsayed, K., 2011, 'Analysis and Optimization of Cyclone Separators Geometry using RANS and LES methodologies', Doctoral thesis, Department of Mechanical Engineering, Vrije Universiteit Brussel.

Fournel, S.; Palacios, J.H.; Godbout, S.; and Heitz, M., 2015, 'Effect of Additives and Fuel Blending on Emissions and Ash-Related Problems from Small-Scale Combustion of Reed Canary Grass', Agriculture 5: 561-576

Grilc, M.; Likozar, B.; and Levec, J., 2015, 'Kinetic model of homogeneous lignocellulosic biomass solvolysis in glycerol and imidazolium-based ionic liquids with subsequent heterogeneous hydrodeoxygenation over NiMo/Al_2O_3 catalyst', Catalysis Today 256(2): 302-314

Höfer, I.; and Kaltschmitt, M., 2017, 'Effect of additives on particulate matter formation of solid biofuel blends from wood and straw', Biomass Conversion and Biorefinery 7(1): 101-116.

Hu, S.; Luo, X.; and Li, Y., 2014, 'Polyols and Polyurethanes from the Liquefaction of Lignocellulosic Biomass', ChemSusChem 7(1): 66–72.

Hu, S.; Wan, C.; and Li, Y., 2012, 'Production and characterization of biopolyols and polyurethane foams from crude glycerol based liquefaction of soybean straw', Bioresource Technology 103(1): 227-233.

Jin, W.; Singh, K.; and Zondlo, J., 2013, 'Pyrolysis Kinetics of Physical Components of Wood and Wood-Polymers Using Isoconversion Method', Agriculture 3(12): 32.

Jose, S.; and Bhaskar, T., 2015, 'Advanced Biorefineries for Sustainable production and distribution', Chapter 1.5, book by Carol L. Williams.

Kobayashi, M.; Asano, T.; Kajiyama, M.; Tomita, B., 2004, 'Analysis on residue formation during wood liquefaction with polyhydric alcohol', Journal of Wood Science 50(5): 407-414.

Krause, H.H.; Hillenbrand, L.J.; Weller, A.E.; and Locklin, D.W., 1977, 'Combustion additives for pollution control -- A State-of-the Art Review', Environmental Protection Technology Series, Prepared for U.S. Environmental Protection Agency: S-4.

Kunsagi, L., 1983, 'Electrogasdynamically assisted cyclone system for cleaning flue gases at high temperatures and pressures', US Patent number US4398928 A.

Li, Y.; Luo, X.; and Hu, S., 2015,'Bio-based Polyols and Polyurethanes', SpringerBriefs in Green Chemistry for Sustainability, ebook, chapter 3.3: 52.

Liu, H.; Qiu, G.; Shao, Y.; and Riffat, B.S., 2010, 'Experimental investigation on flue gas emissions of a domestic biomass boiler under normal and idle combustion conditions', International Journal of Low-Carbon Technologies 5(2): 88–95

Lu, Z.; Wu, Z.; Fan, L.; Zhang, H.; Liao, Y.; Zheng, D.; and Wang, S., 2016, 'Rapid and solvent-saving liquefaction of woody biomass using microwave–ultrasonic assisted technology', Bioresource Technology 199: 423-426.

Mateus, M.M.; Carvalho, R.; Bordado, J.C.; and Santos, R.J.D, 2015, 'Biomass acid-catalyzed liquefaction – Catalysts performance and polyhydric alcohol influence', Data in Brief 5: 736-738, Elsevier open access article.

Mateus, M.M.; Guerreiro, D.; Ferreira, O.; Bordado, J.C.; and Santos, R.G.D., 2017, 'Heuristic analysis of Eucalyptus globulus bark depolymerization via acid-liquefaction', Cellulose 24:659–668.

Mateus, M.M.; Ventura, P.; Rego, A.; Mota, C.; Castanheira, I.; Bordado, J.M.; and Santos, R.J.D., 2017, 'Acid Liquefaction of Potato (Solanum tuberosum) and Sweet Potato (Ipomoea batatas) Cultivars Peels – Pre-Screening of Antioxidant Activity/Total Phenolic and Sugar Contents', BioResources 12(1): 1463-1478.

Monteiro, C.; Tarelho, L.; Lopes, M.; Monteiro, A.; Machado, L.; Amaral, J.; and Borrego, C., 2011, 'Forest biomass resources for industrial energy conversion in Portugal', 19th European Biomass Conference and Exhibition, Berlin, Germany.

Nevers, N.D., 2000, 'Air Pollution Control Engineering', Second Edition, McGraw-Hill International Editions, Civil Engineering Series.

Ninomiya, Y.; Wang, Q.; Xu, S.; Mizuno, K.; and Awaya, I., 2009, 'Effect of Additives on the Reduction of $PM_{2.5}$ Emissions during Pulverized Coal Combustion', Energy Fuels 23(7): 3412–3417

Nunes, C.P., 2017, 'A Utilização Energética da Biomassa como Prevenção dos Fogos Florestais', Accepted for publication in Energia e Futuro.

Nussbaumer, Th.; and Hasler, Ph., 1998, 'Particle Size Distribution of the Fly Ash from Biomass Combustion', Biomass for Energy and Industry, 10th European Conference and Technology Exhibition, Würzburg, Germany.

Oliveira, L. E.; and Da Silva M.L.C.P., 2013, 'Comparative study of calorific value of rapeseed, soybean, jatropha curcas and crambe biodiesel', International Conference on Renewable Energies and Power Quality (ICREPQ'13) Bilbao, Spain: No.11

Rachel-Tang, D.Y.; Islam, A.; and Taufiq-Yap, Y.H., 2017, 'Bio-oil production via catalytic solvolysis of biomass', RSC Adv. 7: 7820.

Ralph, J.; Lundquist, K.; Brunow, G.; Lu, F.; Kim, H.; Schatz, P.F.; Marita, J.M.; Hatfield, R.D.; Ralph, S.A.; Christensen, J.H.; and Boerjan, W., 2004, 'Lignins: Natural polymers from oxidative coupling of 4-hydroxyphenyl-propanoids', Phytochemistry Reviews 3(1-2): 29-60.

Riaza, J.; Gil, M.V.; Álvarez, L.; Pevida, C.; Pis, J.J.; and Rubiera, F., 2012, 'Oxy-fuel combustion of coal and biomass blends', Energy 41(1): 429-435.

Scheller, H.V.; and Ulvskov, P., 2010, 'Hemicelluloses', Annual Review of Plant Biology 61: 263-289.

Sills, D.L.; and Gossett, J.M., 2012, 'Using FTIR to Predict Saccharification From Enzymatic Hydrolysis of Alkali-Pretreated Biomasses', Biotechnology and Bioengineering109(2): 353-362.

Wang, L.; Hustad, J.E.; Skreiberg, Ø.; Skjevrak, G.; and Grønli, M., 2012, 'A Critical Review on Additives to Reduce Ash Related Operation Problems in Biomass Combustion Applications', Energy Procedia 20: 20-29

Wiinikka, H.; Grönberg, C.; Öhrman, O.; and Boström, D., 2009, 'Influence of TiO_2 Additive on Vaporization of Potassium during Straw Combustion', Energy Fuels 23(11): 5367–5374

Xi, D.; Zhou, R.; Zhou, R.; Zhang, X.; Ye, L.; Li, J.; Jiang, C.; Chen, Q.; Sun, G; Liu, Q.; and Yang, S., 2017, 'Mechanism and optimization for plasma electrolytic liquefaction of sawdust', Bioresource Technology 241: 545-551

Xu, X.; Song, C.; Wincek, R.; Andresen, J.M.; Miller, B.G.; and Scaroni, A.W., 2003, 'Separation of CO2 from Power Plant Flue Gas Using a Novel CO2 "Molecular Basket" Adsorbent', Fuel Chemistry Division Preprints 48(1): 162.

Yamada, T.; and Ono, H., 1999, 'Rapid liquefaction of lignocellulosic waste by using ethylene carbonate', Bioresource Technology 70: 61–67.

Zhang, T.; Zhou, Y.; Liu, D.; and Petrus, L., 2007, 'Qualitative analysis of products formed during the acid catalyzed liquefaction of bagasse in ethylene glycol', Bioresource Technology 98: 1454-1459.

Zhang, W.; Liu, H.; Hai, I.U.; Neubauer, Y.; Schröder, P.; Oldenburg, H.; Seilkopf, A.; and Kölling, A., 2012, 'Gas cleaning strategies for biomass gasification product gas', International Journal of Low-Carbon Technologies 7: 69–74.

Zou, X.; Qin, T.; Huang L.; Zhang, X.; Yang, X.; and Wang, Y., 2009, 'Mechanisms and Main Regularities of Biomass Liquefaction with Alcoholic Solvents', Energy Fuels 23: 5213-5218.

6.2. Other references

ABS – American Bureau of Shipping, 'Notes on Heavy Fuel Oil', 1984; 16/10/2017.

Aspen – Aspen Plus V8.4 help manual; 16/10/2017

BASF – Technical specifications of 2-Ethylhexanol by BASF; http://www.solvents.basf.com/portal/load/fid245412/Technical%20Spec%20-%202%20Ethylhexanol_BPC.pdf, October 3, 2017; 16/10/2017

BHE - Bright hub engineering; http://www.brighthubengineering.com/power-plants/26549-differences-of-a-circulating-fluidized-bed-boiler-and-a-pulverised-coal-boiler/#imgn_0; 16/10/2017

Boman, C.; Dan Boström, D.; Jonathan Fagerström, J.; Marcus Öhman, M.; Ida-Linn Näzelius, I.L.; and Linda Bäfver, L., Report on 'Fuel additives and blending as primary measures for reduction of fine ash particle emissions – state of the art', 2012, ERA-NET FutureBioTec.

Brem, G., 'Biomass co-firing: Technology, barriers and experiences in EU', GCEP Advanced Coal Workshop, March 15th-16th, 2005, Provo (UT), USA.

CFN – C.F. Nielsen Briquetting Company; https://cfnielsen.com/faq/calorific-values-for-different-raw-materials/; 16/10/2017

Clarke, S. and Preto F., 'Biomass Densification for Energy Production', Factsheet, June 2011.

Costa M., ‘Biomass Combustion and Co-firing’, presentation in Bioenergy: Challenges and Opportunities, Guimarães, Portugal, 6-9 April 2008; https://fenix.tecnico.ulisboa.pt/downloadFile/3779572077334/Biomass.pdf; 16/10/2017

DIR08 - Directive 2008/50/EC of the European Parliament and of the council of 21 May 2008 on ambient air quality and cleaner air for Europe.

DIR10 - Directive 2010/75/EU of the European Parliament and of the Council of 24 November 2010 on industrial emissions (integrated pollution prevention and control)

Douglas, D.C., ‘Process Development for biomass Liquefaction’, Pacific Northwest Laboratory operated by BATTELE Memorial Institute, Archived files of American Chemical Society Division of Energy & Fuels; https://web.anl.gov/PCS/acsfuel/preprint%20archive/Files/25_4_SAN%20FRANCISCO_08-80_0257.pdf; 16/10/2017

EUBIONET – European Bioenergy Networks, Report on ‘Biomass Co-firing – An Efficient Way to reduce Greenhouse Gas Emissions’; https://ec.europa.eu/energy/sites/ener/files/documents/2003_cofiring_eu_bionet.pdf; 16/10/2017

FAO - ‘Unified Bioenergy Terminology’, Food and Agricultural Organization Forestry Department’s Wood Energy Programme, December 2004; ftp://ftp.fao.org/docrep/fao/007/j4504e/j4504e00.pdf; 16/10/2017

FAO – Food and Agricultural Organization of the United Nations, ‘The research progress of biomass pyrolysis processes’; http://www.fao.org/docrep/t4470E/t4470e0a.htm; 16/10/2017

Guardian - News article titled ‘Wildfires trap 2000 people in town in Central Portugal’ by The Guardian; https://www.theguardian.com/world/2017/aug/17/wildfires-trap-2000-people-in-macao-village-in-central-portugal; 16/10/2017

IAC - Industrial Accessories Company; http://www.iac-intl.com/baghouse/designs; 16/10/2017

ICNF - ‘Inventário Florestal Nacional 6’ by Instituto da Conservação da Natureza e das Florestas; http://www.icnf.pt/portal/florestas/ifn/resource/ficheiros/ifn/ifn6-res-prelimv1-1; 16/10/2017

IEA - International Energy Agency, Bioenergy and biofuels; https://www.iea.org/topics/renewables/bioenergy/; 21/08/2017

IEA - Key world energy statistics 2016, International Energy Agency; https://www.iea.org/publications/freepublications/publication/KeyWorld2016.pdf; 16/10/2017

INE – Statistics by Instituto Nacional de Estatística; http://smi.ine.pt/Conceito/Detalhes?id=5490&lang=EN; 16/10/2017

Livingston, B., Workshop on ‘Ash related Issues in Biomass Combustion’, September 21, 2006; https://ec.europa.eu/energy/intelligent/projects/sites/iee-projects/files/projects/documents/thermalnet_ash_related_issues_in_biomas_combustion.pdf; 16/10/2017

Livingston, W. R., ‘Biomass ash characteristics and behaviour in combustion, gasification and pyrolysis systems’, report, 20 February 2007; https://antioligarch.files.wordpress.com/2014/12/biomass-fly-ash-characteristics-behaviour-in-combustion.pdf; 16/10/2017

NPL – National Physical Laboratory of the UK, Kale & Laby Tables of Chemical and Physical Constants; http://www.kayelaby.npl.co.uk/chemistry/3_11/3_11_4.html; 16/10/2017

NPTEL – Chemical Engineering – Chemical Engineering Design II – Module #5, an open course by Indian Institute of Technology and Indian Institute of Science, pp-3,4.

Nussbaumer T., ‘Overview on Technologies for Biomass Combustion and Emission Levels of Particulate Matter’, report, Zürich 2010; http://citeseerx.ist.psu.edu/viewdoc/download?doi=10.1.1.459.4781&rep=rep1&type=pdf; 16/10/2017

Obernberger, I., ‘Fly ash and aerosol formation in biomass combustion processes – an introduction’, Presentation, Institute for Resource Efficient and Sustainable Systems, Graz University of Technology.

SRC - Shimi Research Center Pvt. Ltd., http://www.shimiresearch.in/Multistage-Cyclones.php; 16/10/2017

TAURON – Document from TAURON; http://www.tauron-wytwarzanie.pl/SiteCollectionDocuments/wydawnictwa/tryptyk_lagisza_eng.pdf; 16/10/2017

UCLA - Illustrated glossary of organic chemistry by University of California, Los Angeles; http://www.chem.ucla.edu/~harding/IGOC/C/cellulose.html; 16/10/2017

UF - Principal Investigators: Dr. Chang-Yu Wu and Anne Allen, Designers: Heath Wintz, Priscilla Chapman, James Marini, Soung-Chul Yang, Robert Roberg, and Ying Li, ‘Aerosol Science and Engineering – Learning about cyclones’, a course by University of Florida; http://aerosol.ees.ufl.edu/cyclone/section01.html; 16/10/2017

UNCCC - United Nations Climate Change Conference 2015 – Paris Agreement; http://www.cop21paris.org/about/cop21; 16/10/2017

US-DE - ‘Biomass Resource Basics’, August 14 2013, The United States Department of Energy; https://energy.gov/eere/energybasics/articles/biomass-resource-basics; 16/10/2017

WE - ‘Classification, certification and standardization including lifecycle assessments of biofuels’; www.worldenergy.org/wp-content/uploads/2012/10/PUB_Biofuels_Policies_Standards_and_Technologies_2010_Annex6_WEC.pdf; 16/10/2017

WHO - World Health Organization Factsheet updated September 2016; http://www.who.int/mediacentre/factsheets/fs313/en/; 16/10/2017